69-19,054

CATALDO, Joseph C., 1937-

EXPERIMENTAL AND THEORETICAL INVESTIGATION OF THE ONSET OF STATIONARY CONVECTIVE PLASMA CELLS.

The City University of New York, Ph.D., 1969
Physics, plasma
University Microfilms, Inc., Ann Arbor, Michigan

EXPERIMENTAL AND THEORETICAL INVESTIGATION OF THE ONSET OF STATIONARY CONVECTIVE PLASMA CELLS

by

JOSEPH C. CATALDO

A dissertation submitted to the Graduate Faculty in Engineering in partial fulfillment of the requirements for the degree of Doctor of Philosophy, The City University of New York.

1969

This manuscript has been read and accepted for the Graduate Faculty in Engineering in satisfaction of the dissertation requirement for the degree of Doctor of Philosophy.

4/22/1969
date

Chairman of Examining Committee

22 April 1969
date

Executive Officer

Prof. M. Ettenberg

Prof. H.E. Hart

Prof. M.L. Pei

Prof. J.R. Steven

Prof. N.C. Jen, Chairman
Supervisory Committee

The City University of New York

ACKNOWLEDGMENTS

I would like to express my gratitude to several people who assisted and encouraged me in the preparation of this dissertation.

First and foremost, I would like to thank my mentor, Professor Norman C. Jen, who suggested the area of research and skillfully directed it from its inception. His friendly and expert guidance is greatly appreciated. I would also like to thank the members of my Doctoral Committee, Professors M. Ettenberg, H.E. Hart, M.L. Pei, and J.R. Steven for their interest and advice. The constructive suggestions of Professors C.M. Tchen, F.F. Chen, (Princeton Plasma Physics Laboratory) and K. Rogers, (Stevens Institute of Technology), are also gratefully acknowledged.

Thanks are also due to Messrs. Ira Mansfield and Peter Fiore for their assistance in setting up and running the experimental equipment.

I would like to thank both the City University, and the United States Air Force Office of Scientific Research for the financial support given to me, personally, and to Magnetohydrodynamics Laboratory of The City College without which this work could not have been done. The financial aid and services provided by The City College and the Department of Civil Engineering are gratefully acknowledged.

The greatest debt of gratitude is owed to my wife, Peggy, without whose encouragement and cooperation, this dissertation could not have been completed.

TABLE OF CONTENTS

LIST OF FIGURES

NOMENCLATURE

A_1 to A_4	integration constant
A_i	atomic weight of potassium
A_m	inverse variance for a gaussian distribution
a	dimensionless A_m
B	magnetic field
C	constant relating the potential and the density
D_1 to D_4	integration constant
E	electric field
e	charge of an electron
F_1 to F_4	integration constant
G	experimental parameter $(1+\alpha)$
H_1 to H_4	integration constant
J	current density
K_1 to K_4	constant
K	Boltzmann constant
L	angular momentum
M	mass ratio (m_e/m_i)
m	azimuthal wave number

m_i	ion mass
m_e	electron mass
n	number density
n_i	ion number density
n_o	equilibrium ion number density
n_1	perturbed ion number density
P_{ie}	total momentum transfer to ions by collisions with electrons
P_i	ion pressure
Q	the order of differential equation
r	radius
r_o	radius of boundary separating regions I and II
T	temperature
T_i	ion temperature
t	time
U	constant, equal to D_4
u_j	exponent of ρ
V_o	azimuthal equilibrium ion velocity
V_{oe}	azimuthal equilibrium electron velocity
V_{ro}	radial equilibrium ion velocity

V_{eo}	azimuthal equilibrium velocity
V_{zo}	axial equilibrium ion velocity
V_l	perturbed velocity
V_{th}	thermal velocity
v_i	ion velocity
v_e	electron velocity
v_o	dimensionless V_o
v	dimensionless V_l
W	dimensionless ω
X_j	integration constant
Y_j	integration constant
Z	charge units on each ion
α	constant relating the density gradient to the potential gradient
β	T_e/T_i , Temperature ratio
δ	dimensionless density gradient
ϕ	gravitational potential
η	electrical resistivity
λ	mean free path

λ_D	Debye length
μ	viscosity
ν	dimensionless n
π	ion viscous stress tensor
ρ	dimensionless r
ρ_o	dimensionless r_o
τ	dimensionless μ
Φ	constant potential
ϕ	electric potential
χ	dimensionless ϕ
Ω_o	dimensionless angular velocity
ω	frequency
ω_c	ion larmor frequency
∇	gradient operator

ABSTRACT

A low-β collisional plasma cylinder confined in a uniform magnetic field is considered. A stationary convective instability, due to the relative rotation of concentric rings of plasma which leads to an adverse angular momentum between these rings, is studied. This mechanism produces a distinct stationary cellular pattern consisting of eight smaller cells around a large central circular hole at a critical magnetic field around 200 gauss.

A new diagnostic instrument, the plasma camera, which allows photographs of the entire column cross-section to be taken at one time with a high degree of spatial resolution, is used in a single ended Q-machine to observe the density distribution of the cellular pattern. The onset of the cellular pattern is always accompanied by at least an order of a magnitude increase in the density. The presence of the hole and the increase in the current density, at low magnetic fields, is the result of effective trapping of particles at the edge of the plasma column.

A new concept of anomalous diffusion is presented. The mechanism of this diffusion is due to the breaking off and transverse motion of flute-like irregularities from the central core of the plasma

column for magnetic fields above 700 gauss.

The theory of stationary convective instability is used to predict the structure and location of the plasma cells. A stream pattern is theoretically determined which matches the experimentally observed plasma cells. A relationship between the perturbed density and potential is also found to be in good agreement with the experimental values.

CHAPTER 1

INTRODUCTION

In recent years, extensive theoretical and experimental studies[1-10] of the plasma instabilities observed inside a quiescent plasma device have been made. Understanding of the mechanism of plasma instabilities is very important in the field of thermonuclear research because of its close association with the confinement of a high temperature plasma and the diffusion process across the magnetic field lines. Until now, most studies of plasma instabilities were confined within the domain of overstability[11-16] and dealt with characteristic frequencies and amplitudes, while studies of stationary convective instabilities[17] have been almost neglected. Yet this type of instability could be very important in the confinement of a plasma. The onset of such an instability leads the plasma column into a state of zero frequency and reduces the transverse diffusion coefficient by a magnitude of several orders.

A theoretical investigation of a stationary convective instability has been made by Chandrasekar[18] for an incompressible conducting fluid embedded in a magnetic field. In his analysis, the driving force

was the thermal gradient and the restoring force was the gravitational force. Verifying Chandrasekar's prediction, an experimental investigation has been successfully made by Nakagawa[19]. Photographs of patterns of convective cells were obtained using mercury as the incompressible fluid and applying a strong magnetic field. The results of Chandrasekar and Nakagawa stimulated interest in investigating convective instabilities within the quiescent plasma device.

Experimental investigations of the plasma column inside the quiescent device have shown that the plasma rotates azimuthally at the E X B drift velocity[20, 21]. This drift velocity varies in the radial direction and is dependent on the magnitude of the electric and magnetic fields. For certain magnetic fields where large changes in the velocity gradient occur, the plasma becomes unstable as predicted by the well-known concept of interchange of angular momentum[17, 22]. Therefore, the existence of a stationary convective instability inside the quiescent plasma device is possible for a critical magnetic field. For this investigation, the driving force is the self-consistent electric field and the restoring force is the centrifugal force due to rotation of the plasma.

In order to provide a self-consistent electrical potential across the plasma column, a special design of the plasma generator has been made. The visualization of the stationary convective instability and its associated cellular pattern would be virtually impossible by means of the Langmuir probe technique[23, 24], because the probe only measures the plasma properties at a given instant of time at a point. For measuring the spatial distribution of the streaming plasma across the plasma column at a given instant of time, a new diagnostic technique, known as the plasma camera[25], has been developed.

The purpose of this study is:

(1) to verify experimentally the existence of a stationary convective instability and the cellular pattern across the plasma column,

(2) to determine the critical magnetic field for maximum confinement or minimum diffusion,

(3) to confirm the theoretical concept of interchange of angular momentum for the stationary convective instability in a plasma column.

A description of the experimental apparatus including a detailed description of the plasma camera is presented in Chapter 2. In Chapter 3, experimental results of the diffusion pattern and the cellular structure are given. The use of the principle of stationary convective stability in predicting the cellular structure in a plasma column is discussed in Chapter 4. A comparison of the experiment with the theory appears in Chapter 5. The conclusions of this dissertation are summarized at the end of Chapter 5.

CHAPTER 2

EXPERIMENTAL APPARATUS

For experimental studies of the onset of instability in a plasma column embedded in a low magnetic field, ranging from 100 to 300 gauss, a quiescent plasma device with a variable magnetic field strength, known as the Q-machine[26, 27], and a new diagnostic technique, known as the plasma camera, have been specially designed and constructed. The plasma device produces a steady, relatively quiescent and highly ionized plasma which rotates azimuthally in the E X B direction. Since Langmuir probe measurements cannot provide the instantaneous distribution across the plasma column at a given instant of time, the plasma camera has been successfully used. The plasma camera designs previously used for a pulsed plasma[28-30] have been significantly modified here because of the low energy density of the streaming plasma column.

2.1 Quiescent Plasma Device

The specially constructed quiescent plasma device, shown in Figure 2-1, at The City College of The City University of New York, consists of the following major elements:

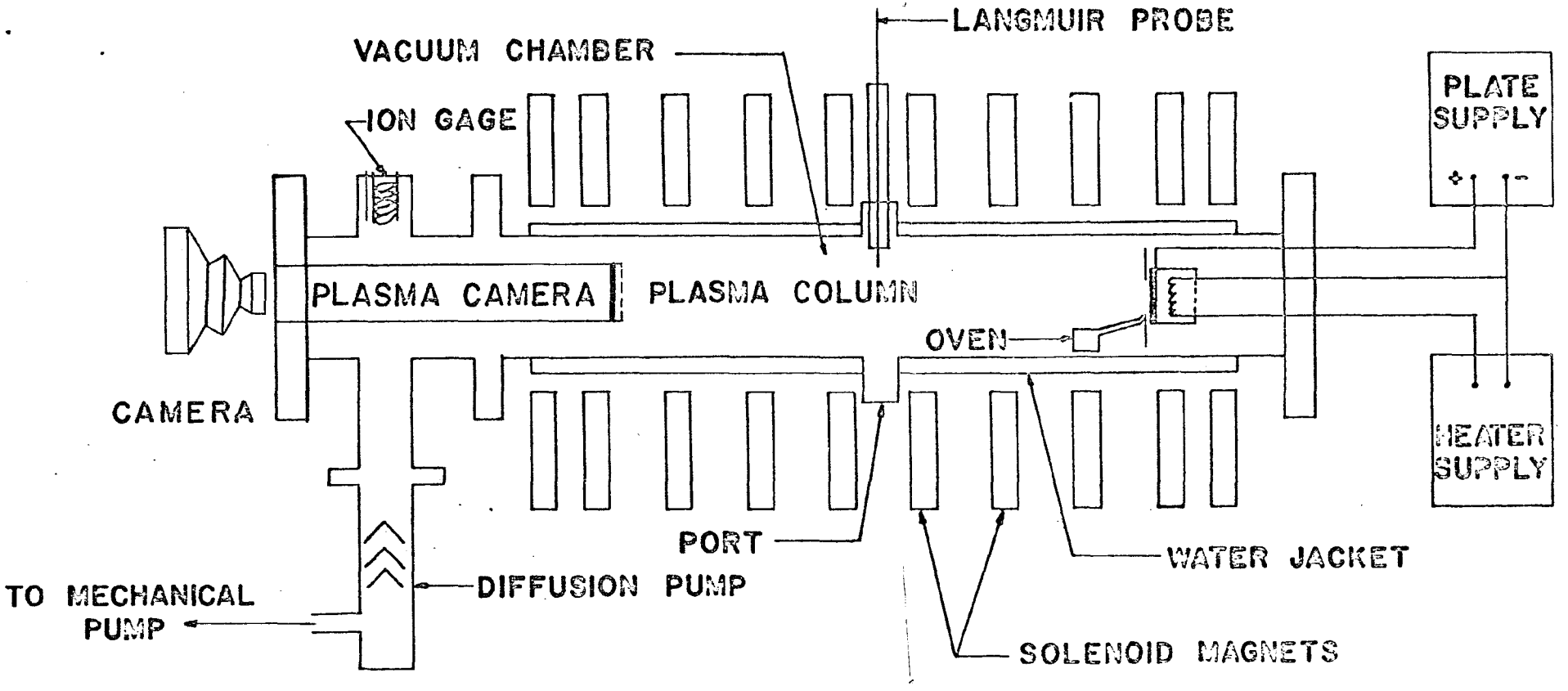

Fig. 2-1. Schematic of Q-machine.

(a) An axial magnetic field with variable strength

(b) A vacuum chamber with a water cooled jacket and

(c) A plasma generator

(a) Magnetic Field: The ten coiled series connected magnetic field unit, manufactured by Magneon Inc., provides a cylindrical test section of 7 inches in inner diameter by 54 inches in length with a variable strength up to 10,000 gauss. The magnets are cooled by a recirculating water system at 90 gallons per minute. The associated power supply, manufactured by Richardson-Allen, has a capacity of 200 volts and 1000 amperes. The end effects have been calculated and minimized by adjusting the spacing between the coils. The final spacing is 4.966, 3.566, 4.366, 4.366, 4.366, 4.366, 4.366, 3.566, 4.966 inches. The variation of the magnetic field intensity along the axis of the plasma column is $\pm 2.0\%$ which is better than the anticipated value given by the manufacturer. The magnetic field was measured by moving a magnetic Hall probe inside, and axially along the length of the chamber. The output is read into an incremental Gauss meter with an accuracy of better than 0.1%. The field is very uniform across the plasma column. A typical magnetic field measurement is shown in Figure 2-2.

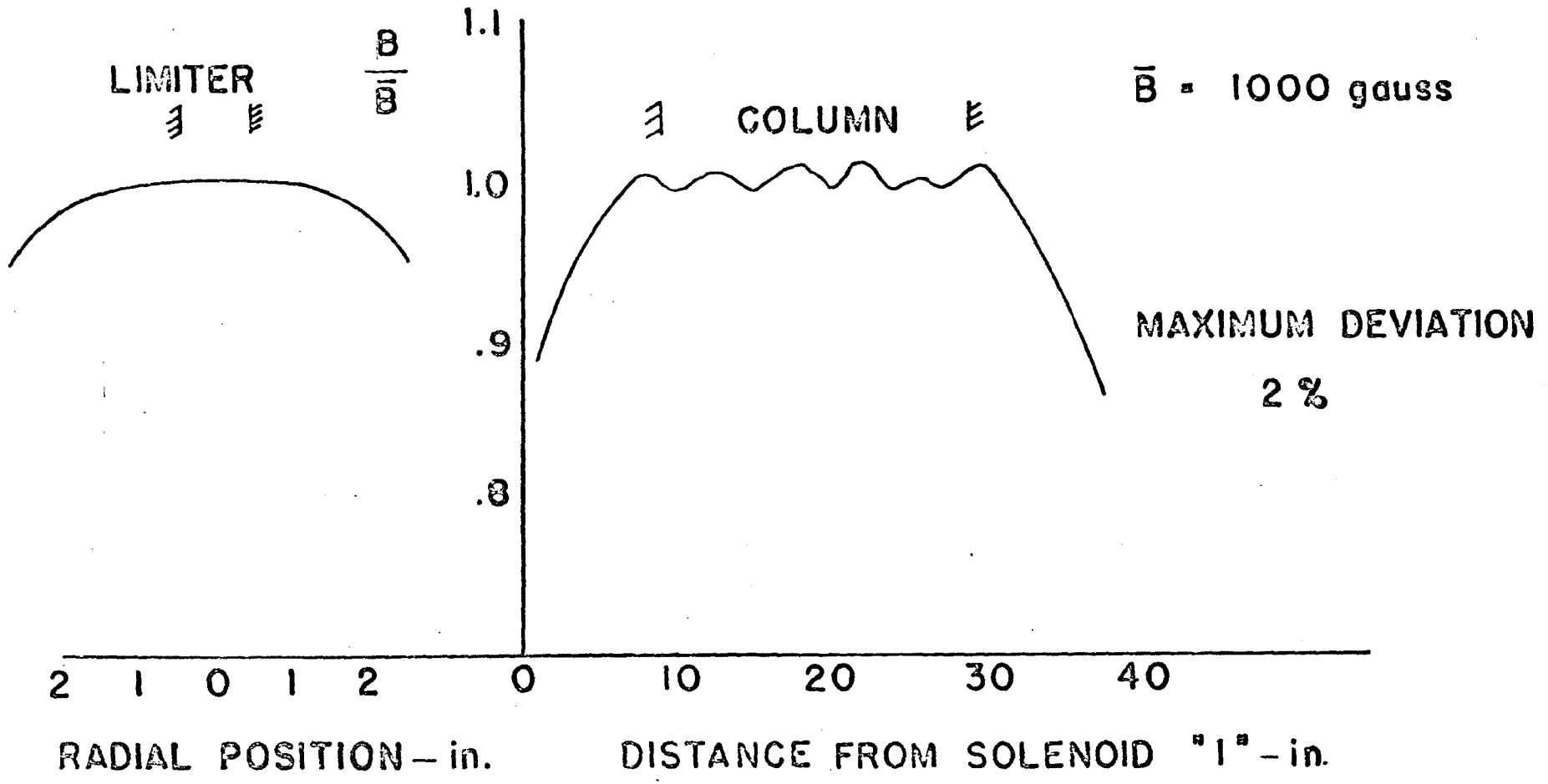

Fig. 2-2. Magnetic field.

(b) Vacuum Chamber: The vacuum chamber has an inside diameter of 4 3/4 inches by 54 inches in length with a water cooling jacket. The chamber water cooling system consists of 1/4 inch copper tubing with an alternate flow system for a constant temperature along the chamber.

The vacuum pumping system consists of a two stage roughing pump, 10 cu.ft. per min. at 0.1 microns in series with a 4 inch diameter diffusion pump, 750 liters per second. The 4 inch vacuum diffusion pump provides a vacuum of up to 10^{-7} mm of mercury. At the midpoint of the chamber, four one inch diameter ports, spaced 90 degrees apart, are provided for instrumentation. A single ended quiescent plasma is produced inside the vacuum chamber, which is terminated by the plasma camera.

(c) Plasma Generator: Within the plasma generator an electron gun is used to heat a tungsten plate onto which a neutral potassium vapor is sprayed. The electron gun heats the tungsten plate to a sufficiently high temperature, 2000 to 2300 degrees kelvin, for surface ionization to take place and at the same time produces neutralizing electrons by thermionic emission. The potassium vapor is ionized by surface ionization on the hot tungsten plate. Since tungsten has a work function

potential of 4.52 volts, which is greater than the ionization potential of the potassium atoms, 4.32 volts, the outer electron of the potassium atom will replace the electron that the tungsten has emitted.

The construction of the gun is similar to a vacuum tube diode in that its elements are a filament type emitter biased negatively with respect to the plate, Figure 2-3. In this plasma generator, the filament is also made of tungsten, 0.012 inches in diameter by 8.7 inches long, placed at a distance of 0.50 inches from the tungsten plate. A constant power supply of 1900 volts and 0.4 amperes is used to accelerate the emitted electrons from the filament to the tungsten plate. The filament-cathode circuit and filament structure are shown in Figures 2-4 and 2-5, respectively. The tungsten plate is 1 inch in diameter and 3/8 inches thick. Current from the power supply is regulated to provide a constant plate temperature. The variation of the temperature, measured by an optical pyrometer, is within the limits of ±10 degrees kelvin around the edge of the tungsten plate. The potassium vapor is produced in an oven and is supplied to the hot plate by a nozzle or an array of nozzles, Figure 2-6. The flux of the potassium vapor is controlled by adjusting the temperature of the oven. A photograph of the plasma generator is shown in Figure 2-7.

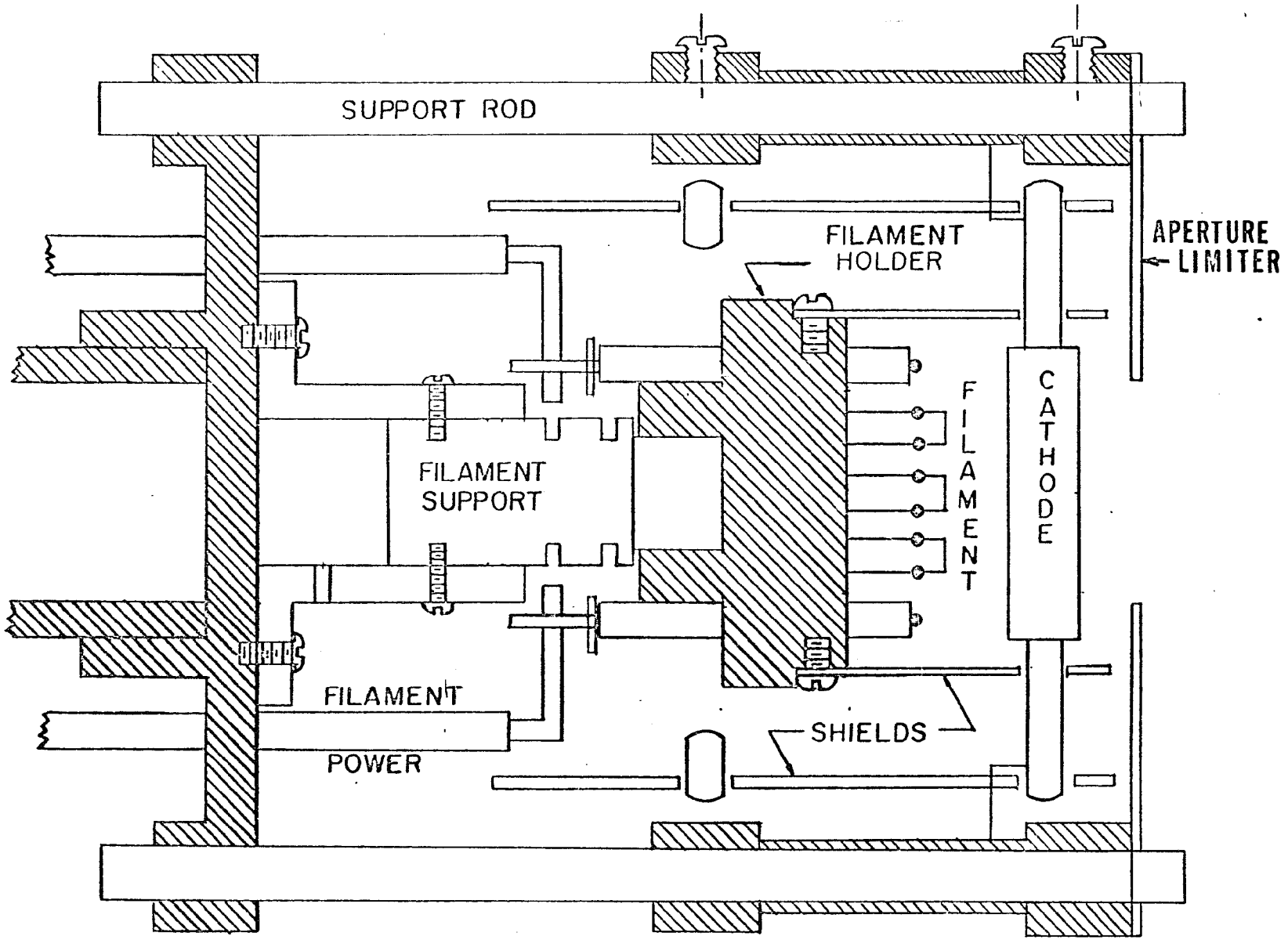

Fig. 2-3. Schematic of electron gun.

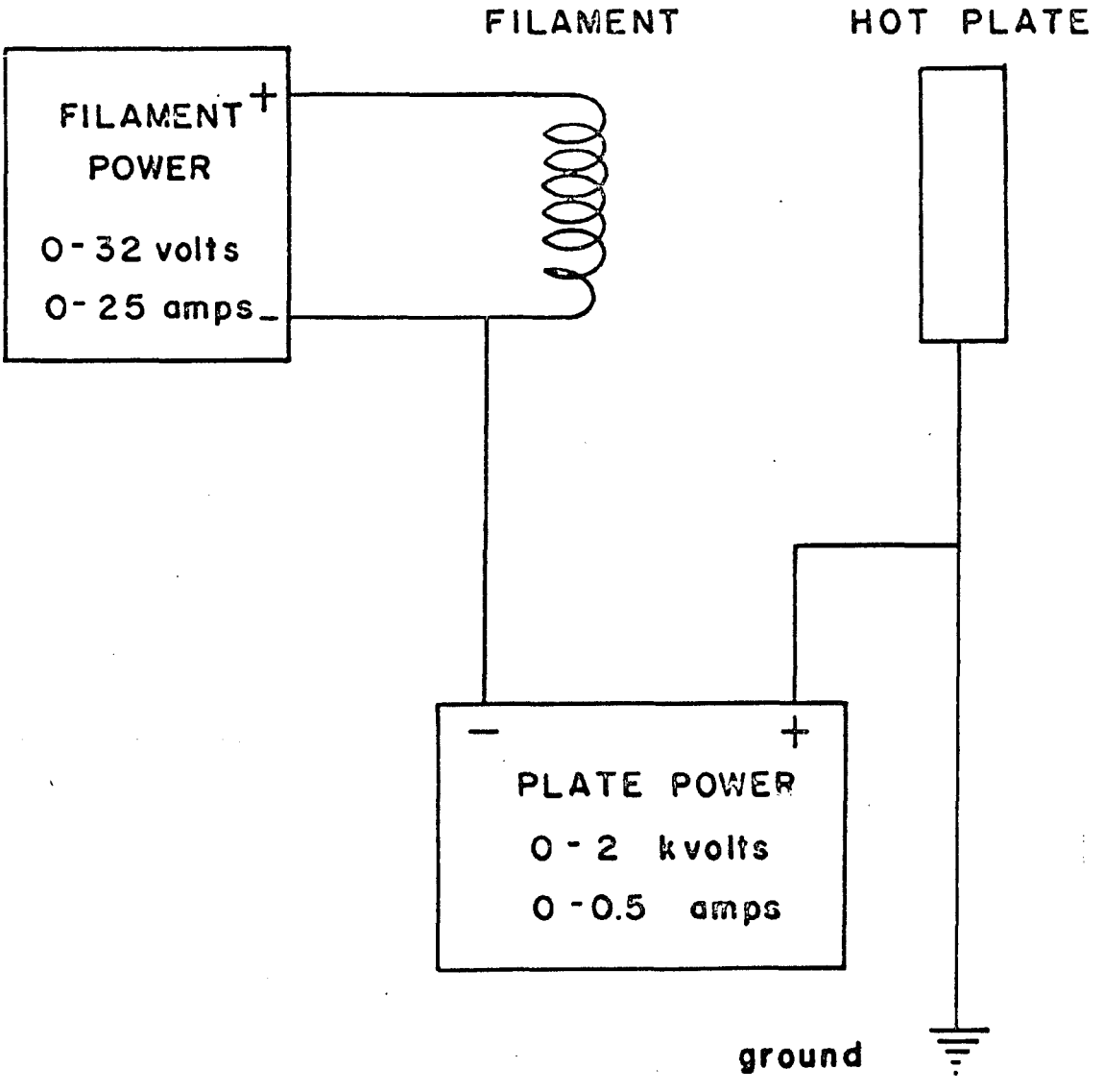

Fig. 2-4. Filament-Cathode circuit.

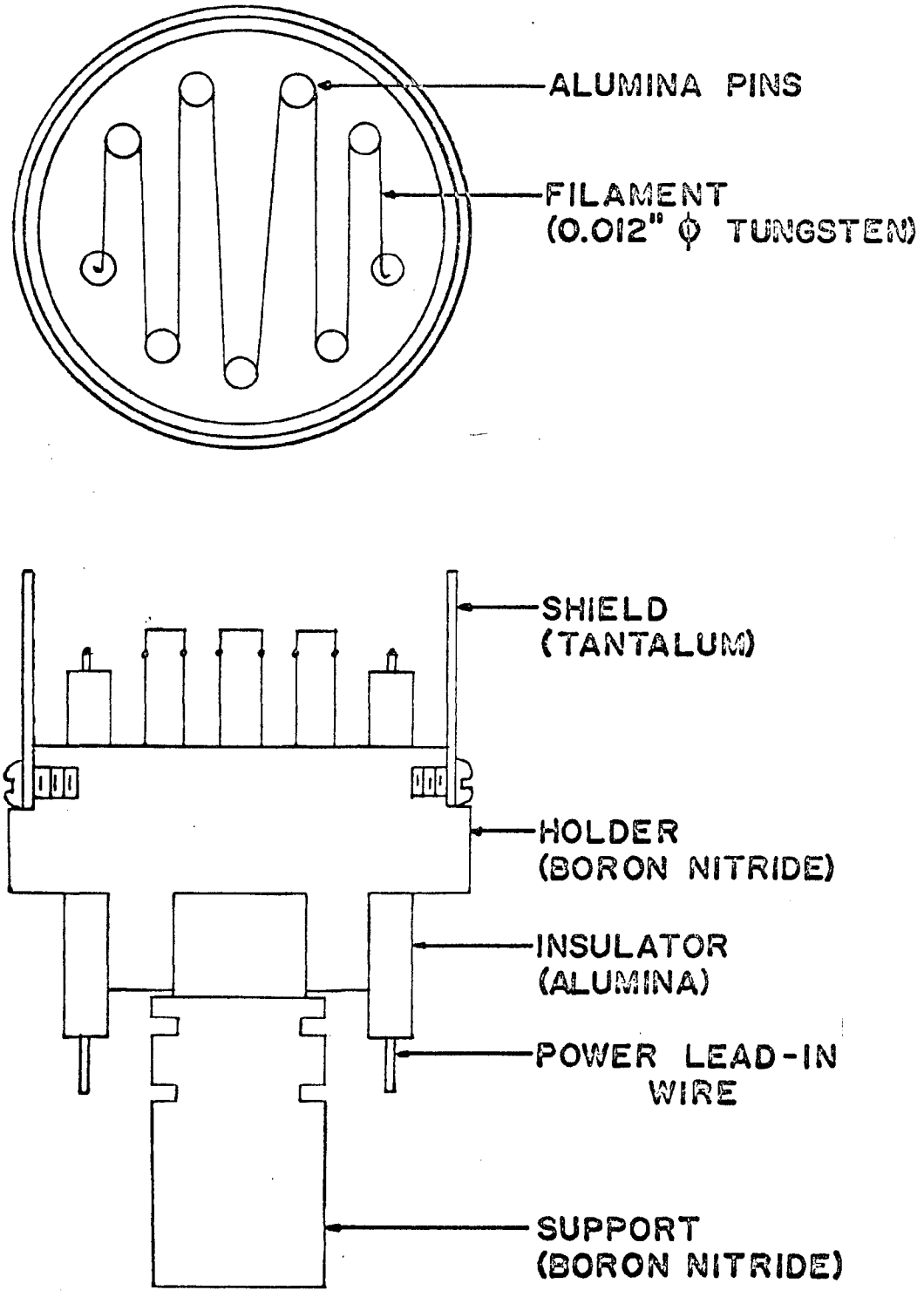

Fig. 2-5. Filament structure.

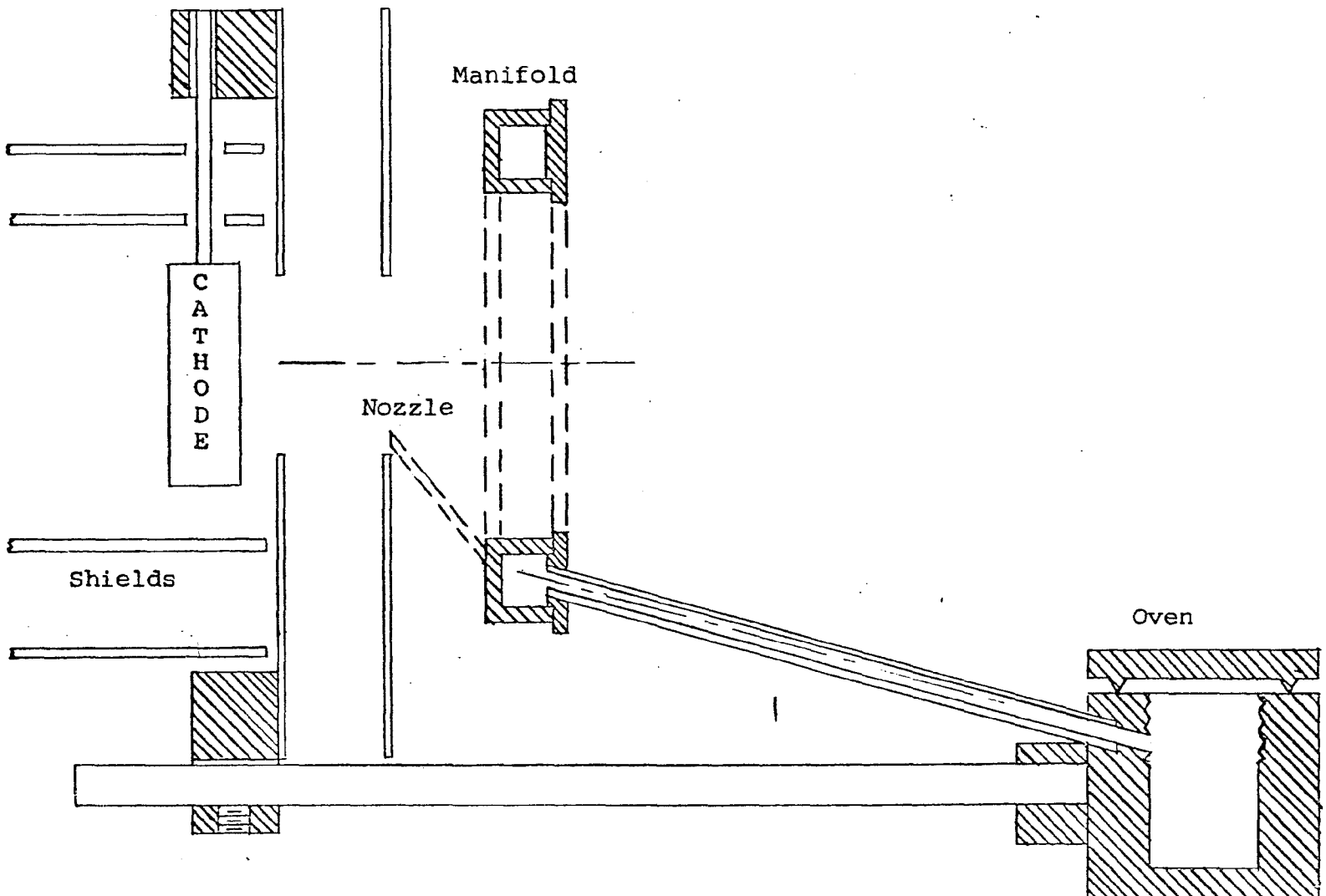

Fig. 2-6. Oven and manifold.

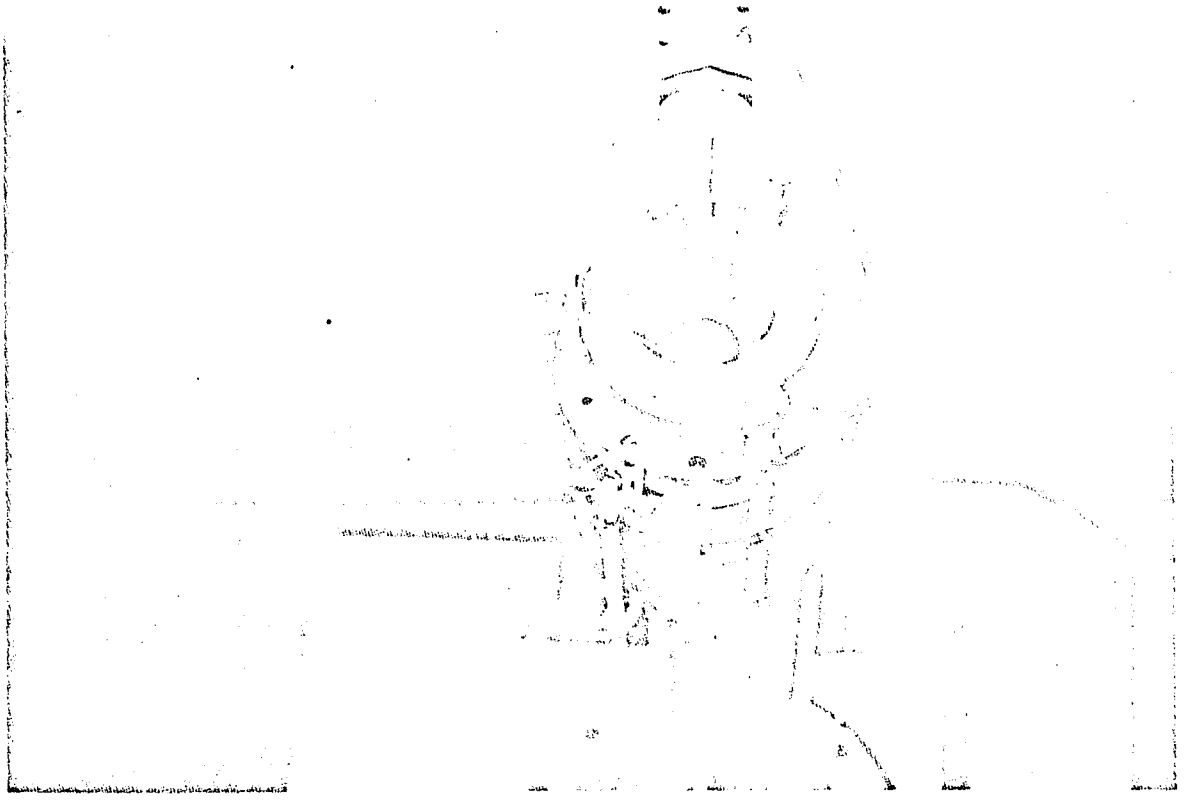

Fig. 2-7. Electron gun assembly.

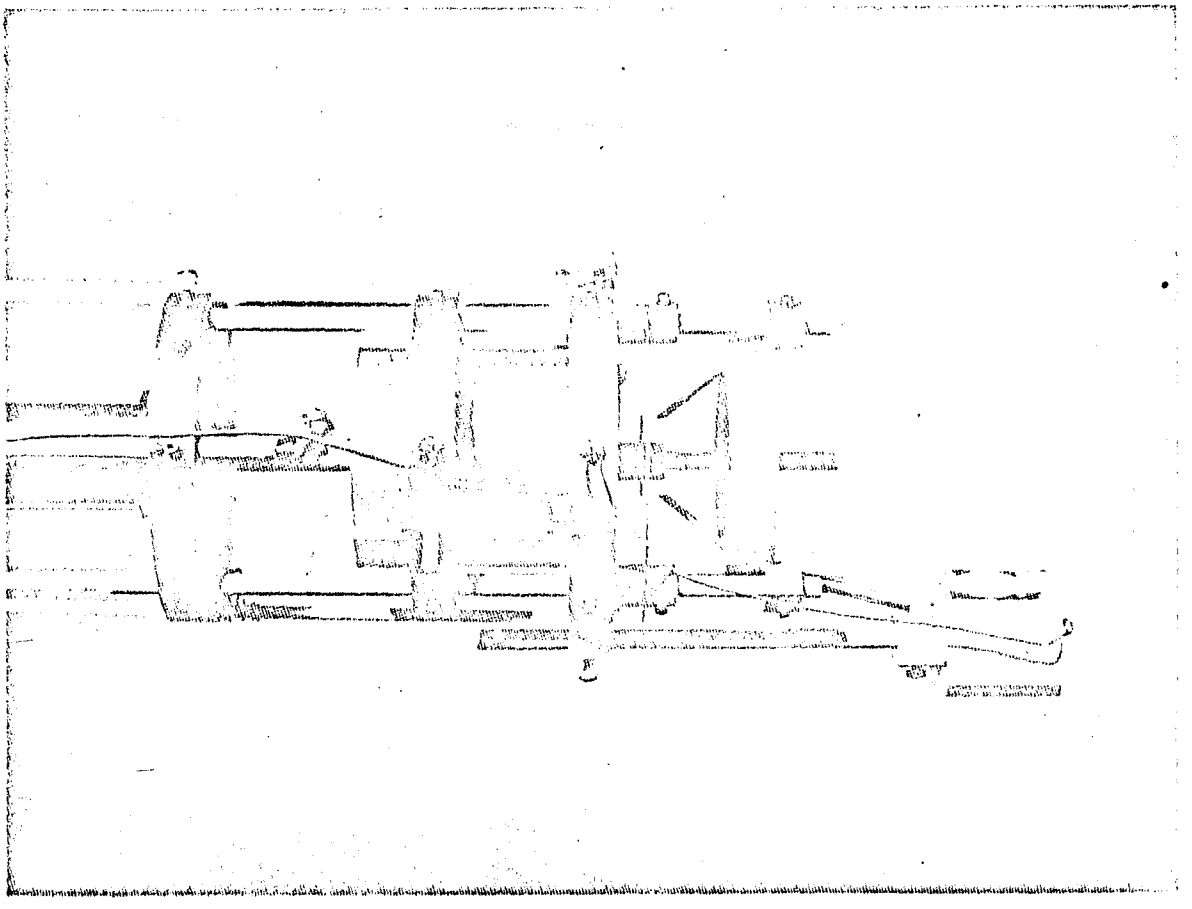

(d) Performance: The water cooled chamber keeps the background of neutrals at a low level. Thus the resulting plasma is confined in a uniform magnetic field with a high degree of ionization. The frequency spectrum analyzer indicates that the plasma column has the characteristics of a quiescent plasma.

(e) Operation: Theoretically, the gun may be operated in the space charge limited regime or in the temperature limited regime. In space charge limited operation, the current voltage characteristic follows the Langmuir-Childs "three halves power" formula. In temperature limited operation, electrons emitted by the filament are accelerated to the plate. Operation of the gun, however, is neither strictly space charge nor temperature limited: The observed mode of operation does not exactly agree with the Langmuir-Childs model. In their model, one type of particle with zero initial velocity is accelerated through the space charge region. In the present case there exists the probability of ions being generated. This means strict adherence to the above formula should not be expected. Some typical operating characteristics of the electron gun are shown in Figure 2-8, along with the applicable portion of the Langmuir-Childs law. It is obvious that the observed current collected by the plate is higher than

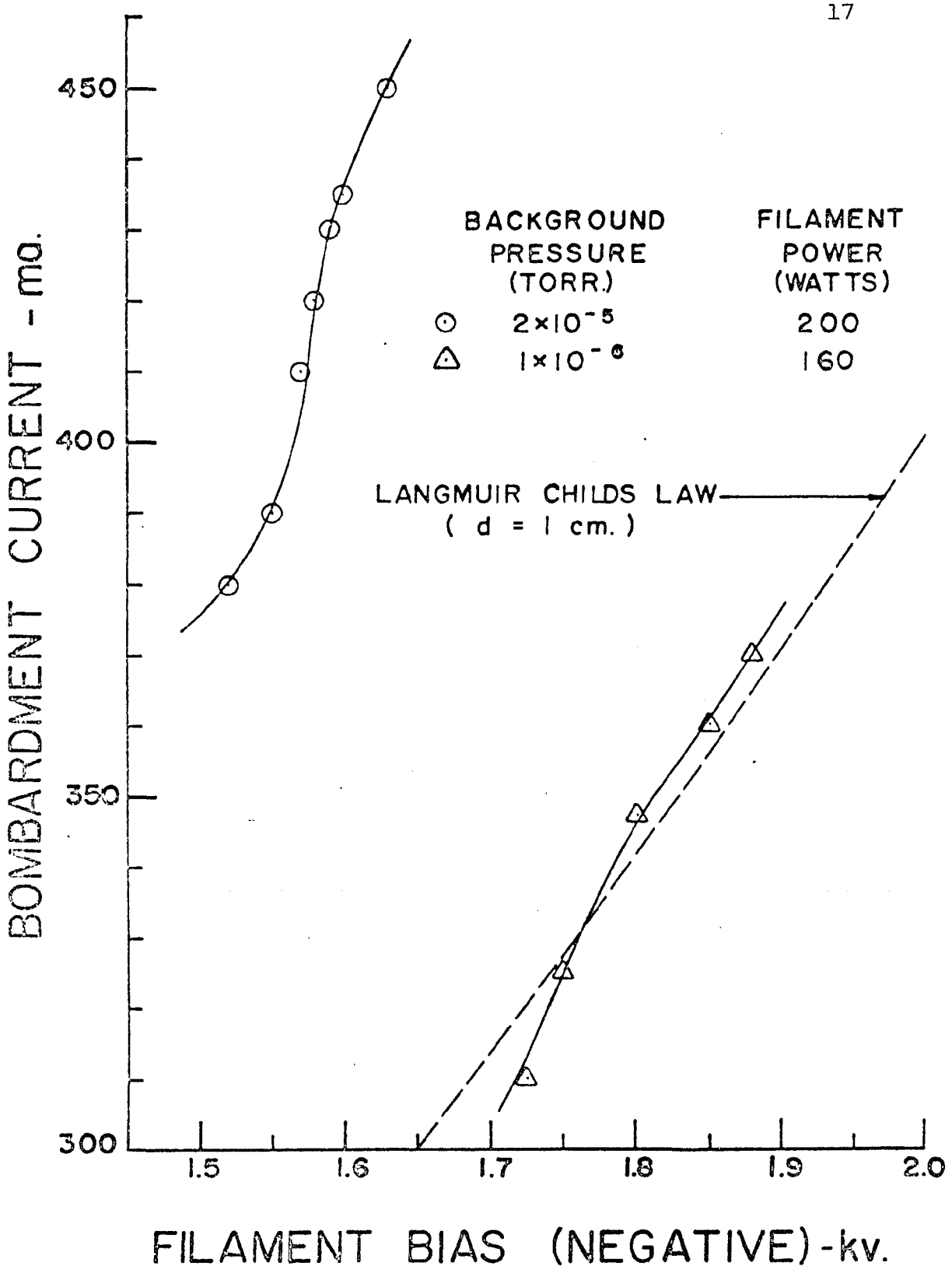

Fig. 2-8. Electron gun characteristic.

that predicted by the Langmuir-Childs law when the pressure is high, but for low pressure the Langmuir-Childs law is followed quite well.

When operating in the space charge limited regime the temperature of the hot plate varies linearly with the input power (Figure 2-9). This is convenient for adjusting the plate temperature especially when the plate is obscured from view by diagnostic equipment and the optical pyrometer cannot be used.

2.2 The Plasma Camera

For the sake of actual visualization of the instantaneous distribution of plasma density across a plasma column, the plasma camera is used, since the Langmuir probe is not feasible here. The Langmuir probe can provide density measurements at different points across the column at a different instant of time. The distribution of plasma density is then plotted or interpreted from those measurements. It becomes obvious that this representative distribution of density is not correct if the time scale of the instability is shorter than the time scale between experimental measurements. For quantitative and pictorial measurements, both plasma camera and Langmuir probes have been used here.

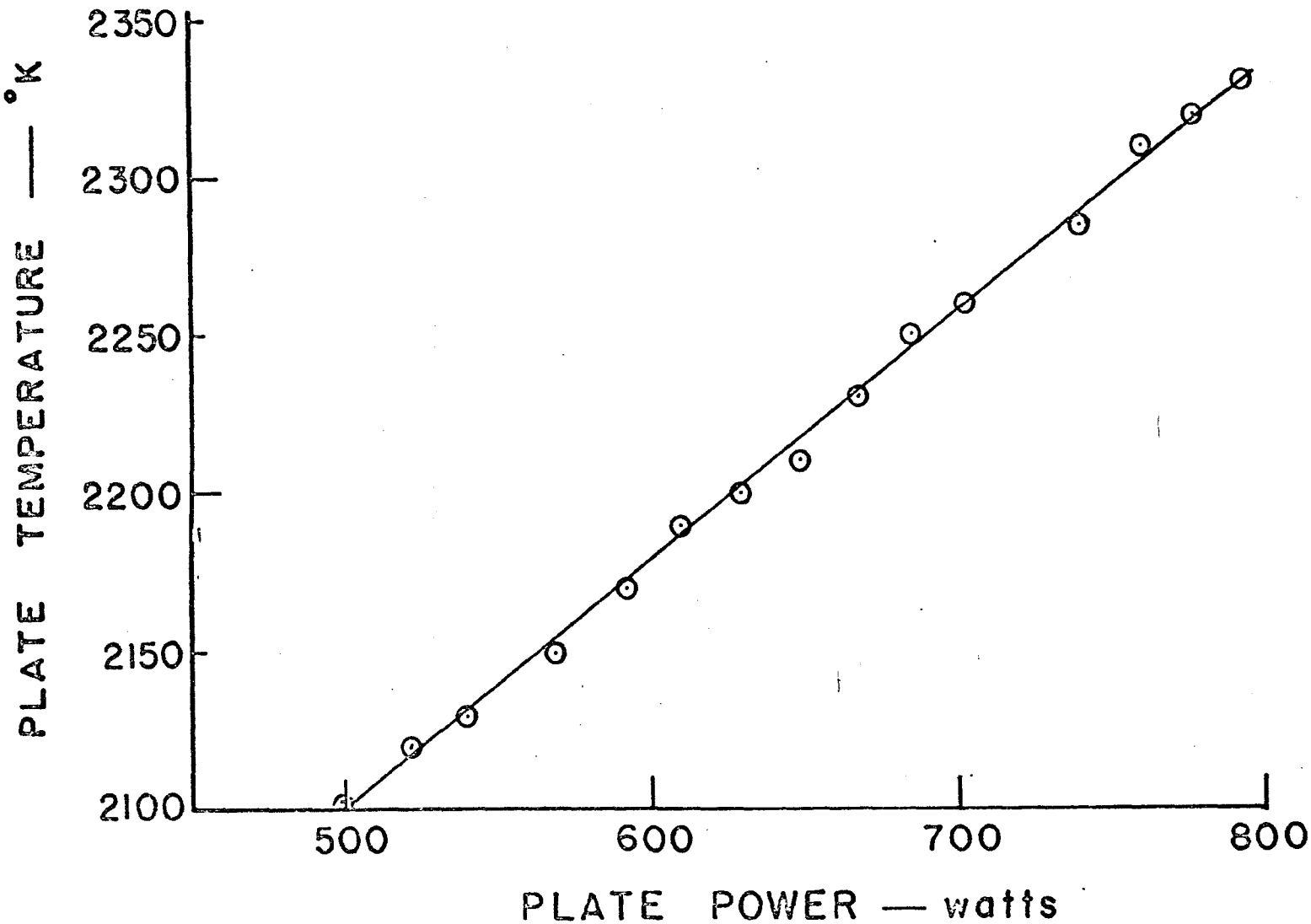

Fig. 2-9. Plate temperature vs. plate input power.

The plasma camera (Figures 2-10 and 2-11) consists of a 50% transmissive stainless steel screen and an aluminum coated scintillator. The general principle of the plasma camera is to accelerate electrons or ions from a continuously streaming plasma column onto a screen. By means of a strong electrical pulse between the screen and the scintillator, those electrons, primary or secondary, produce scintillations which in turn are photographed. For the Q-machine, the design criterions are quite different from the previous design for the pulsed plasma since the energy density of the streaming plasma column is lower and the temperature of the scintillator is higher.

The scintillator consists of a glass disk, 2 3/4 inches in diameter and 1/4 inch thick, coated first with a layer of phosphor and then a layer of aluminum, from 3000 to 5000 angstroms thick. P-1 and P-11 phosphors were found to have the most favorable characteristics for the Q-machine plasma. The minimum voltage required for the scintillations of these phosphors are 3000 volts[31]. The P-1 phosphor scintillates in a yellowish-green, with a rise time to 90% level and persistence to 10% level of from 1 milli sec. to 100 milli sec. The P-11 phosphor scintillates in a blue, with a rise time to 90% level and persistence to 10% level of from 1 μ sec to 10 μ sec.

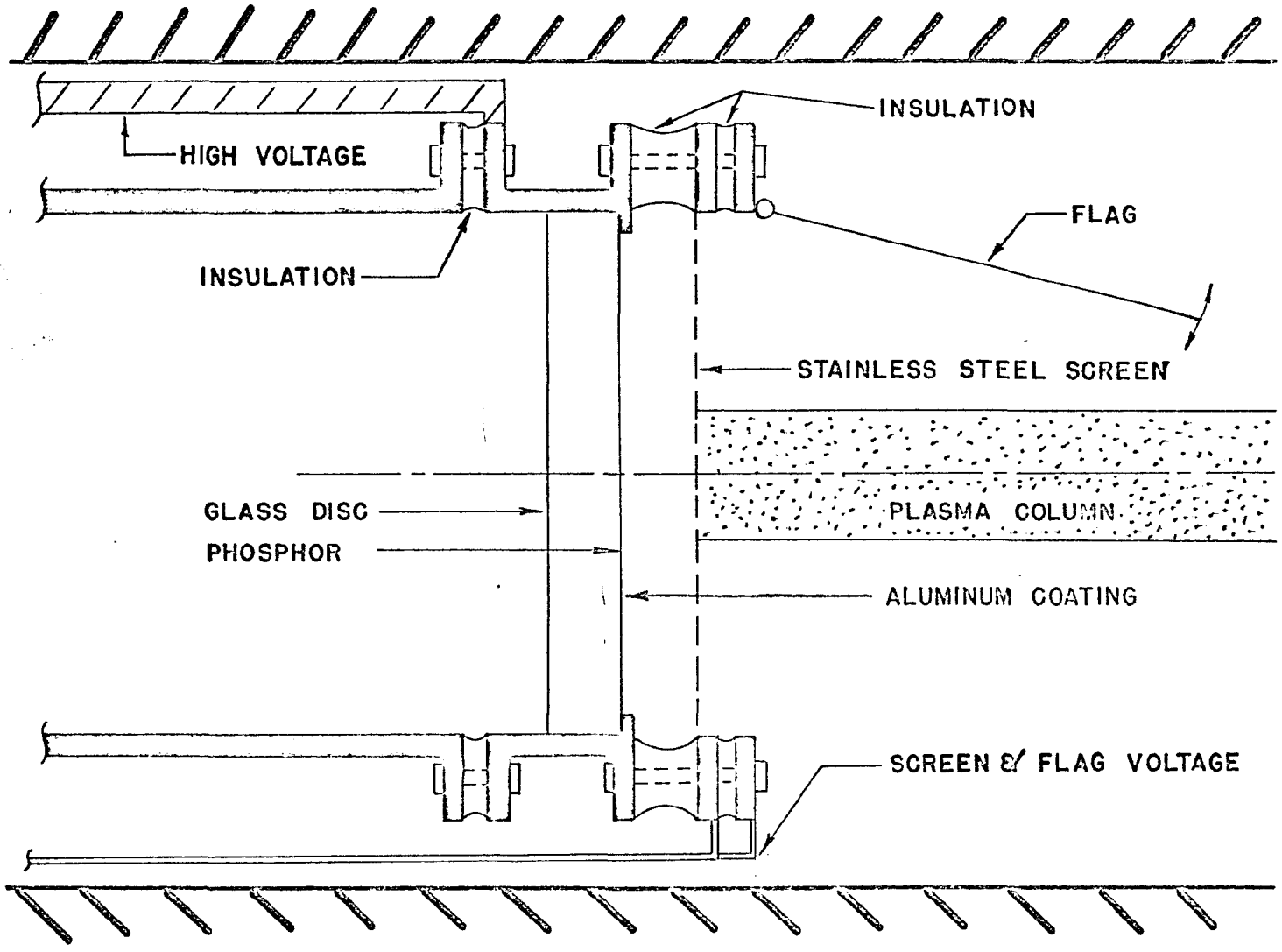

Fig. 2-10. Schematic of plasma camera.

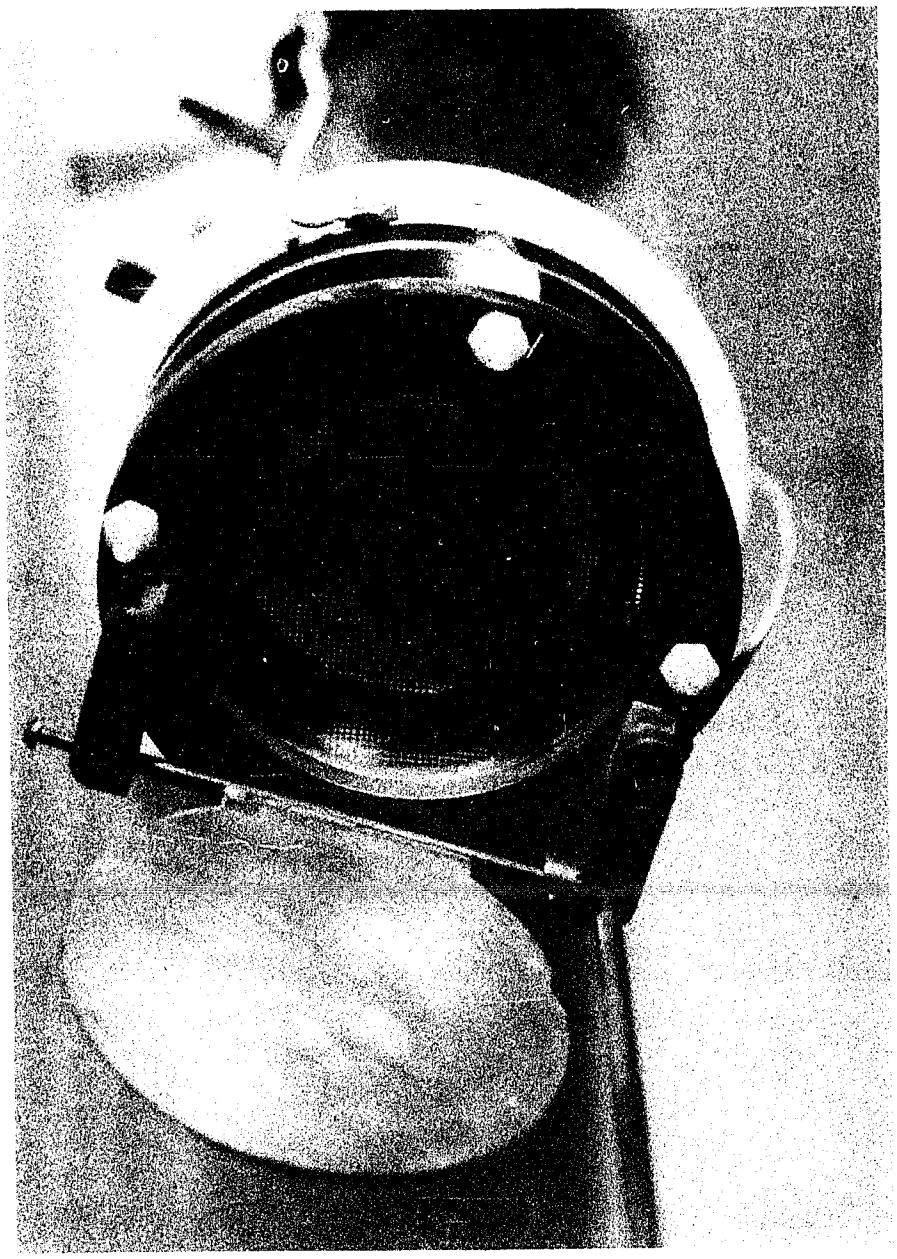

Fig. 2-11. Photograph of plasma camera.

The plasma source is a quite strong source of ultra-violet radiation, which also could produce scintillation. The additional scintillation is superimposed on the scintillation produced by the electrons accelerated in the space between the screen and the phosphor layer, and the over all picture may be considerably different from the effect due to the plasma stream. To eliminate the effect of ultraviolet radiation on the observed distribution of the intensity of the scintillation in the phosphor layer, the layer is covered with a layer of aluminum applied by evaporation in vacuum. The aluminum layer is completely opaque in both the visible and the ultraviolet regions of the spectrum. The ability of the aluminum layer to block out the visible light is an especially important design consideration in a Q-machine since the tungsten plate is extremely bright.

A minimum voltage of 3000 volts is necessary to penetrate the aluminum with an electron[32]. Therefore the electrons must be accelerated through a minimum potential of 6000 volts. From experimental observations on the City College plasma camera, a voltage range of from 7000 to 10,000 volts has been applied in order to produce clear plasma camera pictures.

Experiments have shown that the form of the phosphor scintillations quite accurately reproduces the form of the streaming plasma column, and the distortions that occur do not exceed 1 mm. This is shown by observing Figure 2-12a, with a one-to-one image to object ratio. The shadow of the probe is quite clear and measures 2 mm, the actual size of the probe.

The form and intensity of the distribution of the ion concentrations have also been obtained. Since it is impossible to produce direct scintillations from the ions in a practical way, secondary electrons must be used to indicate the required form. By applying a sufficient negative voltage of 22 1/2 volts to the screen, a sheath forms on the screen in the order of a debye length. The ions are accelerated through the sheath to the screen. By means of a strong pulse, the ions produce emission of secondary electrons upon striking the stainless steel screen. These electrons are accelerated onto the scintillator. Figure 2-12b shows a photograph of the secondary electron emission, a distribution of the ion concentration. One may observe that the brightest portions of the picture are the lines formed by the screen; this is, in fact, due to secondary emission. Comparing Figure 2-12a

Fig. 2-12a. Plasma camera photograph of an electron distribution with probe.

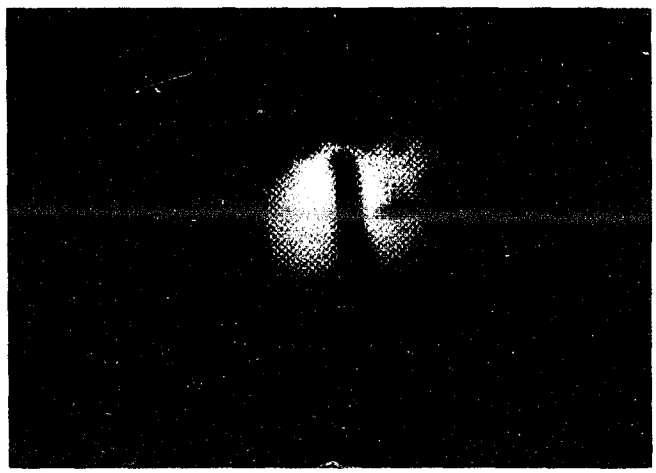

Fig. 2-12b. Plasma camera photograph of an ion distribution with probes.

with Figure 2-12b, one observes that the brightest portions of Figure 2-12a are the space between the grids of the screen. This is the area where the electrons stream through the screen. The reason the probe shadow appears larger in the ion concentration picture is because the ion larmor radius (4.1 mm) is larger than the probe thickness while the electron larmor radius (1.5×10^{-2} mm) is much smaller than the probe thickness.

The positive end of the pulse is applied to a metal holder which is electrically connected to the aluminum layer by a contact ring which overlaps the aluminum layer by 1/8 inch around its outer edge. The negative end of the pulse is connected to the screen which in turn is connected to ground through a dry cell battery.

The main difference between the plasma camera used in the Q-machine[25] and the ones used in a pulse plasma[28-30] is the use of only one screen for the former and two screens for the latter. Since the pulsed plasma is more energetic, the density of particles reaching the scintillator is sufficient to produce scintillation. It has been found experimentally that the number of particles reaching the scintillator in the Q-machine plasma camera is insufficient to produce scintillation when two screens are used. A plastic scintillator is unacceptable

because the collector reaches temperatures of over 150 degrees C. while the melting point temperature of the plastic scintillator is about 80 degrees C. A stainless steel flag that may be rotated out of the way of the plasma stream has been placed in front of the camera. The flag protects the screen and scintillator from constant plasma bombardment.

The optics of the system have been designed to obtain a one-to-one image to object ratio. A 360 mm focal length lens is used to focus the image on a graflex camera with a polaroid attachment.

2.3 The Langmuir Probe

In this study, two Langmuir probes are used to determine the electron and ion current densities, the electrical potentials and the fluctuation of the current densities across the plasma column. The probe construction is shown in Figure 2-13 with the probe circuit shown in Figure 2-14. A tungsten wirer 0.009 inches in diameter and 0.39 inches (1 mm) long is shielded by first inserting the wirer in an alumina ceramic insulating tube with an inner diameter of 0.022 inches, and then winding copper sheathing around the ceramic. For obtaining saturation electron current or ion current, a voltage of $\pm$22 1/2 volts has been used.

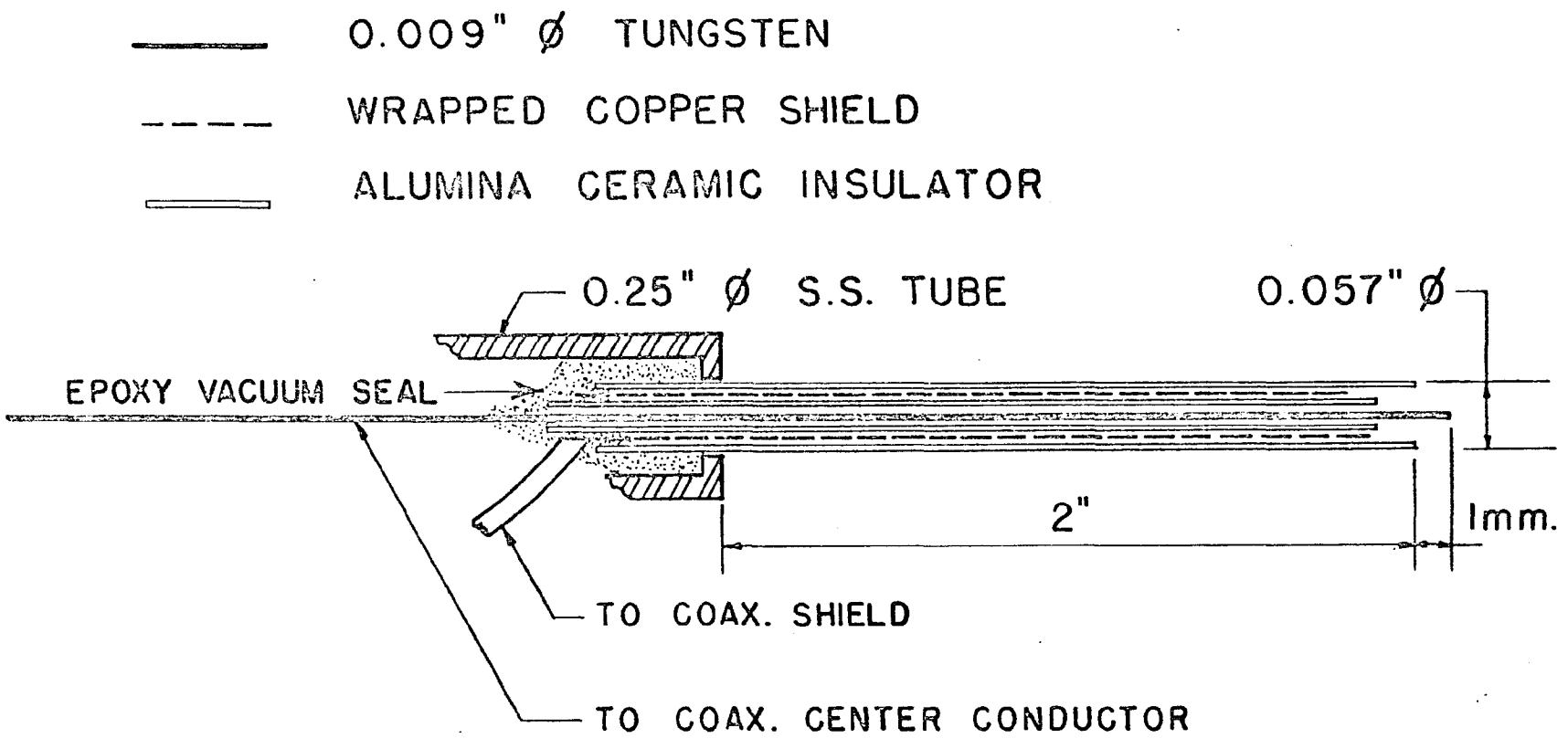

Fig. 2-13. Probe detail.

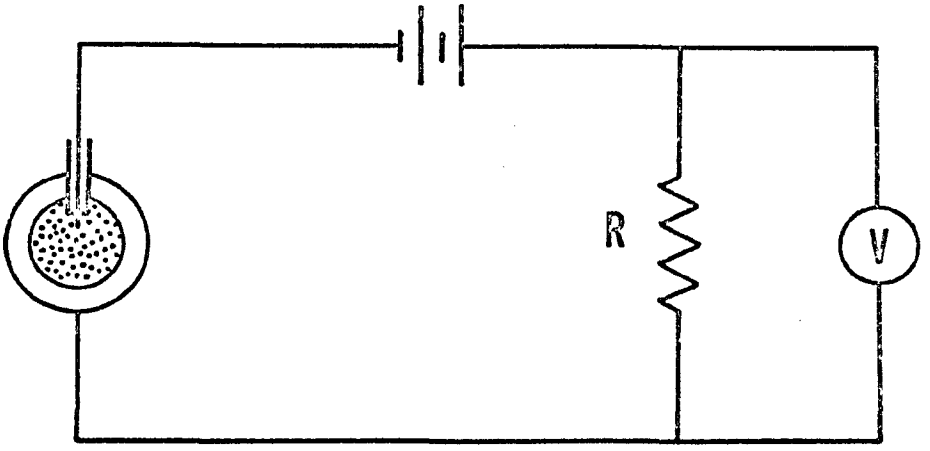

R small, current measurement.

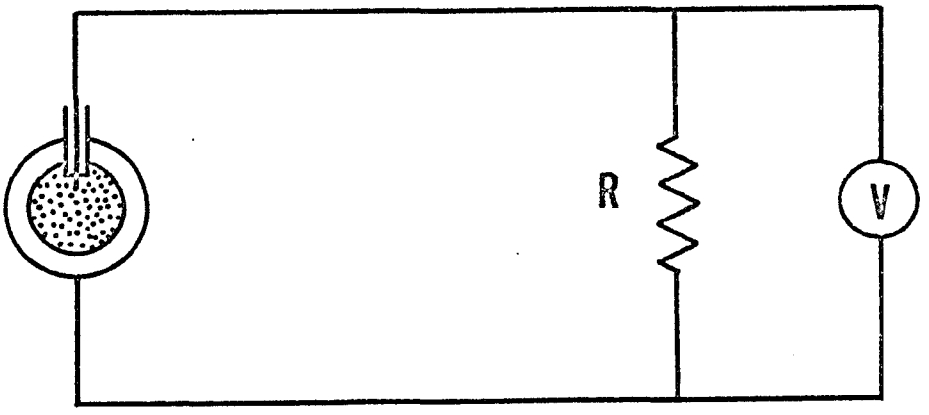

R large, voltage measurement.

Fig. 2-14. Probe circuit.

With reference to the characteristics as shown in Figure 2-15, it is seen that when the probe is biased sufficiently negative with respect to the plasma, almost all the electrons are repelled and the current collected is due mainly to ions; this is called the ion saturation current (region A). In this region, all ions which move towards the probe as a result of their thermal motions are collected by the probe and some are accepted by the sheath. As the potential becomes more positive, fewer electrons are repelled and a point is reached at which the electron current exactly equals the ion current to the probe, hence the net probe current vanishes; this point is called the floating potential. In region B, some of the ions are repelled and the electron current to the probe becomes more positive until the potential is sufficiently positive to repel all the ions and attract all electrons which move to the (effective) probe because of their random velocities (region C); this is electron saturation current.

The slope of the curve in region C is due to sheath which builds up around the probe. Usually the sheath thickness can be neglected, but as the potential is increased the sheath size increases and therefore creates a larger effective probe area which accounts for the increase of electron current with voltage.

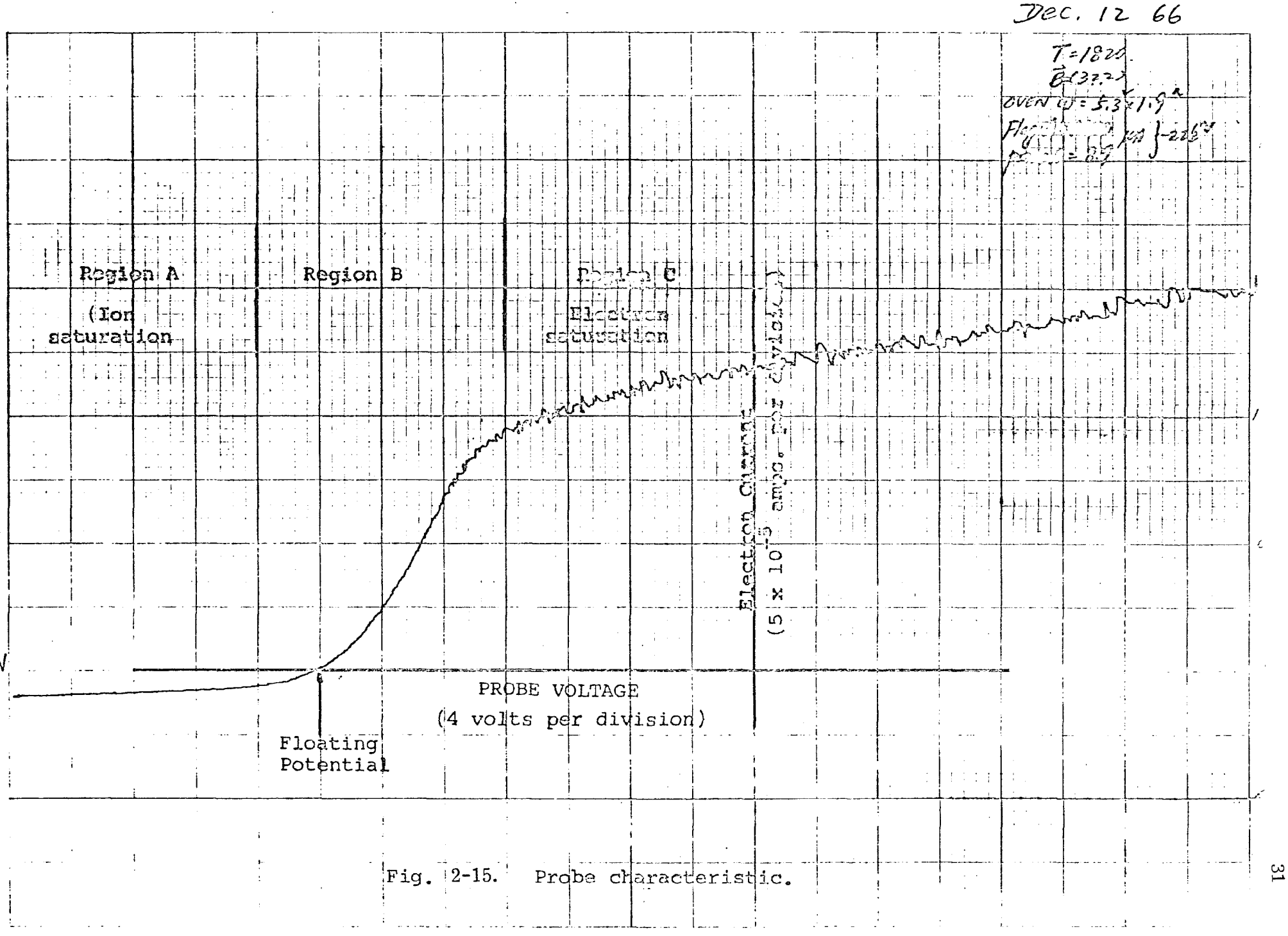

Fig. 2-15. Probe characteristic.

In actual use the probe current is measured by an electrometer and the probe voltage by a vacuum tube voltmeter. The outputs of these meters are used to drive the X and Y axes of a chart recorder all shown in Figure 2-16. The characteristic of Figure 2-15 was recorded in this manner.

Because the ion current saturates rather fast for moderate negative voltages, it is used to calculate the plasma density. In the elementary theory, it is assumed that all the ions which strike the probe because of their thermal motions are collected. For a Maxwellian distribution, the ion saturation current is given by

$$I_{SAT.} = \frac{1}{2} ne\left(\frac{2KT}{\pi m_i}\right)^{1/2}$$

where n is the number density, e is the electric charge, k is Boltzmann's constant, T is the temperature and m_i is the ion mass.

In order to study instabilities, the probes have been shielded (Figure 2-13) to reduce the spurious noise. Ion density oscillations are observed by biasing the probe to collect ion current and letting this current pass through a 1000 ohm resistor, measured with Tektronix 555 Dual-beam oscilloscope, using a type 1 A 7 vertical pre-amplifier. The output of the 1 A 7 is then connected to a spectrum

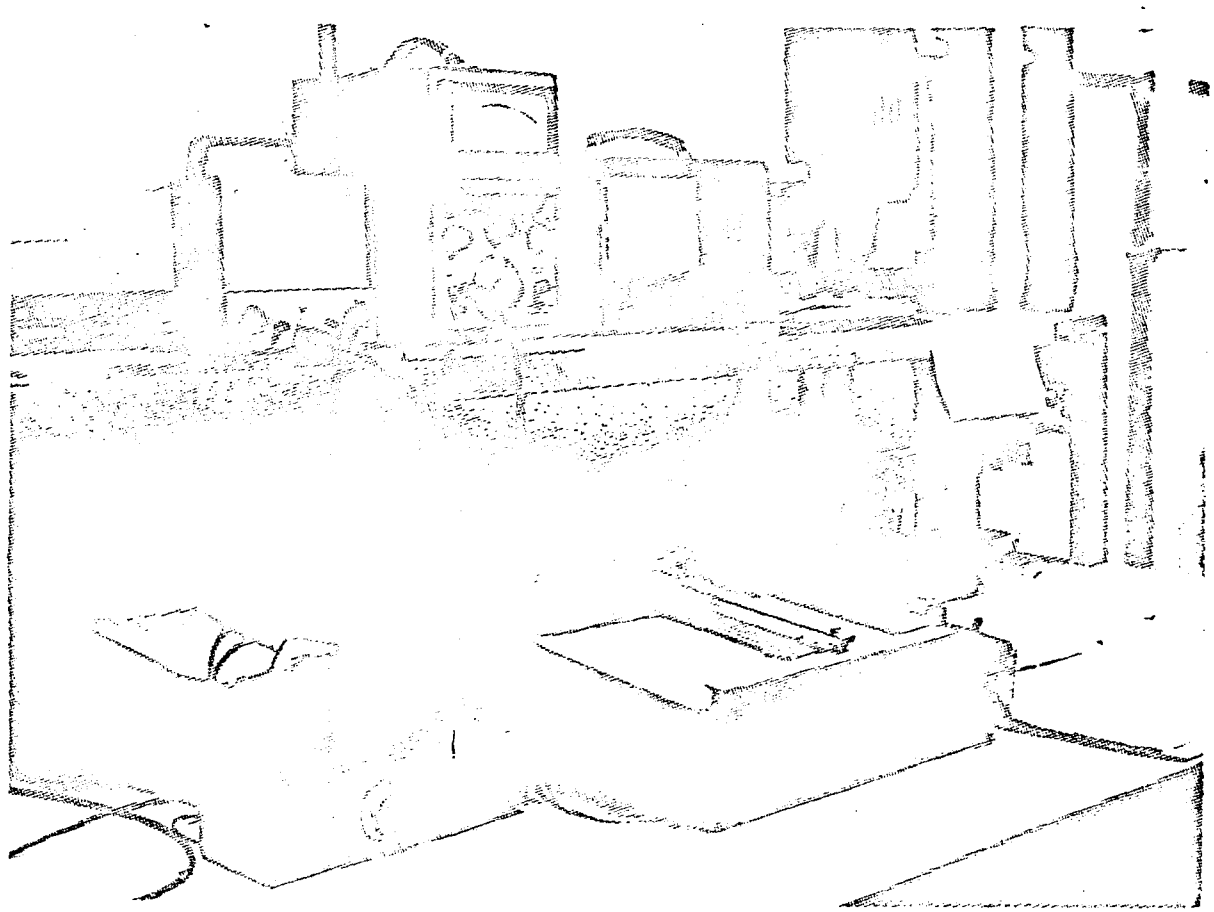

Fig. 2-16. Instrumentation.

analyzer which provides a continuous display in the frequency domain. The Langmuir probe provides the advantage of good spatial resolution at a given point and at a given instant of time. With the addition of the plasma camera technique, a better understanding of the plasma density distribution can be obtained.

2.4 Summary

In this chapter, the experimental apparatus and diagnostic techniques have been described. The plasma camera has the capability of measuring ion or electron spatial resolutions within an accuracy of one millimeter in length and within a time interval of less than one μ second. The Langmuir probe provides quantitative measurements of the physical properties of the plasma column.

The Q-machine generates a relatively quiescent streaming potassium plasma with low energy of 0.2 electron volts. The specially designed Q-machine also provides a unique feature of having a potential gradient along the radius of the plasma column. This potential gradient offers the possibility of the existence of the onset of an instability within the plasma column.

CHAPTER 3

EXPERIMENTS

Previous experimental studies, conducted at the Magneto-hydrodynamics Laboratory[33] at The City College of The City University of New York, have shown that a self-consistent electric field in the radial direction toward the center of the plasma column exists inside the Q-machine. The electric field is not uniform but varies along the radius of the plasma column as a function of the magnetic field. It is believed that the variation of the electric field could lead to the existence of an adverse angular momentum gradient about the axis of the plasma column by means of adjusting the magnetic field. If such a magnetic field exists, the plasma should exhibit a stationary convective instability and show a cellular pattern across the plasma column. It is possible to photograph this pattern by the newly developed plasma camera[25, 33].

The purpose of this experimental study is (1) to verify the existence of such an instability and its associated range of magnetic field; (2) to determine the unique characteristics of such an instability; (3) to establish sufficient data for carrying out a theoretical analysis.

3.1 The Structure of the Plasma Column

For magnetic fields, ranging from 5000 to 50 gauss, a preliminary observation of the structure of the plasma column has been made with the following experimental parameters:

Tungsten plate temperature: 2300 degrees kelvin

Chamber pressure: 2×10^{-6} mm of mercury

Plasma Camera: bias on the screen - 22 1/2 volts and a pulse of 7000 volts for 1 μ sec.

Plasma density: 1×10^{10} to 1.6×10^{11} particles per cu. cm.

(a) Plasma Camera Pictures: The plasma camera photographs show that the distribution of electrons within the plasma column cover a circular cross section of 0.75 inches in diameter for a magnetic field above 1000 gauss. The plasma increases into a larger circular region as the magnetic field decreases below 1000 gauss. The diameters of the plasma column for different magnetic fields are shown in Figure 3-1. At the same time, the plasma camera pictures show a wide range of distributions of the plasma blobs. The plasma blobs are irregular in shape as if they were thrown away from the main body of the rotating plasma column. For a magnetic field around 200 gauss, the formation of plasma blobs disappears

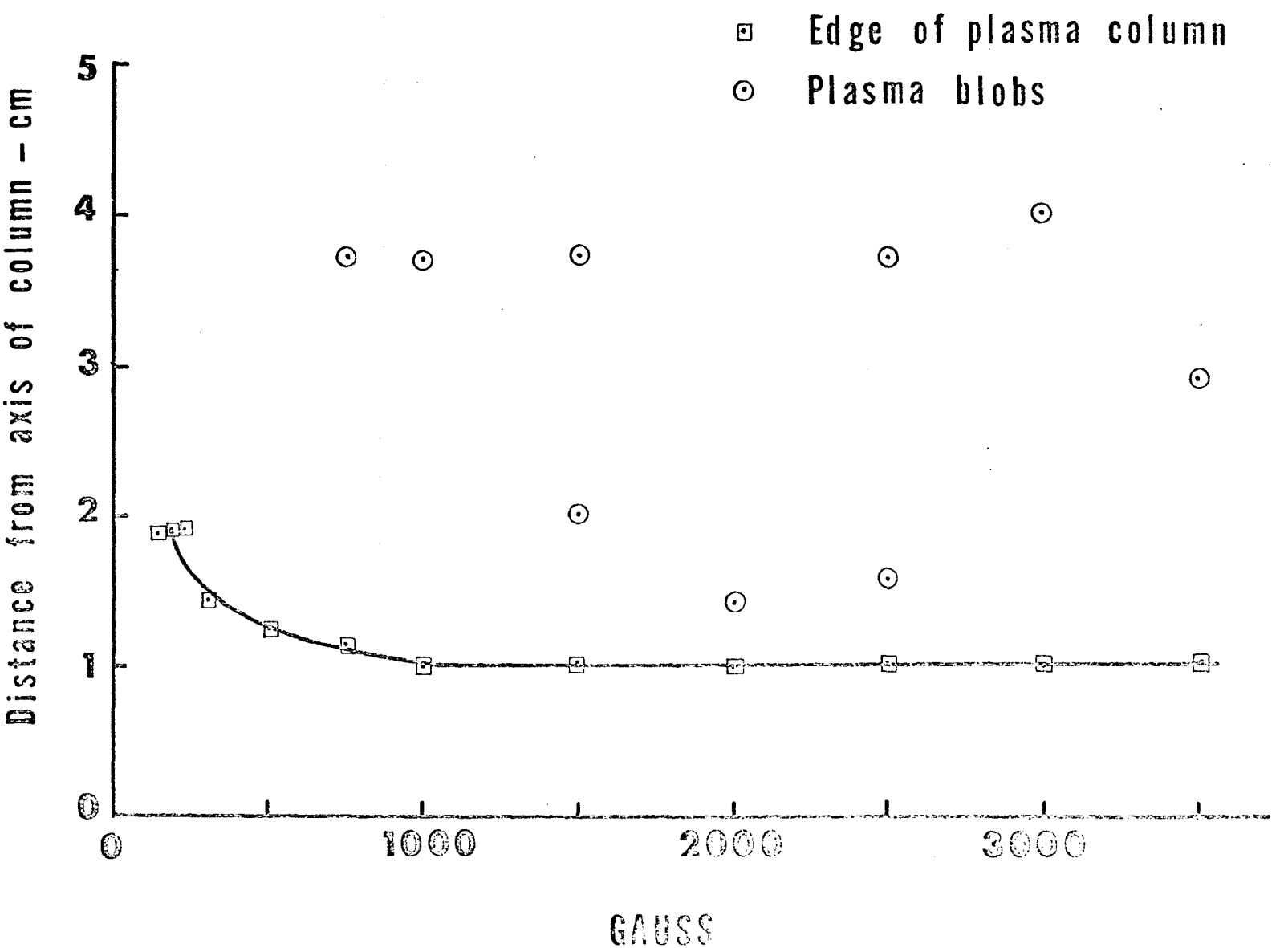

Fig. 3-1. Diameter of the plasma vs. the magnetic field.

and is replaced by a rather well organized cellular picture over the cross section of the plasma column. This cellular formation can be repeatedly photographed and recorded by the plasma camera.

(b) Stationary Characteristics: Above 500 gauss the frequency spectrum analyzer shows a clear sinusoidal frequency pattern. Around 200 gauss, the sinusoidal frequency pattern disappears and the spectrum analyzer shows the characteristics of a stationary or a non-oscillating plasma. These preliminary observations have stimulated the interest in the formation of a cellular plasma with stationary characteristics.

(c) Density and Potential Profiles:

Over the range of magnetic fields the structure of the plasma column varied from a solid core to a cellular shaped pattern as shown in Figure 3-2. From 700 to 5000 gauss, the basic shape of the column was unchanged, that is, a gaussian type density profile with a large electric potential gradient at the edge of the column, as shown in Figure 3-3. An accurate spatial distribution for this range of magnetic field is obtained by taking plasma camera photographs (Figure 3-4).

There appears to be no basic change in the profiles and plasma camera pictures above 700 gauss. But as we lower the magnetic field to 500 gauss, the plasma density profiles flattens out at the

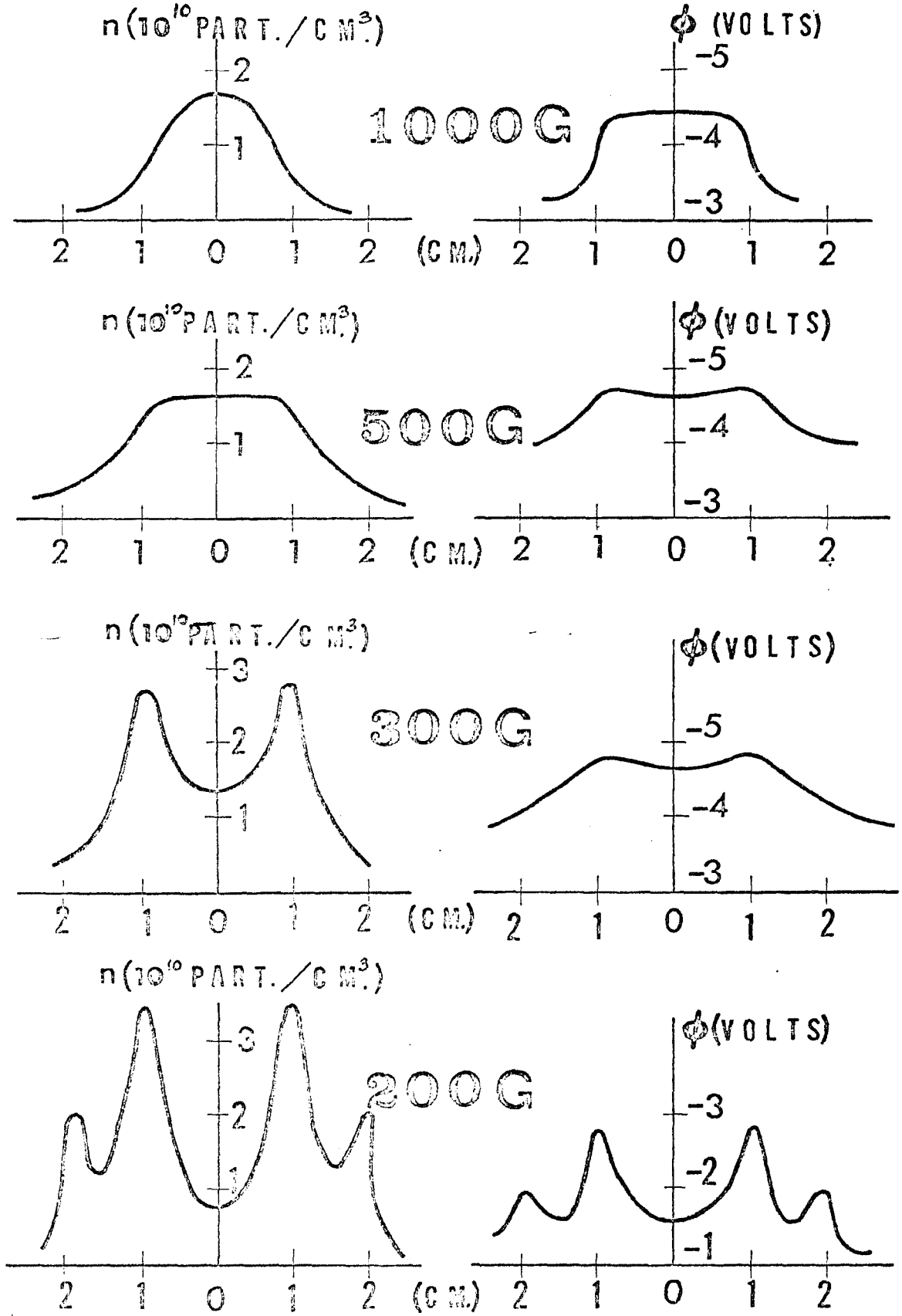

Fig. 3-2. Density and potential profiles for various magnetic fields.

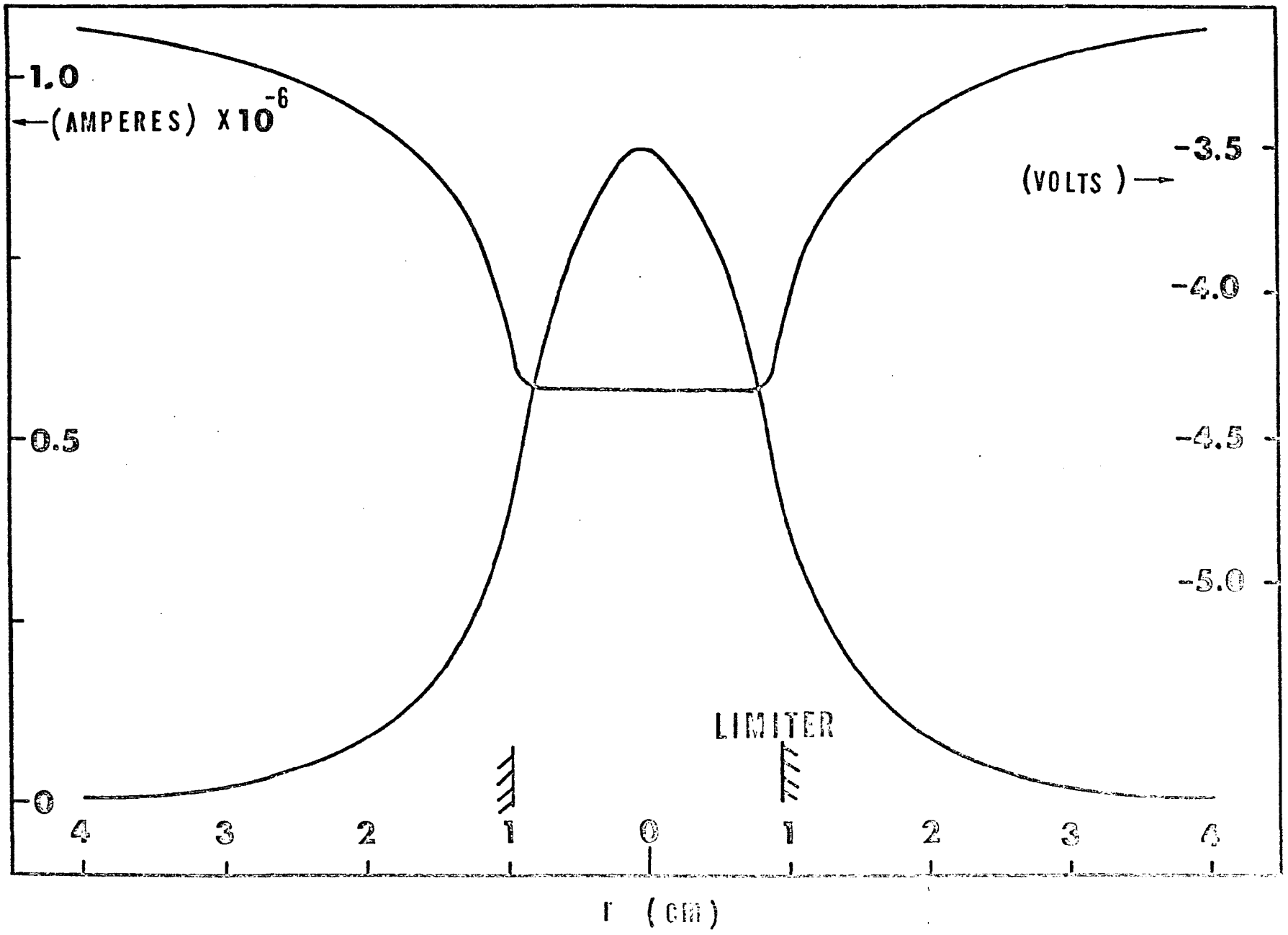

Fig. 3-3. Ion current and potential profiles at 1000 gauss.

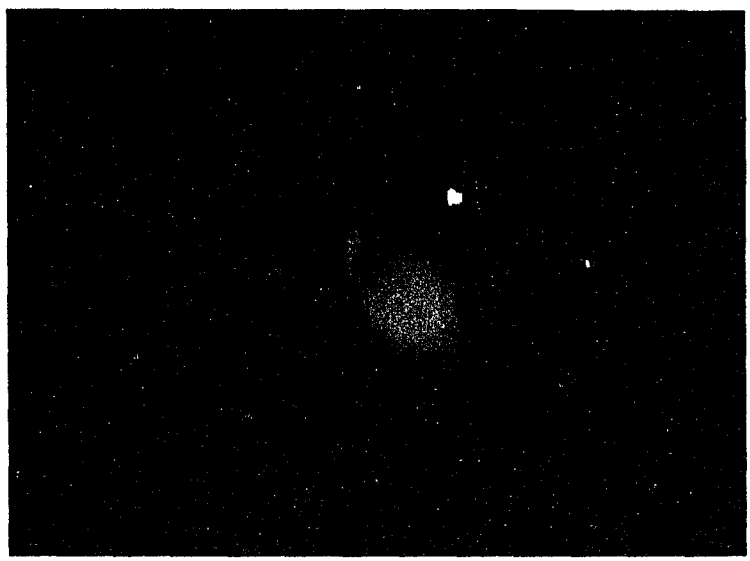

Fig. 3-4. Plasma camera photographs at 1000 gauss.

center of the column (Figure 3-5) and below 350 gauss, the density drops at the center of the plasma column (Figure 3-6). The accompanying plasma camera picture verifies the development of a hole along the axis of the column (Figure 3-7).

Below 300 gauss, the structure of the plasma column develops into a cellular pattern, as shown in the plasma camera photograph (Figure 3-8) and verified by the probe measurement of the ion current density and floating potential (Figure 3-9). This pattern has exactly the same structure and location for all of the experimental data observed. The pattern is eight small stationary circles arranged around a larger central circle. This particular configuration gradually deforms into a gaussian distribution if the magnetic field is further reduced to a range of 50 to 100 gauss.

The electrical potential across the plasma column also has been correspondingly recorded with the Langmuir probe and the x-y recorder. In general, the potential profile follows the change in the density profile. The plasma density potential relation has been experimentally determined in section 3.4.

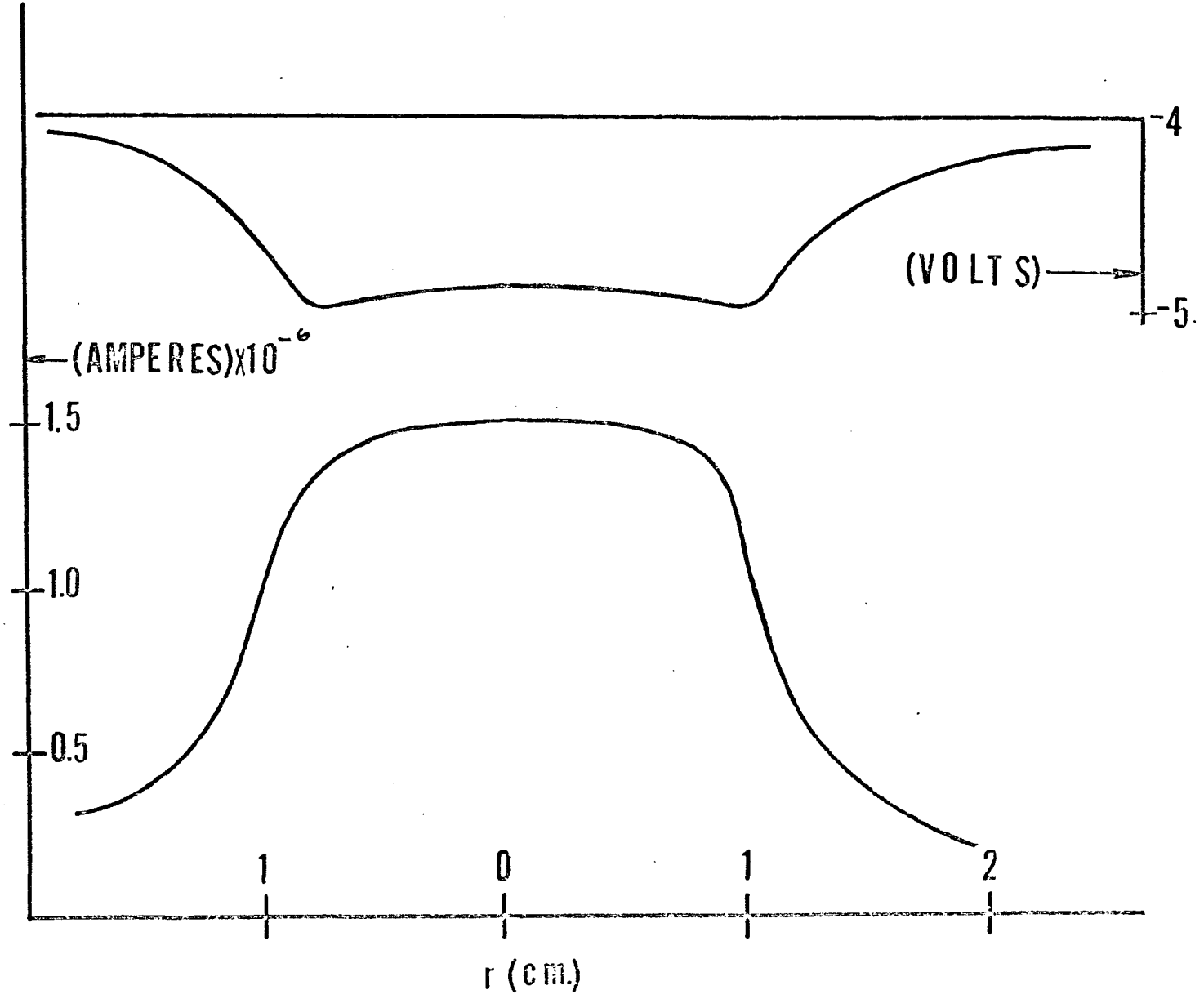

Fig. 3-5. Ion current and potential profiles at 500 gauss.

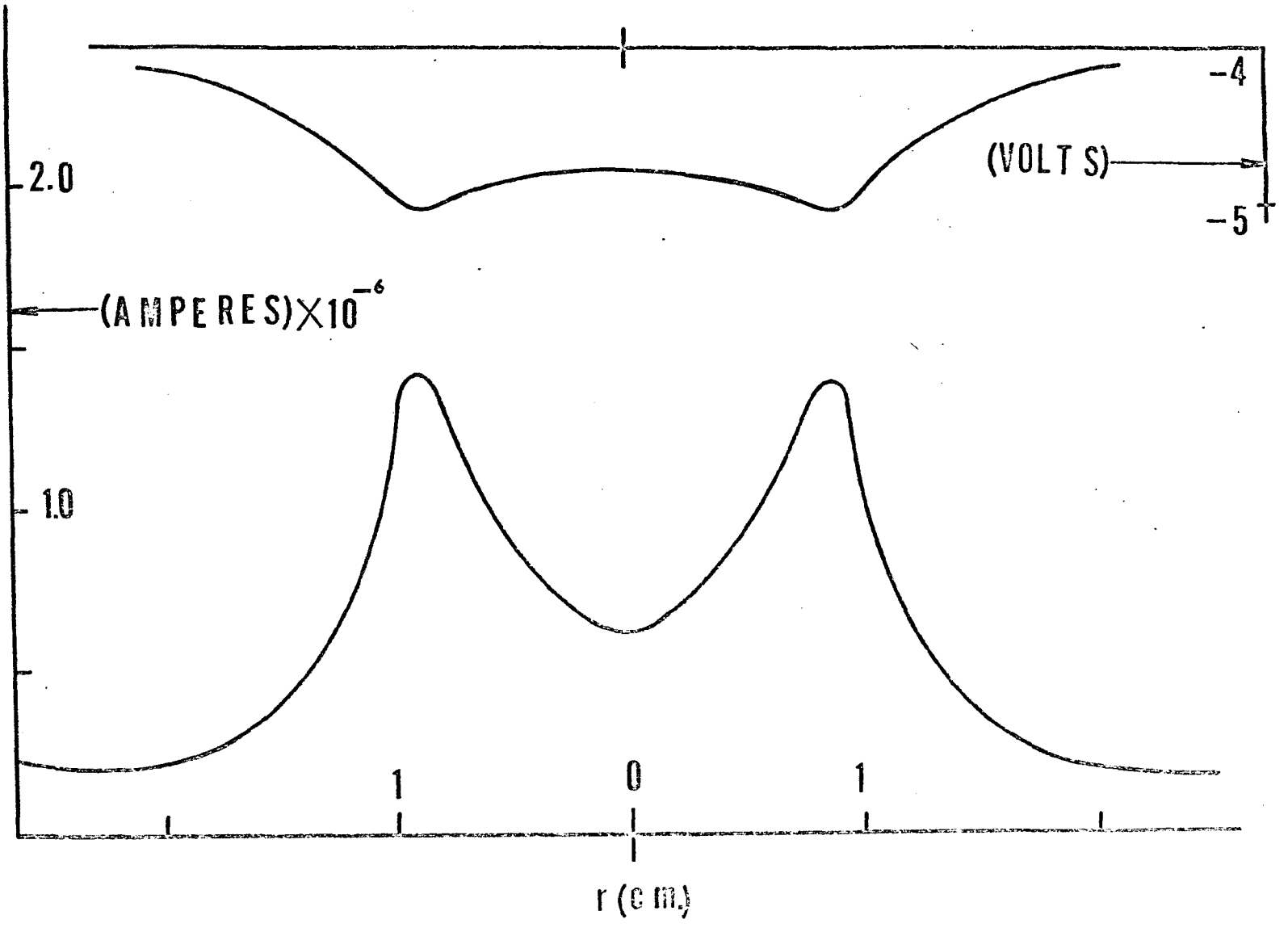

Fig. 3-6. Ion current and potential profiles at 300 gauss.

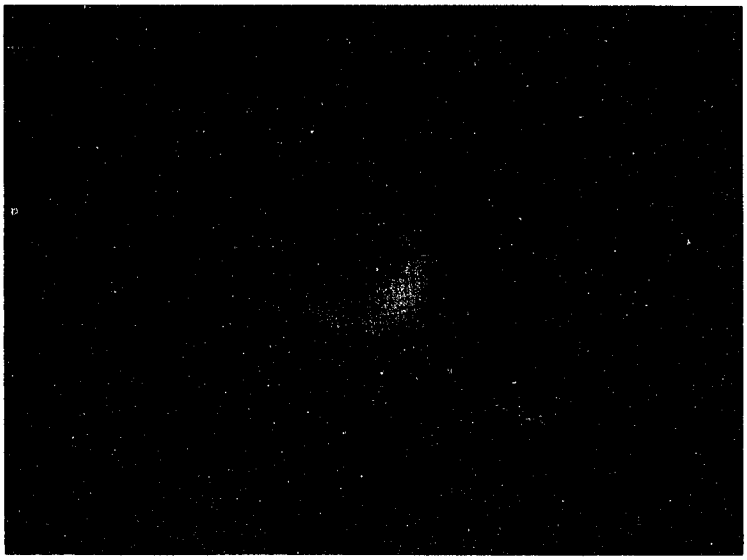

Fig. 3-7. Plasma camera photograph at 300 gauss.

Fig. 3-8. Plasma camera photograph at 200 gauss showing the plasma cells.

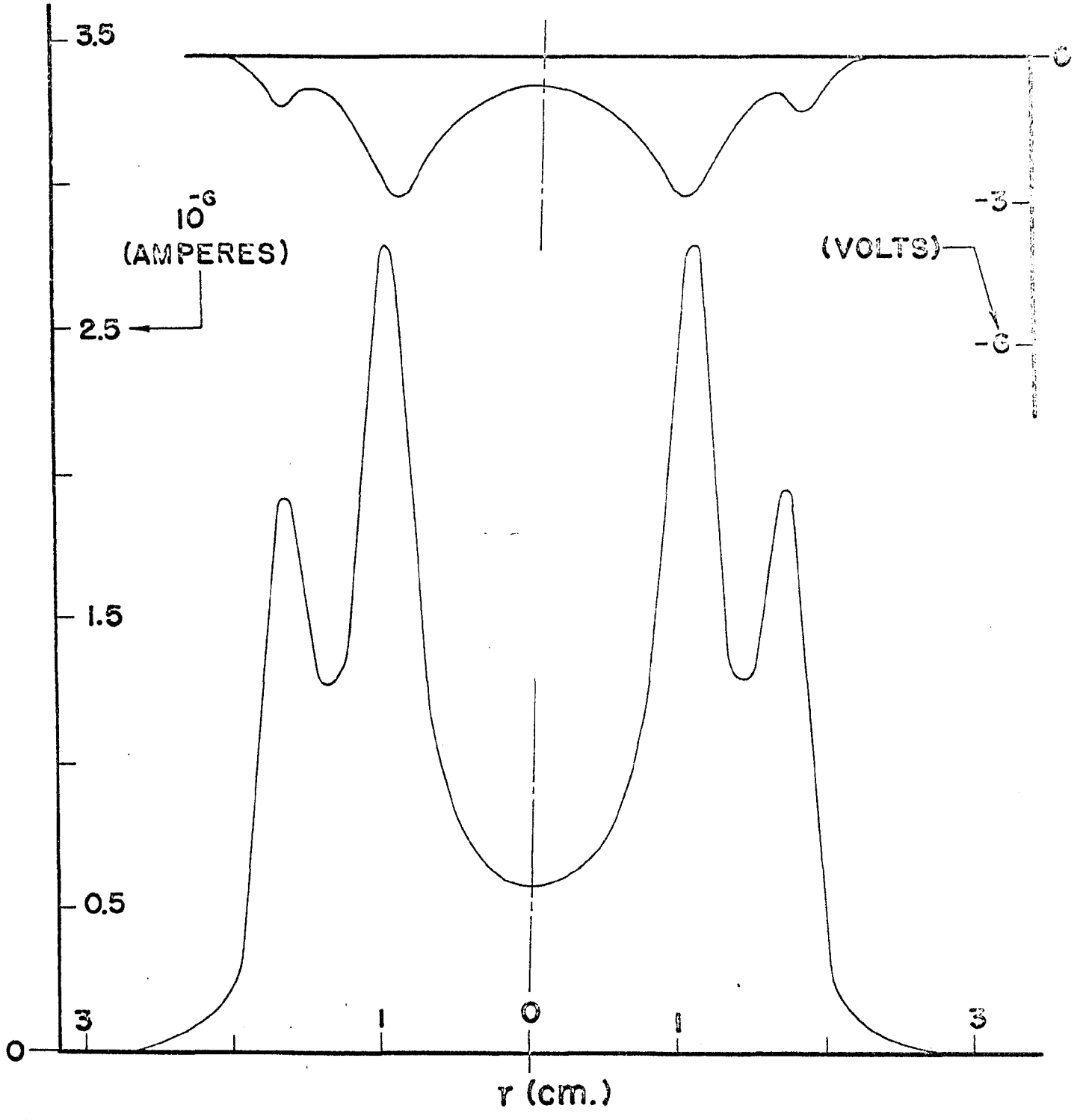

Fig. 3-9. Ion current and potential profiles at 200 gauss.

(d) Plasma Rotation:

Figure 3-4 shows a plasma camera photograph of an electron distribution taken at a magnetic field of 1000 gauss. It is seen that the plasma column cross-section is circular, 1.9 cm. in diameter, with one irregularity extending from the periphery of the column.

Langmuir probe measurements indicate an electric field at the periphery of the plasma column but no electric field in the central core of the plasma column. The irregularity is rotating in the $E_r \times B$ direction, which is rotating clockwise in Figure 3-4.

The plasma camera photograph shown in Figure 3-10b was taken by applying the high voltage pulse twice and leaving the film plane exposed to the light produced by the scintillations. This figure shows two irregularities which were photographed one second apart. The column is still circular in shape and the irregularity has rotated around the column. This is basically the same irregularity as shown in Figure 3-10a but taken at a different time in its development. From Figures 3-4, 3-10a and 3-10b and the probe measurements, the irregularity forms at the periphery of the plasma column in the region of maximum electric field. From one to three irregularities have been observed at the periphery of the column, rotating in the azimuthal direction. The irregularities have large variations in their

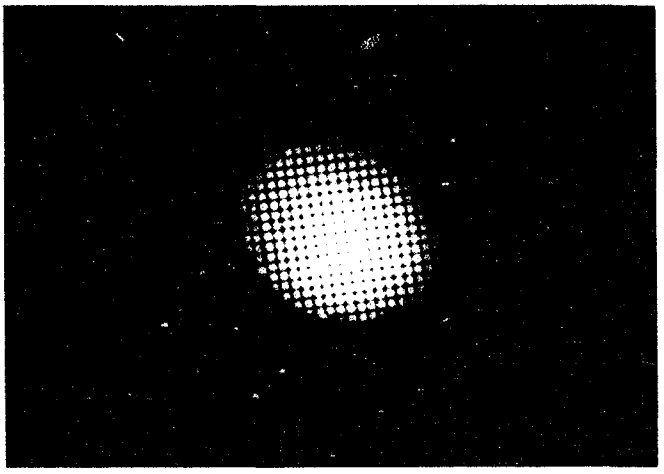

Fig. 3-10a. Plasma camera photograph (single exposure) showing one irregularity at 1000 gauss.

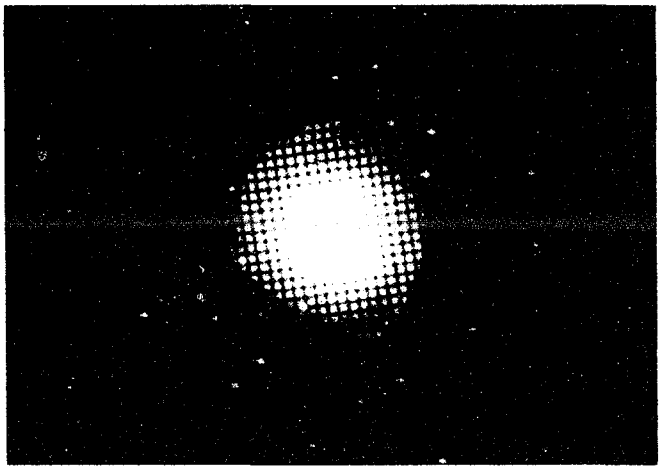

Fig. 3-10b. Plasma camera photograph (double exposure) showing rotation of the irregularity at 1000 gauss.

shapes with almost no change in the circular shape of the central core of the plasma.

(e) Explanations:

The mechanism that leads to the different forms of the density profiles is described in the following manner: At higher magnetic fields, above 500 gauss, the major portion of the plasma does not experience the electric field at the edge of the column because the ion larmor radius is much smaller than the radius of the column. As the magnetic field is lowered, there is an ever increasing number of ions experiencing the electric field at the periphery of the column. The electric field is pointing into the center of the column. Therefore, as the ions pass through the electric field they experience a resistive force which slows them down and turns them back into the column. Because of this motion the ions spend a longer time at the periphery of the column than at the central core, so that the density profiles appear to be peaked at the outer edges, as shown in the experimental data. The ions pull electrons out to the edge of the column due to ambipolar diffusion. The first indication that the plasma is moving out of the center of the column is observed around 375 gauss. The ion larmor radius is large enough so that the ions leaving the hot plate

will experience the electric field. At 300 gauss, the plasma density is 0.6×10^{11} particles per cu.cm. This corresponds to a means free path of 0.167 cm., and a larmor radius of 0.947 cm. Therefore, every ion will experience the electric field and make at least one collision while doing so, thereby losing kinetic energy and becoming effectively trapped in the electric field around the periphery of the plasma core. Because of the loss of kinetic energy due to collisions, the ions cannot attain enough energy to escape from the potential well.

3.2 New Concept of Transverse Diffusion

By measuring the longitudinal plasma current vs. the magnetic field it is seen that as the magnetic field is lowered from 1,000 to about 300 gauss, the plasma current increased at a somewhat faster rate than its increase from 1,000 to 5,000 gauss. At 300 gauss there is a very large increase in the plasma current that finally leveled off at 200 gauss, as shown in Figure 3-11. There is a decrease in the plasma current from 200 gauss to 125 gauss. Below 50 gauss the plasma density did not show a definite pattern and therefore is not shown in Figure 3-11. This increase in current at 200 gauss is 10 times greater than the plasma current measured at 1,000 gauss.

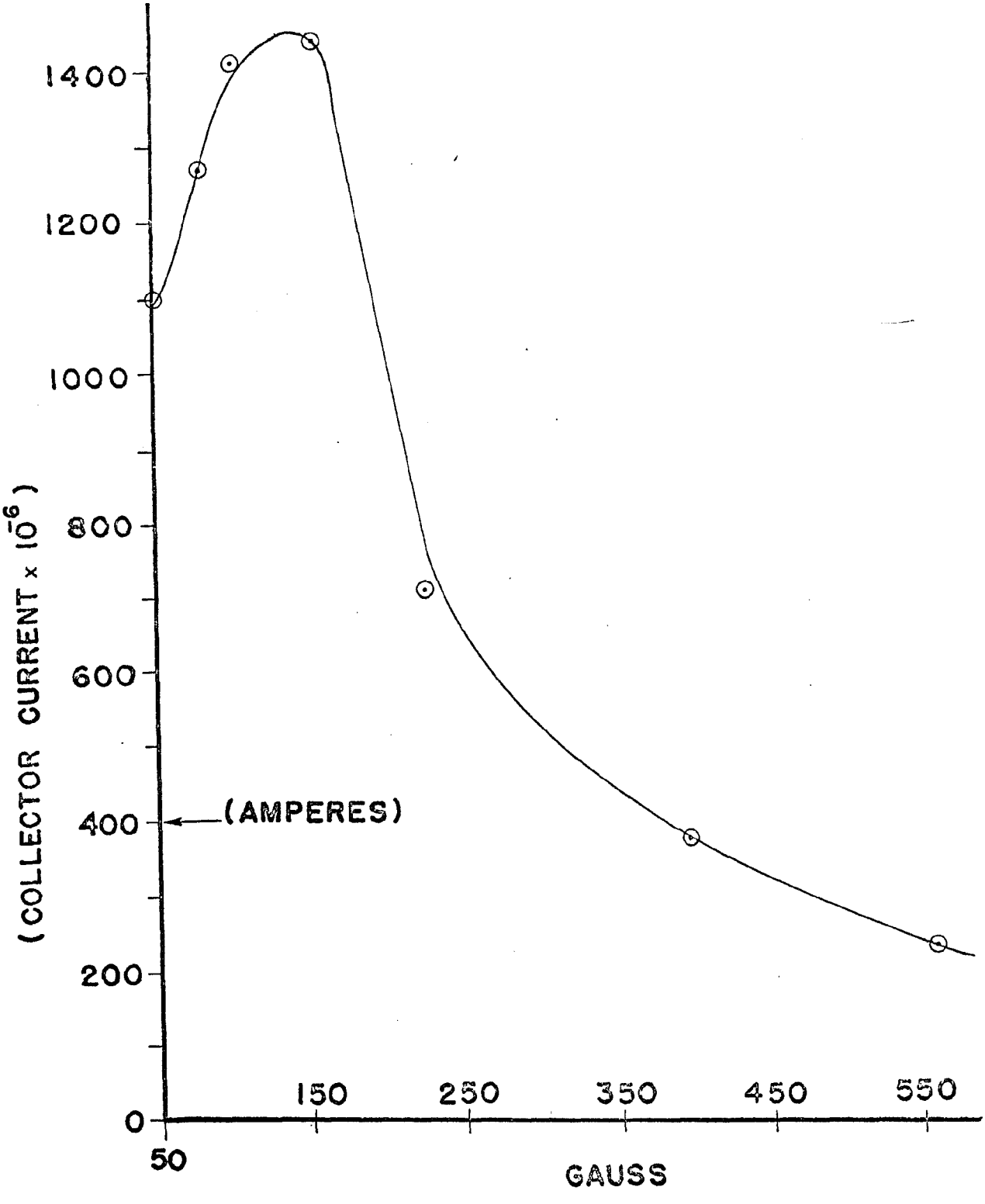

Fig. 3-11. Ion collector current vs. magnetic field.

One of the most interesting features concerning this increase in the plasma current is that when the plasma cells set in they are always accompanied by at least one order of magnitude increase in the plasma current.

With a bias of $\pm$22 1/2 volts, the screen of the plasma camera acts as a collector plate. The plasma current measured by the collector plate is in close agreement with the plasma current calculations obtained from the ion current measured by the Langmuir probe.

By means of plasma camera photographs, the explanation of longitudinal current-magnetic field relation becomes obvious. The flute-like irregularities or plasma blobs seem to grow in the radial direction, Figure 3-12, and finally break off from the central core of the plasma. At the same time the basic diameter of the plasma column remains circular. The plasma blobs appear to decrease as the magnetic field is lowered. From the previous experimental results, the transverse diffusion of the plasma across the magnetic field lines, known as anomalous diffusion, is due to collective mass transfer through the breaking off of the irregularities.

At higher magnetic fields, about 500 gauss, large portions of the plasma are carried across field lines as seen by the plasma

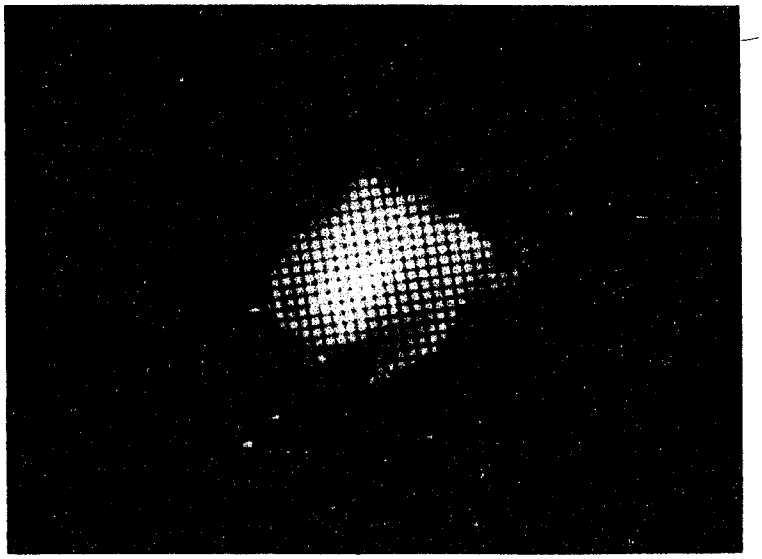

Fig. 3-12. Plasma camera photograph at 1000 gauss showing the diffusion of the plasma.

camera photographs in Figures 3-4, 3-10, and 3-12. These observations were verified by placing a circular ring, 6.5 cm. in diameter, 3.8 cm. long and 1.6 mm. thick, around the plasma column. The ring was biased negatively with nine volts. Plasma camera pictures and profiles were taken to verify that the plasma column was not disturbed by the presence of the ring.

The experimental results reveal that at 1,000 gauss, at the same location that the plasma camera pictures were taken, the ring collected, over a longitudinal distance of 3.8 cm., a transverse ion current of 24 microamperes. The current at the end collector plate, at 1,000 gauss, during this experiment measured 150 microamperes. At 200 gauss, with the ring in exactly the same location as it was for 1,000 gauss, the ring did not collect any transverse ion current. This was in complete agreement with the plasma camera pictures taken at 200 gauss, since there was no plasma observed outside of the plasma column.

Since the anomalous diffusion is one of the most important problems in the field of thermal nuclear fusion research[34-38], a number of investigations has been carried out in order to understand the fundamental mechanism of such a phenomenon. At present it is

believed that the mechanism causing this transversal diffusion is due to random oscillations as a result of an instability in the plasma. Experimental results indicated that the diffusion follows the classical theory if the magnetic field is weak and follows Bohm's theory[39] on anomalous diffusion if the magnetic field is strong. As the result of this research by means of plasma camera, a new concept of plasma blob formation and its breaking off from the central core of the rotating plasma column becomes clear.

3.3 Description of the Plasma Cells

As the magnetic field is lowered, the plasma cells first appear at a magnetic field just under 300 gauss, the clearest plasma camera pictures of the cells are taken at about 200 gauss, and the cells are no longer visible at and under 100 gauss. The cellular structure appeared to lock in at its onset and remain in a stationary position, as shown by a series of plasma camera photographs in Figure 3-13. The stationary structure of the cells may also be observed by the results of a series of probe measurements shown in Figure 3-14. The diameter of the smaller circles and the larger circles remained constant in the range of the magnetic fields where

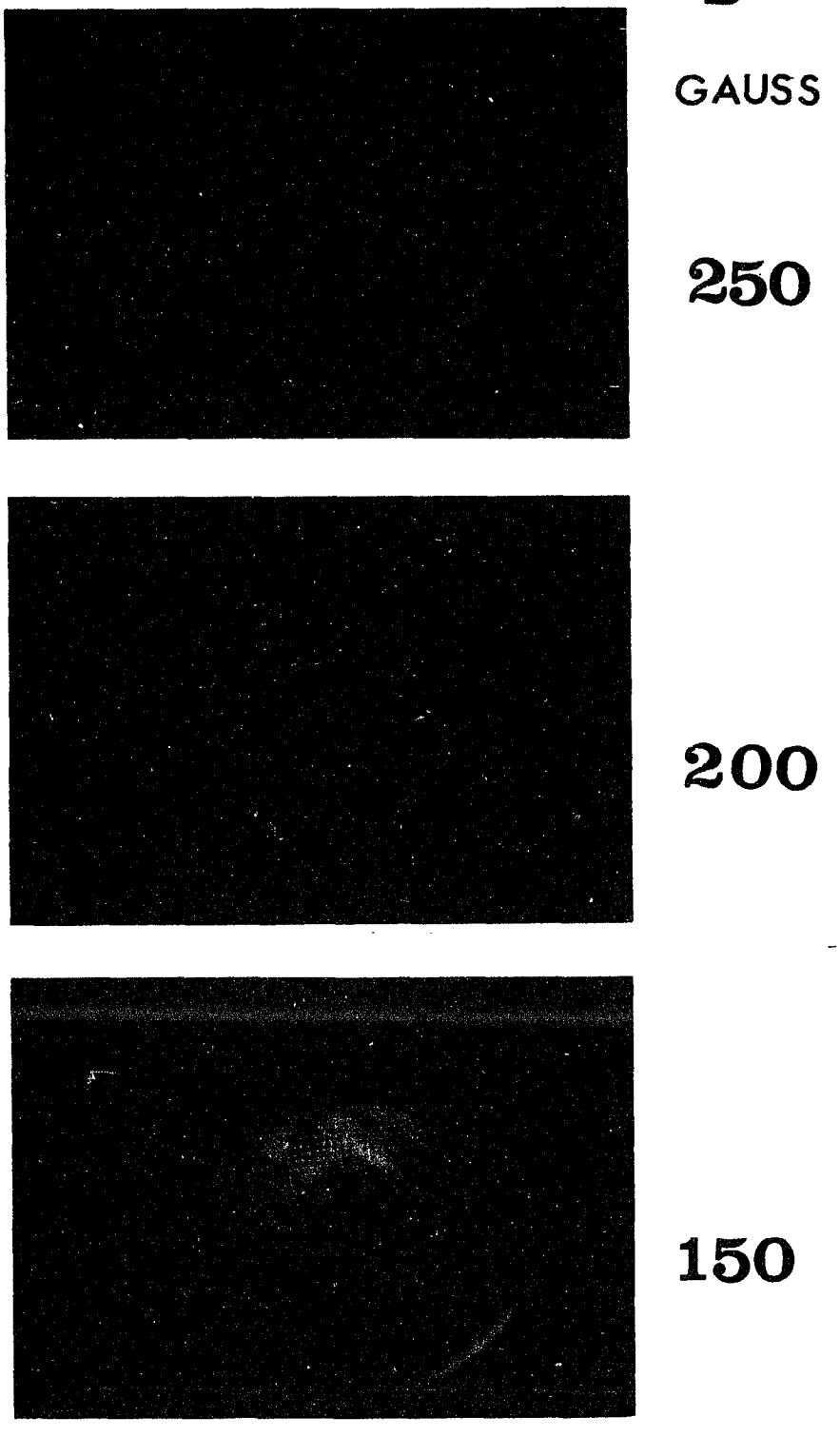

Fig. 3-13. Plasma camera photographs of the plasma cells.

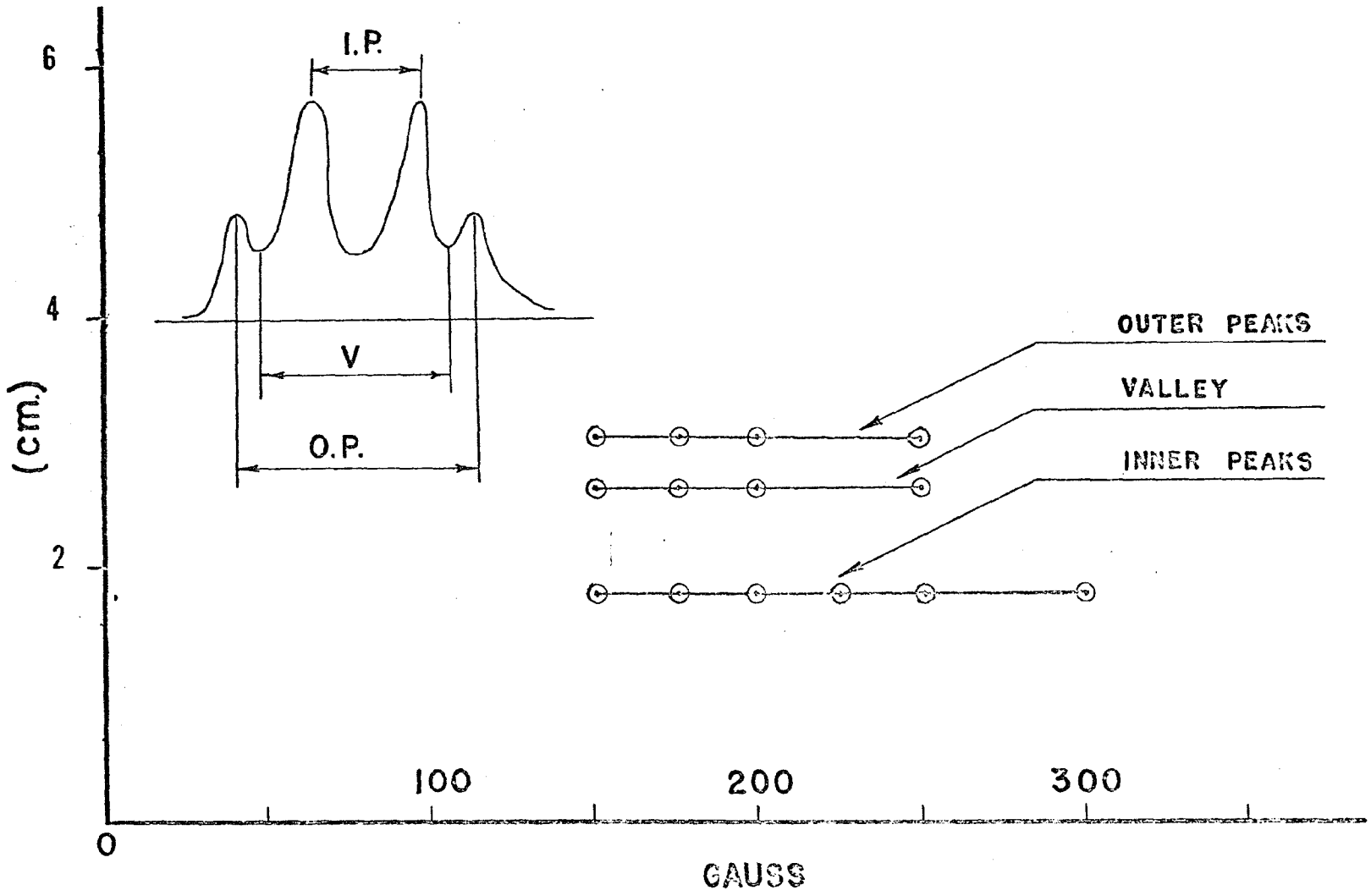

Fig. 3-14. Peak and Valley diameters vs. magnetic field.

the pattern exists. The diameter of the inner ring is 1.73 cm., the diameter of the outer ring is 2.93 cm. and the diameters of the smaller cells range from 0.466 cm. to 0.635 cm.

However, the peak and valley currents do vary between the values of the critical magnetic field, 100 to 300 gauss. The ion current at the center of the column remains approximately constant from 125 to 250 gauss, Figure 3-15. The ion current at the edge of the column increases by a factor of 2.5 from 250 to 200 gauss. The ratio of ion current at the edge of the column to the ion current at the center of the column is approximately 3.5 to one at 200 gauss.

The electric field, measured from the fall-off of the floating potential, increase sharply from 0.3 volts/cm at 500 gauss to 3.0 volts/cm at 200 gauss. The density gradient, measured from the fall-off of the ion current density also increases sharply from 3×10^{-6} amp/cm at 500 gauss to 14.0×10^{-6} amp/cm at 200 gauss.

At higher magnetic fields, above 500 gauss, there is a distinct frequency, 10 kc, at the edge of the plasma column. Under 350 gauss the frequency is very low and incoherent. A well defined frequency is not observed on the spectrum analyzer and it is impossible to detect a coherent wave form on the oscilloscope.

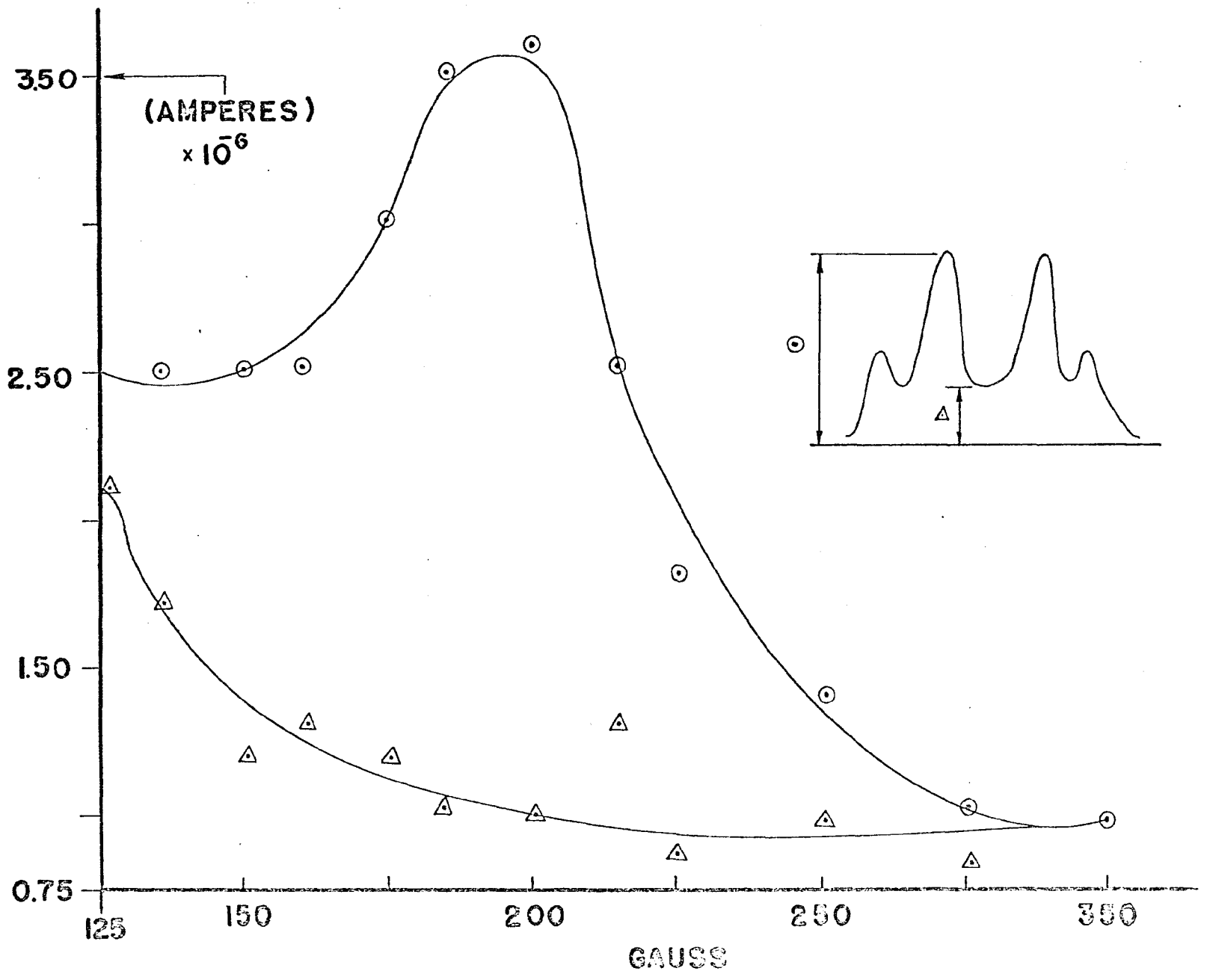

Fig. 3-15. Peak and axial ion current vs. magnetic field.

3.4 Parameters Controlling the Plasma Cells

From the previous experimental results, one of the controlling parameters for the onset and development of the plasma cells is the magnetic field. The other parameters varied are the length of the column, the temperature of the hot plate, the density and the end conditions. The effects on the cellular structure due to a change in these parameters are as follows:

(a) The Length of the Column:

The structure of the plasma cells are independent of the length of the plasma column. Figure 3-16 shows plasma camera pictures of the plasma cells taken at different magnetic fields, for a column length of 45 cm. The structure and the position of these cells, Figure 3-16, are the same as shown in Figure 3-8 for a column length of 50 cm. The cells appear to be smaller in Figure 3-16 because of the optics in photographing the cells.

(b) The Temperature:

The temperature of the hot plate was varied from 2350 degrees K to 2200 degrees K without a noticeable change in the cellular structure observed on the plasma camera pictures. Below 2200 degrees K the current density was too low to take plasma

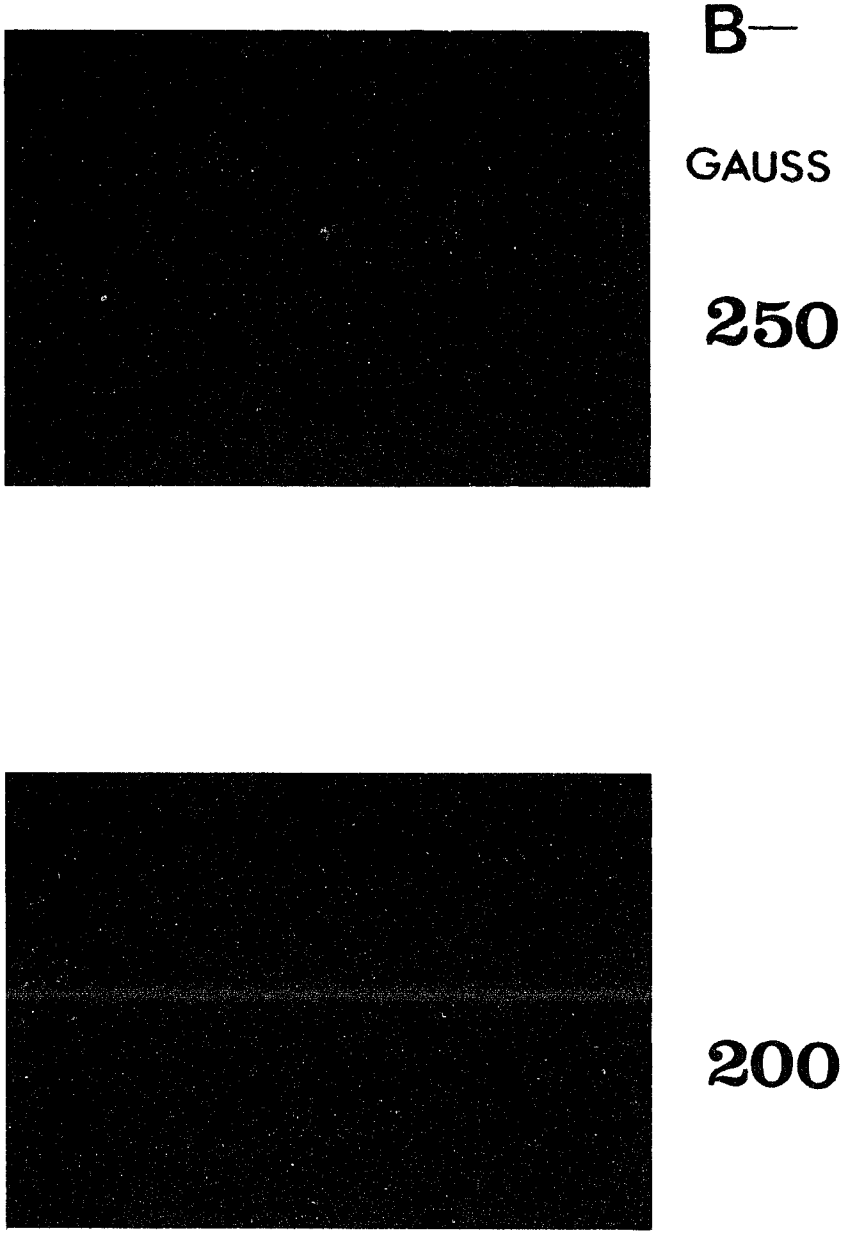

Fig. 3-16. Plasma camera photographs for a column length of 45 cm.

camera pictures but the shape of the ion current profile was unchanged down to a temperature of 2000 degrees K as shown in Figure 3-17.

By optical pyrometer measurements, the maximum variation of the temperature of the hot plate was $\pm$10 degrees K across a diameter. From these measurements it is believed that the plasma is in an isothermal state.

(c) Plasma Density:

The density was varied by controlling the spray of neutral potassium on the hot plate. Once the cellular pattern set in, the magnitude of the density did not affect the structure of the cells or shape of the profiles.

(d) The End Conditions:

The size of the apperture limiter was changed from 3/4 in. in diameter to 1/2 in. in diameter with no basic change in the cell pattern. The distance between the inner peaks was changed from 1.72 cm. to 1.14 cm. and the value of the current at the center of the column was increased. In all the experiments described, the neutral potassium was spread onto the hot plate through a nozzle 1.5 mm. in diameter. The edge of the nozzle was placed at the edge

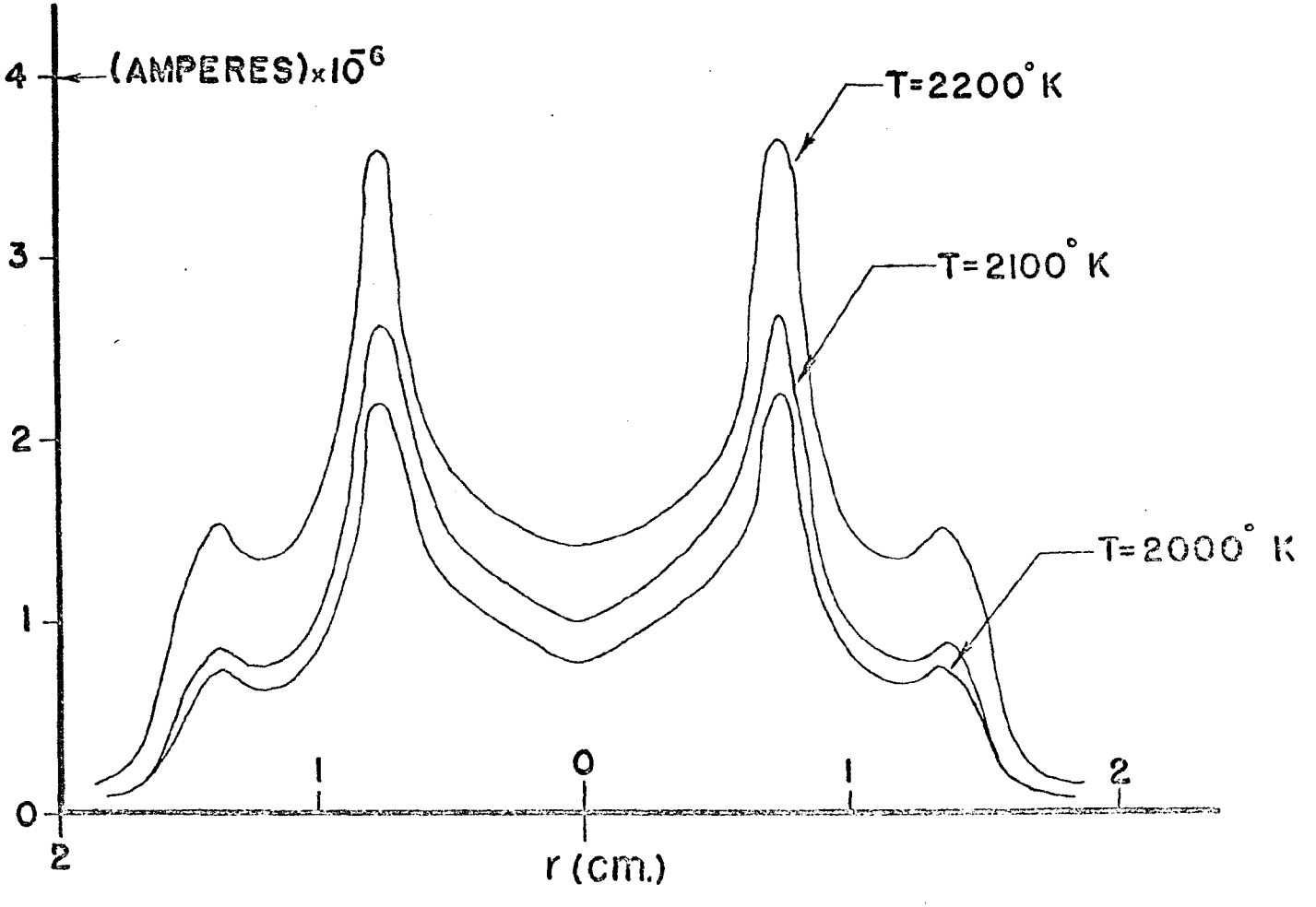

Fig. 3-17. Ion current profiles at 200 gauss.

of the apperture limiter and its position was varied by moving the edge of the nozzle 1/4 in. into the apperture limiter opening; the nozzle was also rotated up to 10 degrees over the course of the original experiments. There was no change in the structure, location, or the magnitude of the plasma cells due to these translations and rotations of the nozzle.

Therefore, the main parameter that controls the plasma cells is the magnetic field and the other parameters do not have a major effect on the structure or magnitude of the cells.

3.5 Plasma Density - Electrical Potential Relationship

Based on experimental data, a relation between the density and potential for a magnetic field of 300 gauss, that is, just before the onset of the plasma cells, can be mathematically expressed as

$$n_I \doteq \exp(A_{mI} r^2/2), \quad r \leq r_o \tag{3.1}$$

$$n_{II} \doteq \exp(A_{mII} r^2/2), \quad r \geq r_o \tag{3.2}$$

where n_I and n_{II} are the number densities in region I and II, respectively, r_o is the radius at which the regions meet and A_{mI} and A_{mII} are empirical constants, (Figure 3-18).

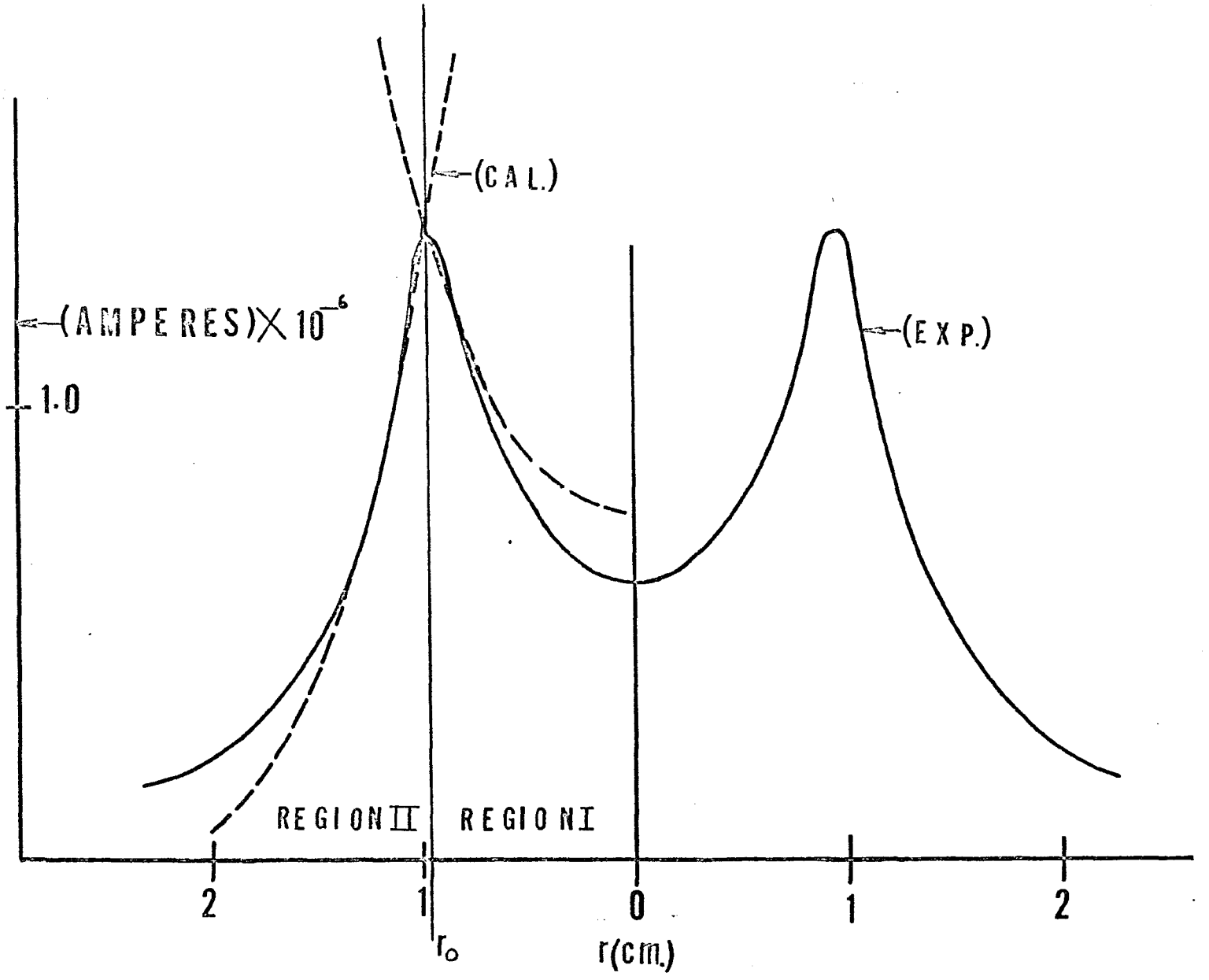

Fig. 3-18. Idealized ion current profiles at 300 gauss.

In a similar manner, the electric potential profile can be expressed as, Figure 3-19,

$$\phi_I = C_I A m_I r^2/2 - \Phi_I \quad , \quad r \leq r_o \tag{3.3}$$

$$\phi_{II} = C_{II} A m_{II} r^2/2 - \Phi_{II} \quad , \quad r \geq r_o \tag{3.4}$$

where ϕ_I and ϕ_{II} are the electric potentials in region I and II, respectively, C_I and C_{II} are constants and Φ_I and Φ_{II} are constant potentials. The sign of Am_I is positive and Am_{II} is negative, therefore the sign of C_I and C_{II} must be negative to obtain an equilibrium potential that corresponds to the experimental potential (Figure 3-19).

By combining eqs. (3.1) and (3.3) or eqs. (3.2) and (3.4) a general relationship between the potential and density can be written as

$$\phi = C \ln n - \Phi \tag{3.5}$$

By differentiating eq. (3.5) we will obtain a general expression between the potential gradient and the density gradient as follows

$$\frac{d\phi}{dr} = \frac{C}{n} \frac{dn}{dr} \tag{3.6}$$

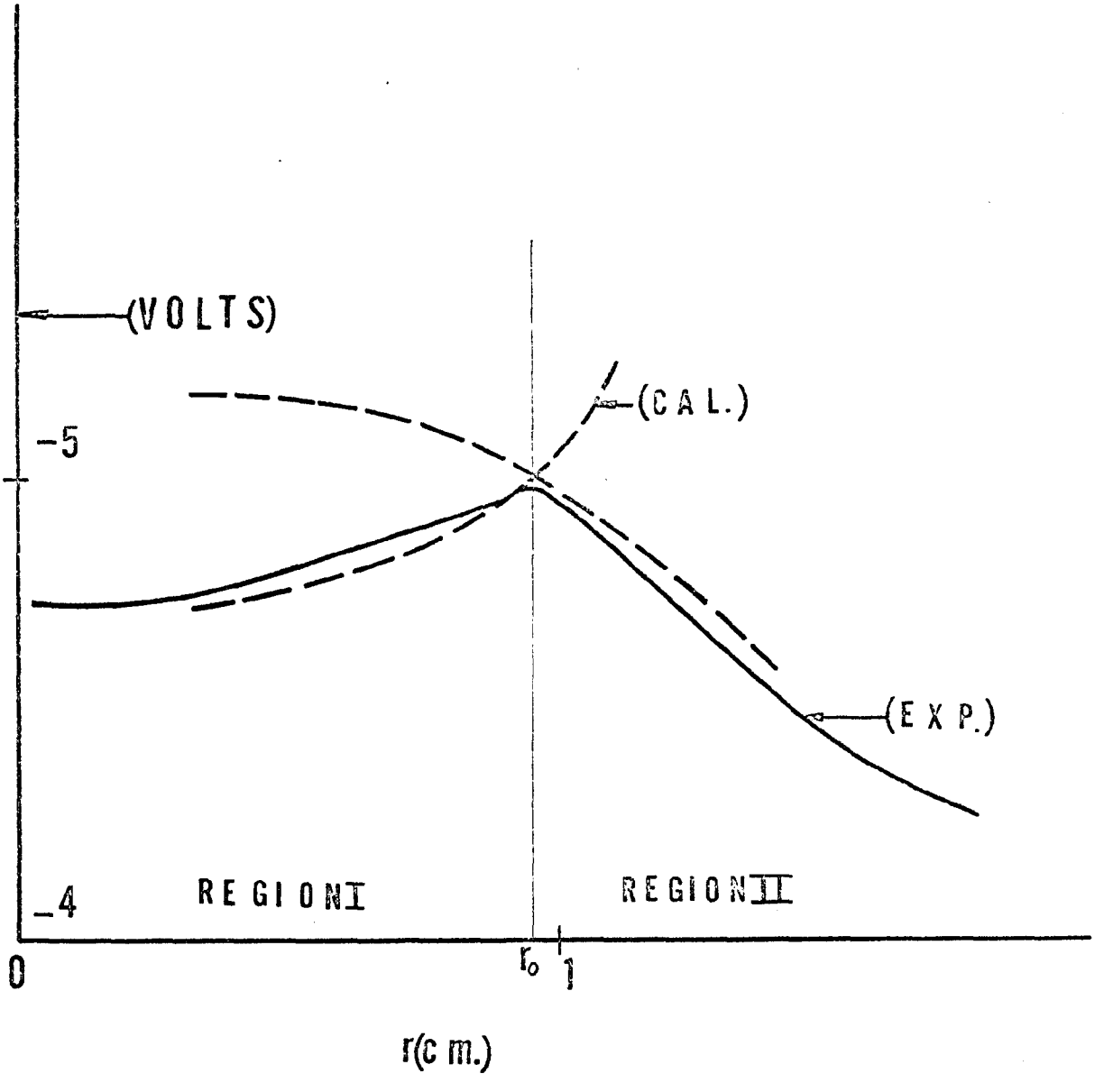

Fig. 3-19. Idealized potential profiles at 300 gauss.

3.6 Summary

In this chapter the characteristics of the plasma cells have been successfully found by means of the plasma camera technique, for a range of magnetic field of 100 to 300 gauss.

This set of experiments leads to the following important results:

(1) The photographs of the plasma camera have shown the formation of plasma blobs, its breaking-off mechanism from the central core of the rotating plasma column and offers a new concept of anomalous diffusion across the magnetic field. The problem of anomalous diffusion is considered as one of the most important problems in the field of plasma research today.

(2) For a range of magnetic fields from 100 to 300 gauss, the cross section of the plasma column shows a clear and well patterned formation of eight convection cells. At the same time the plasma column changes its oscillating nature into a stationary convection.

(3) Detailed studies for different parameters, such as plasma column length, plasma temperature, plasma density and

the end conditions, have been performed. It has been concluded that the magnetic field is the most influential factor in order to achieve the formation of convection cells and minimum diffusion across the magnetic field.

(4) At a magnetic field of 300 gauss, just before the onset of the plasma convection cells, a logarithmatic relationship between plasma density and plasma potential has been obtained as in equation (3.5) for use in the theoretical analysis.

CHAPTER 4

THEORETICAL ANALYSIS

In this chapter, a theoretical analysis of the mechanics of the cell formation obtained by plasma camera observations is attempted, a stability criterion is established, and the concept of angular momentum interchange as the criterion for the instability is confirmed. The plasma is considered as a mixture of equal number of ions and electrons with a small mean free path in comparison with the characteristic length of the plasma column. The plasma is classified as low beta plasma for the low range of magnetic field around 200 gauss, since the dynamic pressure of the plasma is much smaller than the pressure of the magnetic field.

4.1 Fundamental Equations

The second moment of the Boltzmann equation gives the equation of motion for a fully-ionized plasma[40, 41]. In e.m.u. system the equation for ions is

$$n_i m_i\left(\frac{\partial \vec{v}_i}{\partial t} + \vec{v}_i \cdot \vec{\nabla} \vec{v}_i\right) = n_i z e\left(\vec{E} + \vec{v}_i \times \vec{B}\right) - \nabla p_i + \vec{\nabla} \cdot \vec{\vec{\Pi}} - n_i m_i \vec{\nabla} \phi + \vec{P}_{ie} \tag{4.1}$$

where the subscript i stands for ions and e for electrons:

m_i the ion mass, $\vec{v}_i$ the ion velocity, Z the charge units on each ion, e the value of the electric charge which equals 1.6×10^{-20} abcoulombs, $\vec{E}$ the self-consistent electric field, $\vec{B}$ the magnetic field, p_i the ion scalar pressure, $\vec{\vec{\pi}}$ the viscous stress tensor[41]

$$\vec{\nabla}\cdot\vec{\vec{\pi}} = \mu\left(\nabla^2\vec{v}_i + 1/3\,\vec{\nabla}[\vec{\nabla}\cdot\vec{v}_i]\right) \tag{4.2}$$

which is defined in terms of the coefficient of viscosity μ, $\mathcal{J}$ the gravitational potential, and $\vec{P}_{ie}$ the total momentum transferred to the ions per unit volume per unit time by collisions with electrons[40] as defined by

$$\vec{P}_{ie} = n^2 e^2 \eta (\vec{v}_e - \vec{v}_i) \tag{4.3}$$

where η is the electrical resistivity.

In this study, the ions are singly charged particles, that is Z = 1. Both gravitational and momentum transfer to ions are neglected.

For an isothermal plasma[42] the equation of state becomes

$$\vec{\nabla} p_i = K T \vec{\nabla} n_i \tag{4.4}$$

where K is the Boltzmann's constant which equals 1.38×10^{-16} erg. per degrees kelvin, and T is the temperature in degrees kelvin. The first moment of the Boltzmann equation gives the equation of continuity

$$\frac{\partial n_i}{\partial t} + \vec{\nabla} \cdot (n_i \vec{v}_i) = 0 \tag{4.5}$$

A similar set of equations for electrons can be established by replacing the subscript i by e, e by -e and dropping the viscous stress tensor since the ions are the mass carrying species.

The Maxwell's equations and Ohm's law are

$$\frac{\partial \vec{B}}{\partial t} = - \vec{\nabla} \times \vec{E} \tag{4.6}$$

$$\vec{\nabla} \times \vec{B} = 4\pi \vec{J} + \frac{1}{c^2} \frac{\partial \vec{E}}{\partial t} \tag{4.7}$$

$$\vec{J} = \frac{1}{\eta} \left(\vec{E} + \vec{v} \times \vec{B} - \frac{1}{e n_i} \vec{\nabla} p_i \right) \tag{4.8}$$

where $\vec{J}$ is the current density and C the speed of light. It is noted that the Ohm's law couples the fluid dynamics equations together with the electromagnetic equations.

Experimental results suggest the problem under investigation meets the conditions for magnetohydrodynamic approximations[20] rather well and the displacement current term in the Maxwell's equation may be neglected. The approximations for the streaming plasma column are (1) the speed of velocity of the plasma is much smaller than the speed of light; (2) the self-consistent electric field is in the same order of $v \times B$; (3) the oscillating frequency for a magnetic field of 300 gauss is small.

The fact that the magnetic field pressure for this problem is much larger than the dynamic pressure of the plasma implies the motion of plasma particles cannot disturb the intensity of the magnetic field, that is, the magnetic field remains constant. The experimental data has also shown that the magnetic field is rather uniform within the test section. From these considerations, the Maxwell's equations for the streaming plasma column can be satisfied if

$$\vec{\nabla} \times \vec{E} = 0 \tag{4.9}$$

and

$$\vec{J} \doteq 0 \tag{4.10}$$

By introducing an electric potential Φ , the equation of motion for ions becomes

$$n_i m_i\left(\frac{\partial \vec{v}_i}{\partial t} + \vec{v}_i \cdot \vec{\nabla} \vec{v}_i\right) = n_i e\left(-\vec{\nabla}\phi + \vec{v}_i \times \vec{B}\right) - K T_i \vec{\nabla} n_i + \mu\left(\nabla^2 \vec{v}_i + 1/3\, \vec{\nabla}\left[\vec{\nabla} \cdot \vec{v}_i\right]\right) \tag{4.11}$$

Now the equations (3.5), (4.5) and (4.11) completely describe the motion of the ions for a fully ionized plasma. Similar equations for electrons can also be developed.

From the experimental data for a magnetic field of 300 gauss, the calculated mean free path for ions is 0.167 cm. The characteristic length which is the diameter of the plasma column is 2 cm. It is obvious that the mean free path is at least one order smaller than the characteristic length. Therefore the use of the continuum equations[43] is justified here.

4.2 Equilibrium

For the equilibrium conditions, the equation of motion for ions can be written as

$$m_i n_0 \vec{V}_0 \cdot \vec{\nabla} \vec{V}_0 = n_0 e\left(-\vec{\nabla}\phi_0 + \vec{V}_0 \times \vec{B}\right) - K T_i \vec{\nabla} n_0 + \vec{\nabla} \cdot \vec{\vec{\pi}} \tag{4.12}$$

where the subscript "o" indicates equilibrium.

For the streaming plasma column geometry, it is natural and convenient to use polar coordinates to describe the motion. The Z-axis is chosen parallel to the magnetic field lines.

The motion of the plasma column is assumed to be rotating about the axis of the column and moving with a constant velocity along the Z-axis. Therefore, the velocity components are expressed as

$$\begin{aligned} V_{r0} &= 0 \\ V_{\theta 0} &= \lambda r \\ V_{z0} &= \text{CONSTANT} \end{aligned} \tag{4.13}$$

where λ is a constant in any one region.

Under these conditions the equations of motion in the θ and Z direction are identically satisfied. The equation of motion in the r direction becomes

$$-\frac{V_0^2}{r} = -\frac{e}{m_i}\phi' + \frac{e}{m_i} V_0 B - \frac{K T_i}{m_i}\frac{n_0'}{n_0} \tag{4.14}$$

where V_o is the ion velocity in the θ direction and the prime denotes $\frac{d}{dr}$. The relationship between the electric potential and the plasma density has been determined experimentally as

$$\phi_o = C \ln n_o - \Phi \tag{4.15}$$

In order to obtain a common factor in eq. (4.20) set

$$C = \alpha \frac{K T_i}{e} \tag{4.16}$$

where α is a constant scale factor for any one region representing the ratio of the electric force to the force due to the pressure gradient. The experimental value of α range from 1.0 to 2.0 for a magnetic field of 300 gauss. Therefore eq. (4.14) becomes

$$\frac{V_o^2}{\omega_c r V_{th}} + \frac{V_o}{V_{th}} - (\alpha+1) \frac{V_{th}}{\omega_c} \frac{n_o'}{n_o} = 0 \tag{4.17}$$

where

$$\omega_c = \frac{eB}{m_i}$$
$$V_{th} = \left(\frac{K T_i}{m_i}\right)^{1/2} \tag{4.18}$$

a similar treatment for electrons gives

$$-\frac{V_{oe}^2}{r} = \frac{e}{m_e} \phi' - \frac{e}{m_e} V_{oe} B - \frac{K T_e}{m_e} \frac{n_o'}{n_o} \tag{4.19}$$

substitute eqs. (4.15), (4.16) and (4.18) into eq. (4.19), we obtain

$$(4.20)\quad \frac{M V_{oe}^2}{\omega_c r V_{th}} - \frac{V_{oe}}{V_{th}} + \left(\frac{\alpha}{\beta} - 1\right)\beta \frac{V_{th}}{\omega_c} \frac{n_o'}{n_o} = 0$$

where

$$(4.21)\quad \beta = \frac{T_e}{T_i}$$

$$M = \frac{m_e}{m_i}$$

since $M << 1$ eq. (4.20) becomes

$$(4.22)\quad \frac{V_{oe}}{V_{th}} = \left(\frac{\alpha}{\beta} - 1\right)\beta \frac{V_{th}}{\omega_c} \frac{n_o'}{n_o}$$

It will be convenient to express eq. (4.17) into dimensionless form by introducing the following dimensionless parameters

$$\rho = \frac{r\omega_c}{V_{th}}$$

$$(4.23)\quad \upsilon_o = \frac{V_o}{V_{th}}$$

$$\Omega_o = \frac{\upsilon_o}{\rho}$$

The solution of eq. (4.17) in terms of these dimensionless parameters, represents the angular velocity of ions Ω_o and can be expressed as

$$\Omega_o = \frac{-1 \pm \left(1 + 4[\alpha + 1] \frac{1}{\rho n_o} \frac{dn_o}{d\rho}\right)^{1/2}}{2} \tag{4.24}$$

Since Ω_o is a constant the form of the density profile is

$$n_o \doteq \exp\left(\frac{a\rho^2}{2}\right) \tag{4.25}$$

where a is a dimensionless parameter defined by

$$a = Am\left(\frac{V_{eh}}{\omega_c}\right)^2 \tag{4.26}$$

Equation (4.25) is the dimensionless form of equations (3.1) and (3.2). Therefore the choice for $V_{\theta o} = \lambda r$, equation (4.19), satisfies the experimental equilibrium profile. By substituting equation (4.25) into equation (4.24), we will obtain the dimensionless angular velocity in terms of the dimensionless parameters α and a.

$$\Omega_o = \frac{-1 \pm (1 + 4[\alpha + 1]a)^{1/2}}{2} \tag{4.27}$$

The experimental values for the parameters a and α for region I and II have been determined at 300 gauss and are:

$$
\begin{aligned}
a_I &= +1.12 \\
a_{II} &= -1.80 \\
\alpha_I &= -1.150 \\
\alpha_{II} &= -1.653
\end{aligned}
\tag{4.28}
$$

Substituting these values into equation (4.27), we obtain

$$
\begin{aligned}
\Omega_{oI} &= -0.786,\ -0.214 \\
\Omega_{oII} &= +0.692,\ -1.692
\end{aligned}
\tag{4.29}
$$

These equilibrium conditions are as shown in Figure 4-1. The inner core of the cylindrical column rotates with a constant angular velocity Ω_{oI} and an outer cylinder rotates at a constant angular velocity Ω_{oII}. These equilibrium conditions, equation (4.29), may lead to a potentially unstable arrangement of flow resulting from a prevailing adverse gradient of angular momentum.

The mechanism of this instability may be looked at in the following way. Consider the angular momentum $(L = \rho^2 \Omega_o)$ of two rings of plasma, at $\rho = \rho_1$, and $\rho = \rho_2$ within region I and region II respectively, as shown in Figure 4-1. The plasma mass in ring I is chosen to be equal to the plasma mass in ring II. Under equilibrium conditions, the angular momentum of a plasma element remains

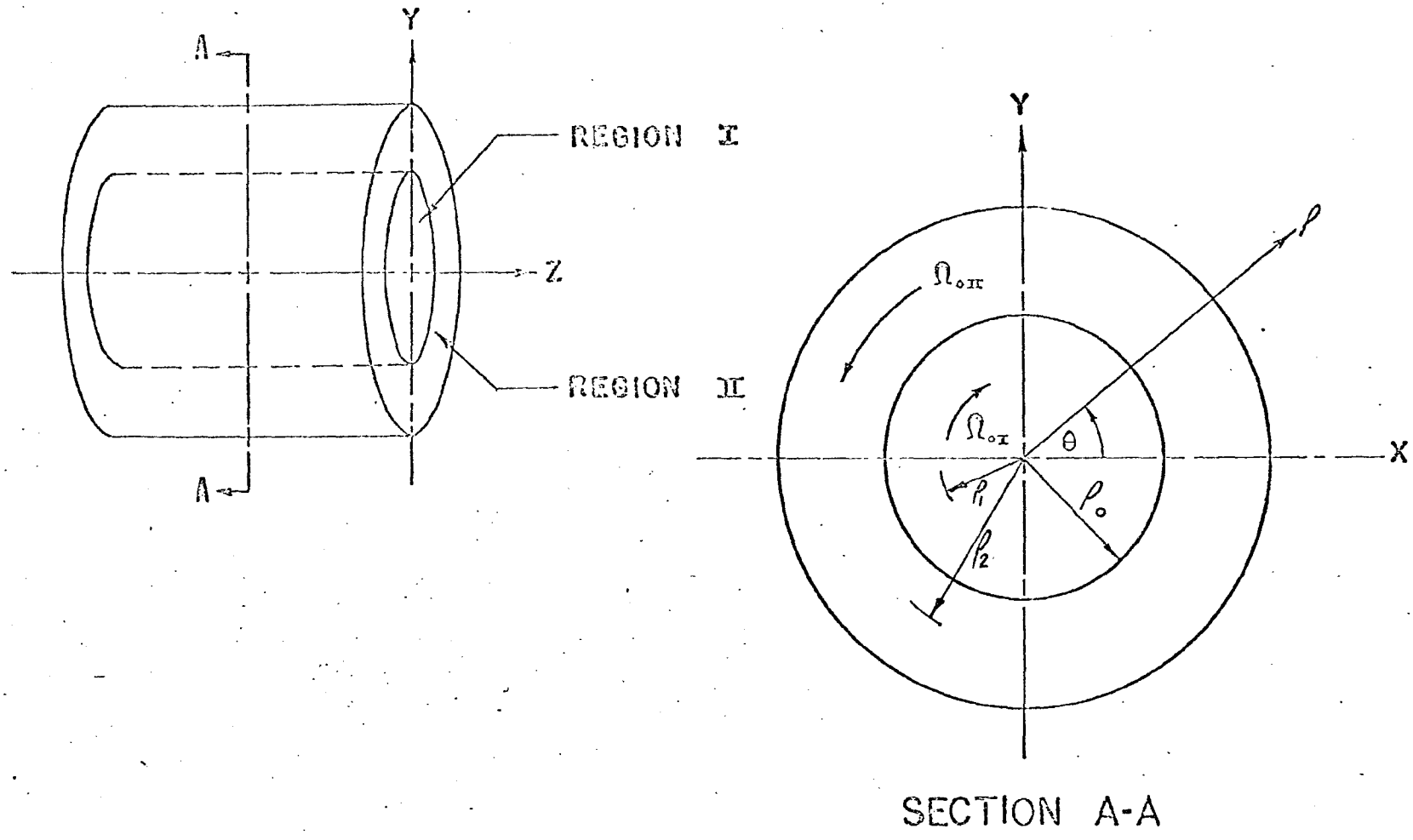

Fig. 4-1. Idealized plasma column at 300 gauss.

constant. Suppose that we interchange the plasma contained in the two rings. The plasma at ρ_2 after the interchange will have the angular momentum L_1 which it had at ρ_1 before the interchange, similarly, the plasma at ρ_1 after the interchange, will have the angular momentum L_2 which it had at ρ_2. As a result, the change in the kinetic energy per unit mass for these rings is equal to

$$\Delta K.E. = \frac{1}{2}\left\{\left(\frac{L_2^2}{\rho_1^2} + \frac{L_1^2}{\rho_2^2}\right) - \left(\frac{L_1^2}{\rho_1^2} + \frac{L_2^2}{\rho_2^2}\right)\right\} \tag{4.30}$$

Therefore

$$\Delta K.E. = \frac{1}{2}\left(L_2^2 - L_1^2\right)\left(\frac{1}{\rho_1^2} - \frac{1}{\rho_2^2}\right) \tag{4.31}$$

Since ρ_2 is greater than ρ_1, the change in the kinetic energy merely depends upon the difference of $L_2^2 - L_1^2$. Consequently, if the angular momentum is a monotonic increasing function of ρ, no interchange of plasma rings can occur without a source of energy, and, this means stability. On the other hand, if the angular momentum should decrease anywhere, then an interchange of rings in this region

will result in a liberation of energy, and this means instability. A stability condition may now be obtained for the plasma

$$\frac{\Omega_2}{\Omega_1} > \left(\frac{\rho_1}{\rho_2}\right)^2 \tag{4.32}$$

which is known as Rayleigh's criterion in ordinary fluid mechanics. In this case, the only pair of roots which leads into instability is

$$\begin{aligned} \Omega_{oI} &= -0.786 \\ \Omega_{oII} &= 0.692 \end{aligned} \tag{4.33}$$

The other combinations are stable and satisfy the Rayleigh's criterion. The root of -0.214 is disregarded since the large ratio of the angular momentums between the two rings places the situation far into the stable region. However, the pair of roots, -0.786 and -1.692, will be discussed later in this chapter.

In the equilibrium case the driving forces which are due to electromagnetic and pressure gradient effects, are balanced by inertia. A test for stability may be performed by increasing these driving effects an infinitesimal amount, that perturbs the system, in this case by changing the magnetic field. If the increased energy is completely absorbed by a dissipative mechanism then the system

is stable. If it is larger than the dissipation, then the system is unstable. In this problem the dissipative mchanism is viscosity. A classic analogy to this problem exists in hydrodynamics, [17, 22, 44] known as couette flow.

Couette flow is the steady circular flow of a liquid between two rotating coaxial cylinders. At a critical ratio of the angular velocities, instability will set in resulting-in-convection. This convection will produce a stationary cellular pattern, known as Taylor cells[22]. If at the onset of instability stationary convection prevails, the frequency of the perturbed variables vanishes for all wave numbers and the wave amplitude remains constant. If the perturbed variables take the form of an exp. $(-i\omega t)$, the real part of the complex frequency ω vanishes and the imaginary part of the frequency will be set equal to zero at the marginal state.

4.3 Method of Analysis

The flow pattern at the onset of the instability will be determined from the equations of motion and continuity. When this instability occurs the changes from equilibrium are small so that the equations are linearized. From the experimental evidence, the

perturbed variables will be assumed to have a sinusoidal variation in the θ direction and no variation in the axial direction. This assumption which follows the normal mode analysis is widely used in the theory of hydromagnetic stability[17, 44]. Because of the stationary structure of the cells a convective cell analysis will be proposed. This implies that the variables are independent of time at the onset of the instability. It remains to determine the variation in the radial direction.

There are five variables to be determined; the electric potential, the ion and electron velocities, and the ion and electron densities. From the assumption of quasi-neutrality, the ion and electron densities are equal. Combining the equations of motion and continuity for the electrons, a relationship between the density and the potential is obtained. This relationship is used to eliminate the potential in the equation of motion for ions. Combining the equations of motion and continuity for ions two second order, coupled, ordinary differential equations for the components of the ion velocity are obtained. These differential equations will be simplified by the use of experimental results.

4.4 Perturbation

The linearized quantities for the ion equation of motion are:

$$
\begin{aligned}
n(r,\theta,t) &= n_0(r) + n_1(r,\theta,t) \\
\vec{V}(r,\theta,t) &= \vec{V}_0(r) + \vec{V}_1(r,\theta,t) \\
\Phi(r,\theta,t) &= \Phi_0(r) + \Phi_1(r,\theta,t)
\end{aligned}
\tag{4.34}
$$

where n_1 , $\vec{V}_1$, Φ_1 are perturbed quantities and vary as exp. ($-i\omega t$) where ω is a complex frequency.

By substituting the above quantities into the above equations of motion for ions and dropping higher order terms, the linearized equations become

$$
\begin{aligned}
m_i n_0(-i\omega\vec{V}_1 + \vec{V}_0\cdot\vec{\nabla}\vec{V}_0 + \vec{V}_1\cdot\vec{\nabla}\vec{V}_0 \\
+ \vec{V}_0\cdot\vec{\nabla}\vec{V}_1) + m_i n_i \vec{V}_0\cdot\vec{\nabla}\vec{V}_0 &= e n_0(-\vec{\nabla}\Phi_0 - \vec{\nabla}\Phi_1 + \vec{V}_0\times\vec{B} + \vec{V}_1\times\vec{B}) \\
&\quad + e n_1(-\vec{\nabla}\Phi_0 + \vec{V}_0\times\vec{B}) \\
&\quad - KT_i\vec{\nabla}n_0 - KT_i\vec{\nabla}n_i \\
&\quad + \mu\left(\nabla^2\vec{V}_1 + \tfrac{1}{3}\vec{\nabla}[\vec{\nabla}\cdot\vec{V}_1]\right)
\end{aligned}
\tag{4.35}
$$

By multiplying the equation of motion by $(1 + \frac{n_1}{n_0})$ and subtracting the result from eq. (4.35), the difference is

$$
\begin{aligned}
m_i n_0(-i\omega\vec{V}_1 + \vec{V}_1\cdot\vec{\nabla}\vec{V}_0 + \vec{V}_0\cdot\vec{\nabla}\vec{V}_1) &= e n_0(-\vec{\nabla}\Phi_1 + \vec{V}_1\times B) \\
&\quad - KT_i\left(\vec{\nabla}n_1 - \frac{n_1}{n_0}\nabla n_0\right) \\
&\quad + \mu\left(\nabla^2\vec{V}_1 + \tfrac{1}{3}\vec{\nabla}[\vec{\nabla}\cdot\vec{V}_1]\right)
\end{aligned}
\tag{4.36}
$$

The linearized equation of continuity can be written as

$$\omega n_1 + i\vec{\nabla}\cdot(n_0\vec{v}_1) + i\vec{\nabla}\cdot(n_1\vec{v}_0) = 0 \tag{4.37}$$

It will again be convenient to introduce the following dimensionless quantities

$$\begin{aligned}
\rho &= r\omega_c/v_{th} \\
\vec{u} &= \vec{v}_1/v_{th} \\
\vec{u}_0 &= \vec{v}_0/v_{th} \\
W &= \omega/\omega_c \\
\vec{\delta} &= \vec{\nabla} n_0 v_{th}/n_0\omega_c \\
a &= A_m(v_{th}/\omega_c)^2 \\
\chi &= e\phi_1/kT_i \\
\nu &= n_1/n_0 \\
\tau &= \mu\omega_c/m_i n_0 v_{th}^2
\end{aligned} \tag{4.38}$$

We shall also replace $\vec{\nabla}$ by $(\omega_c/v_{th})\vec{\nabla}$.

In terms of these dimensionless variables the equation of motion eq. (4.36) becomes

$$(W + i\vec{u}_0\cdot\vec{\delta})\vec{u} + i\vec{\delta}(\chi+\nu) - \tau\vec{u}\times\frac{\vec{B}}{|B|} = \tau\vec{u}\cdot\vec{\delta}\vec{u}_0 + \tau i\tau\left(\delta^2\vec{u} + \frac{1}{3}\vec{\delta}(\vec{\delta}\cdot\vec{u})\right) \tag{4.39}$$

and the equation of continuity eq. (4.37) becomes

$$(4.40)\quad (W+i\vec{v}_0\cdot\vec{\nabla})\mathcal{V}+i\vec{\nabla}\cdot\vec{v}+i\vec{v}\cdot\vec{\delta}=0$$

The mechanism of the instability, from equilibrium conditions and its dissipative factors lead to the formation of stationary cells this implies that the real part of the complex frequency will vanish for all wave numbers and the imaginary part of the frequency will be set equal to zero at the marginal state. Therefore all the perturbed quantities will vary in the following way

$$(4.41)\quad \begin{aligned}\vec{v}(\rho,\theta)&=\vec{v}(\rho)\exp(i m\theta)\\ \mathcal{V}(\rho,\theta)&=\mathcal{V}(\rho)\exp(i m\theta)\\ \chi(\rho,\theta)&=\chi(\rho)\exp(i m\theta)\end{aligned}$$

By substituting eq. (4.41) into eqs. (4.39) and (4.40), we obtain

$$(4.42)\quad \begin{aligned}&\left(-m\Omega_0+\frac{i[4/3]\tau+im^2\tau}{\rho^2}\right)v_\rho-\left(\frac{i4\tau}{3}\right)v_\rho'-\left(\frac{i4\tau}{3}\right)v_\rho''\\ &+\frac{m\tau}{3\rho}v_\theta'+\left(-2i\Omega_0-i-\frac{7m\tau}{3\rho^2}\right)v_\theta+i(\mathcal{V}+\chi)'=0\end{aligned}$$

$$(4.43)\quad \left(-m\Omega_0 + i\tau + i[4/3]m^2\tau\right)v_\theta - \left(\frac{i\tau}{\rho}\right)v_\theta' - (\tau i\tau)v_\theta'' + \frac{m\tau}{3\rho}v_\rho' + \left(2i\Omega_0 + i + \frac{7m\tau}{3\rho^2}\right)v_\rho - \frac{m}{\rho}(\nu+\chi) = 0$$

$$(4.44)\quad \frac{i v_\rho}{\rho} + i v_\rho' - \frac{m}{\rho}v_\theta + i\,\partial\rho\, v_\rho - m\Omega_0\nu = 0$$

The prime denoting $\frac{\partial}{\partial\rho}$ and n_0 has been eliminated by using eq. (4.25). Eqs. (4.42) and (4.43) are the ρ and θ components of the equations of motion, and eq. (4.44) is the equation of continuity. v_ρ, v_θ, ν, and χ are only a function of ρ in eqs. (4.42), (4.43) and (4.44). For the limiting case of zero viscosity, eqs. (4.42) and (4.43) become

$$(4.45)\quad (-m\Omega_0)v_\rho - i(2\Omega_0+1)v_\theta + i(\nu+\chi)' = 0$$

$$(4.46)\quad (-m\Omega_0)v_\theta + i(2\Omega_0+1)v_\rho - \frac{m}{\rho}(\nu+\chi) = 0$$

Solving eqs. (4.45) and (4.46) for v_ρ and v_θ in terms of ν, χ, Ω_0, and m and substituting the result into equation (4.44) the equation of continuity becomes

$$-\Omega_0\left(m^2-[2\Omega_0+1]^2\right)\nu-(\chi+\nu)\left([2\Omega_0+1]a-\frac{m^2}{\rho^2}\Omega_0\right)$$

$$-\Omega_0\left((\chi+\nu)''+\frac{(\chi+\nu)'}{\rho}+a\rho\,(\chi+\nu)'\right)=0 \tag{4.47}$$

Eq. (4.47) is the combined equation of motion and continuity for ions when $\mathcal{C}$ = 0. The corresponding equation for electrons can be obtained by replacing Ω_0 by $-M\Omega_{oe}$, χ by $-\beta^{-1}\chi$, a by $M\beta a$, ρ by $-\rho M^{1/2}\beta^{-1/2}$ and prime by-prime $\beta^{1/2}M^{1/2}$. These changes are necessary because the values for V_{th} and ω_c in eq. (4.38) are defined in terms of T_i and M_i.

The equivalent equation for electrons is

$$M\Omega_{oe}\left(M^2m^2\Omega_{oe}-[-2\Omega_{oe}M+1]^2\right)\nu$$

$$-\left(-\frac{\chi}{\beta}+\nu\right)\left([-2\Omega_{oe}M+1]aM\beta+M^2\beta\frac{m^2\Omega_{oe}}{\rho^2}\right) \tag{4.48}$$

$$+M\Omega_{oe}\left(\left(-\frac{\chi}{\beta}+\nu\right)''M\beta+\frac{(\chi+\nu)'}{\rho}M\beta+a\beta M\rho\left(-\frac{\chi}{\beta}+\nu\right)'\right)=0$$

because $M \ll 1$ eq. (4.48) becomes

$$-\Omega_{oe}\nu=\left(\nu-\frac{\chi}{\beta}\right)a\beta \tag{4.49}$$

From eq. (4.22) the equilibrium electron equation of motion, and eq. (4.25), the density versus radius relationship, eq. (4.49) becomes

$$\chi = \alpha \nu \tag{4.50}$$

Eq. (4.50) implies that the perturbed electric potential varies in exactly the same manner as the perturbed density, only differing by a multiplicative constant. By using equation (4.50) for eliminating χ and equation (4.44) for eliminating ν, the equations (4.42) and (4.43) become

$$\left(\frac{-G}{m\Omega_0} - \frac{i4\tau}{3}\right)v_\rho'' - \left(\frac{(1+\Omega_0)}{m}\rho - \frac{G}{\rho m\Omega_0} - \frac{i4}{3\rho}\tau\right)v_\rho'$$
$$+\left(-m\Omega_0 - \frac{(1+\Omega_0)}{m} + \frac{G}{m\Omega_0\rho^2} + \frac{i(4/3)\tau + im^2\tau}{\rho^2}\right)v_\rho \tag{4.51}$$
$$+\left(\frac{-iG}{\Omega_0\rho} + \frac{m\tau}{3\rho}\right)v_\theta' + \left(-i2\Omega_0 - i + \frac{iG}{\Omega_0\rho^2} - \frac{7m\tau}{3\rho^2}\right)v_\theta = 0$$

$$-i\tau v_\theta'' - \frac{i\tau}{\rho}v_\theta' + \left(-m\Omega_0 + \frac{mG}{\Omega_0\rho^2} + \frac{i\tau + i(4/3)m^2\tau}{\rho^2}\right)v_\theta \tag{4.52}$$
$$+\left(\frac{-iG}{\rho\Omega_0} + \frac{m\tau}{3\rho}\right)v_\rho' + \left(i2\Omega_0 + i - i(1+\Omega_0) - \frac{iG}{\rho^2\Omega_0} + \frac{7m\tau}{3\rho^2}\right)v_\rho = 0$$

where

$$G = 1 + \alpha \tag{4.53}$$

The numerical values determined by the experimental data for the coefficients of the above equation have shown that the magnetic force, the pressure and the inertia forces are nearly zero and the coefficients can be mathematically represented just by the viscosity terms. With close approximations, the above equations can be written as

$$(4.54)\quad v_\rho'' + \frac{v_\rho'}{\rho} - \frac{(3/4)m^2+1}{\rho^2} v_\rho + \frac{i m}{4\rho} v_\theta' - \frac{i\,7m}{4\rho^2} v_\theta = 0$$

$$(4.55)\quad v_\theta'' + \frac{v_\theta'}{\rho} - \frac{(4/3)m^2+1}{\rho^2} v_\theta + \frac{i m}{3\rho} v_\rho' + \frac{i\,7\,m}{3\rho^2} v_\rho = 0$$

Eqs. (4.54) and (4.55) are linear coupled ordinary homogeneous differential equations with variable coefficients of a classic type known as the Euler equation[45]. The general solutions of these equations are:

$$(4.56)\quad v_\rho = \sum_{j=0}^{j=Q} X_j \rho^{u_j}$$

$$(4.57)\quad v_\theta = \sum_{j=0}^{j=Q} Y_j \rho^{u_j}$$

where Q is related to the degree of the differential equation. By combining the differential equations (4.54) and (4.55), a fourth order differential equation, Q = 4, can be obtained. This implies four constants of integration. Eqs. (4.56) and (4.57) involve eight constants of integration, therefore there must be a relationship between X_j and Y_j that can be obtained by satisfying eqs. (4.54) or eq. (4.55).

Substitution of eqs. (4.56) and (4.57) into eqs. (4.54) and (4.55) leads to

$$\begin{bmatrix} u_j(u_j-1)+u_j-\left(\frac{3}{4}m^2+1\right) & \frac{\tau m}{4}(u_j-7) \\ \frac{\tau m}{3}(u_j+7) & u_j(u_j-1)+u_j-\left(\frac{4}{3}m^2+1\right) \end{bmatrix} \begin{bmatrix} X_j \\ Y_j \end{bmatrix} = 0 \tag{4.58}$$

For a nontrivial solution set the determinant

$$\begin{pmatrix} u_j^2-\frac{3}{4}m^2-1 & \frac{\tau m}{4}(u_j-7) \\ \frac{\tau m}{3}(u_j+7) & u_j^2-\frac{4}{3}m^2-1 \end{pmatrix} = 0 \tag{4.59}$$

This implies that

$$u_j^4-2(1+m^2)u_j^2+(m^2-1)^2=0 \tag{4.60}$$

or

(4.61) $$\mu_j = \pm(m+1), \pm(m-1)$$

then the velocity components in region I and II can be expressed as

(4.62) $$v_{\rho I} = A_1\rho^{(m+1)} + A_2\rho^{(m-1)} + A_3\rho^{-(m+1)} + A_4\rho^{-(m-1)}$$

(4.63) $$v_{\rho II} = D_1\rho^{(m+1)} + D_2\rho^{(m-1)} + D_3\rho^{-(m+1)} + D_4\rho^{-(m-1)}$$

(4.64) $$v_{\theta I} = F_1\rho^{(m+1)} + F_2\rho^{(m-1)} + F_3\rho^{-(m+1)} + F_4\rho^{-(m-1)}$$

(4.65) $$v_{\theta II} = H_1\rho^{(m+1)} + H_2\rho^{(m-1)} + H_3\rho^{-(m+1)} + H_4\rho^{-(m-1)}$$

We shall consider the following boundary conditions. The velocity in the radial and azimuthal direction are finite throughout regions one and two, that is

(4.66) Region I: $0 \leq \rho \leq \rho_0$, $v_{\rho I}$ and $v_{\theta I}$ are finite as $\rho \to 0$

(4.67) Region II: $\rho \leq \rho$, $v_{\rho II}$ and $v_{\theta II}$

are finite as ρ becomes large. The above conditions lead to

$$A_3 = A_4 = F_3 = F_4 = 0$$
$$D_1 = D_2 = H_1 = H_2 = 0$$

Therefore equations (4.62) through (4.65) may be simplified into the following form:

$$v_{\rho I} = A_1 \rho^{(m+1)} + A_2 \rho^{(m-1)} \tag{4.68}$$

$$v_{\rho II} = D_3 \rho^{-(m+1)} + D_4 \rho^{-(m-1)} \tag{4.69}$$

$$v_{\theta I} = F_1 \rho^{(m+1)} + F_2 \rho^{(m-1)} \tag{4.70}$$

$$v_{\theta II} = H_3 \rho^{-(m+1)} + H_4 \rho^{-(m-1)} \tag{4.71}$$

Now the eight constants can be further reduced by the substitution of equations (4.68) through (4.71) into the two differential equations. The constants are related as follows:

$$F_1 = \frac{\tau(m+8)}{m-6} A_1 \tag{4.72}$$

$$F_2 = \tau A_2 \tag{4.73}$$

$$H_3 = -\tau D_3 \tag{4.74}$$

and

$$H_4 = \frac{i(8-m)D_4}{m+6} \tag{4.75}$$

Therefore the perturbed velocities become

$$v_{\rho I} = A_1 \rho^{(m+1)} + A_2 \rho^{(m-1)} \tag{4.76}$$

$$v_{\rho II} = D_3 \rho^{-(m+1)} + D_4 \rho^{-(m-1)} \tag{4.77}$$

$$v_{\theta I} = i\left(\frac{m-8}{m-6} A_1 \rho^{(m+1)} + A_2 \rho^{(m-1)}\right) \tag{4.78}$$

$$v_{\theta II} = i\left(-D_3 \rho^{-(m+1)} + \frac{8-m}{m+6} D_4 \rho^{-(m-1)}\right) \tag{4.79}$$

For the four independent constants of integration, A_1, A_2, D_2, and D_4, four boundary conditions are necessary in order to find the particular solutions of eqs. (4.54) and (4.55). At least one boundary condition must be non-homogeneous; that is, a relationship between the perturbed velocity and the equilibrium quantities. Such a relationship is impossible to find, because in the process of linearizing a differential equation the magnitude of the perturbed

quantities are never specified. The perturbed velocities will then be obtained within a multiplicative constant, giving the form of the variation. Only three boundary conditions are required to determine this form. They are:

(a) The perturbed radial velocities must be equal at the boundary of the two regions;

$$v_{\rho I} = v_{\rho II} \quad \text{at } \rho=\rho_0 \tag{4.80}$$

(b) The perturbed azimuthal velocities must be equal at the boundary of the two regions,

$$v_{\theta I} = v_{\theta II} \quad \text{at } \rho=\rho_0 \tag{4.81}$$

(c) The perturbed density of the two regions must be equal at the boundary of the two regions,

$$v_I = v_{II} \quad \text{at } \rho=\rho_0 \tag{4.82}$$

By using eqs. (4.76) and (4.77), eq. (4.80) becomes

$$A_1 + A_2 \rho_0^{-2} = \rho_0^{-2m}(D_3 \rho_0 + D_4) \tag{4.83}$$

By using eqs. (4.78) and (4.79), eq. (4.81) becomes

$$(4.84)\quad \frac{m+8}{m-6} A_1 + A_2 \rho_0^{-2} = \rho_0^{-2m}\left(-D_3 \rho_0^{-2} + \frac{8-m}{m+6} D_4\right)$$

By using eqs. (4.76) through (4.79) and eq. (4.44), eq. (4.82) becomes

$$(4.85)\quad \frac{A_1}{m-6}\left(12m+12-a_I(m-6)\rho_0^2\right) - A_2 a_I = \frac{\Omega_{0I}}{\Omega_{0II}}\left(-D_3 a_{II} + \frac{D_4}{m+6}\left(12m-12-a_{II}(m+6)\rho_0^2\right)\right)\rho^{-2m}$$

Theoretically, a relation may be found to reduce the four constants of integration to the one from eqs. (4.83), (4.84) and (4.85), but the algebraic expression becomes long and complicated. The pattern of the plasma cells could not be clearly seen from such a complicated and long expressions.

In order to interpret the above mathematical results, numerical values from the experimental data are used here.

For a magnetic field of 300 gauss and the experimental conditions as described in Chapter 3, the numerical values are listed as follows:

α_I	=	-1.15	
α_{II}	=	-1.653	
AmI	=	1.25	
AmII	=	-2.00	
a_I	=	1.12	
a_{II}	=	-1.80	
V_{th}	=	0.698×10^5	cm per sec
ω_c	=	0.737×10^5	rad per sec
$\Omega_{o\,I}$	=	-0.786	
$\Omega_{o\,II}$	=	0.692	
m	=	8	
r_o	=	0.95	cm
ρ_o	=	1.0	

From the above numerical values, the four constants can be expressed in terms of an arbitrary constant, U

(4.86) $A_1 = -0.143\,U$

(4.87) $A_2 = 1.144\,U$

(4.88) $D_3 = 0.000543U$

(4.89) $D_4 = U$

The value of the perturbed velocities becomes

(4.90) $v_{\rho I} = U(-0.143\rho^9 + 1.144\rho^7)e^{i8\theta}$

(4.91) $v_{\rho II} = U(.000543\rho^{-9} + \rho^{-7})e^{i8\theta}$

(4.92) $v_{\theta I} = iU(-1.145\rho^9 + 1.144\rho^7)e^{i8\theta}$

(4.93) $v_{\theta II} = -iU(0.000543)\rho^{-9}e^{i8\theta}$

The value for v_ρ and v_θ are functions of ρ and θ in eqs. (4.90) through (4.93).

The total velocity components may be found by superimposing the perturbed velocity onto the equilibrium velocity.

(4.94) $V_\rho = 0 + v_\rho = v_\rho$

(4.95) $$V_\theta = v_o + v_\theta \doteq v_o$$

The value for $v_o = \Omega_o \rho$

(4.96) $$v_{oI} = -0.786\rho$$

(4.97) $$v_{oII} = 0.692\rho$$

From eqs. (4.90) and (4.91) v_ρ becomes

(4.98) $$v_{\rho I} \doteq \rho^7 (U_1 \cos.8\theta - U_2 \sin.8\theta)$$

(4.99) $$v_{\rho II} \doteq \rho^7 (U_1 \cos.8\theta - U_2 \sin.8\theta)$$

where $U = U_1 + iU_2$

By using the results of the velocity components, the equation of the streamlines can be obtained as

Region I: $0 \leq \rho \leq 1.00$

$$\frac{K_1 \rho^7 (U_1 \cos.8\theta - U_2 \sin.8\theta)}{-0.786\rho} = \frac{d\rho}{\rho d\theta}$$

(4.100) $$\rho = \left(K_2[U_1 \sin.8\theta + U_2 \cos.8\theta] + C_1\right)^{-1/6}$$

Region II: $$1.00 \leq \rho$$

$$\frac{K_3 \rho^{-7}(U_1 \cos.8\theta - U_2 \sin.8\theta)}{0.692\rho} = \frac{d\rho}{\rho d\theta}$$

(4.101) $$\rho = \left(K_4[U_1 \sin.8\theta + U_2 \cos 8\theta] + C_2\right]^{1/8}$$

where K_2, K_4, C_1 and C_2 are constants. The streamlines are shown in Figure 4-2. It is clear that the fluid tends to separate and come together at eight equally spaced angles. By substituting the velocity components, equations (4.90) through (4.93) into the equation of continuity, the dimensionless density $\mathcal{V}$ varies as i exp. ($\tau 8\theta$). The perturbed density has a maximum value when the perturbed radial velocity is zero and the perturbed radial velocity has a maximum value when the perturbed density is zero. This implies, referring to Figure 4-2. that the perturbed density has a maximum value at the center of each hole and at the center of the two adjacent holes where the plasma is the most concentrated. For the variation in the flow pattern discussed up to this point, the values of $\Omega_{oI} = -0.786$ and $\Omega_{oII} = 0.692$. The values of $\Omega_{oI} = -0.786$ and $\Omega_{oII} = -1.692$ are considered. In the same manner, the four constants are determined as follows:

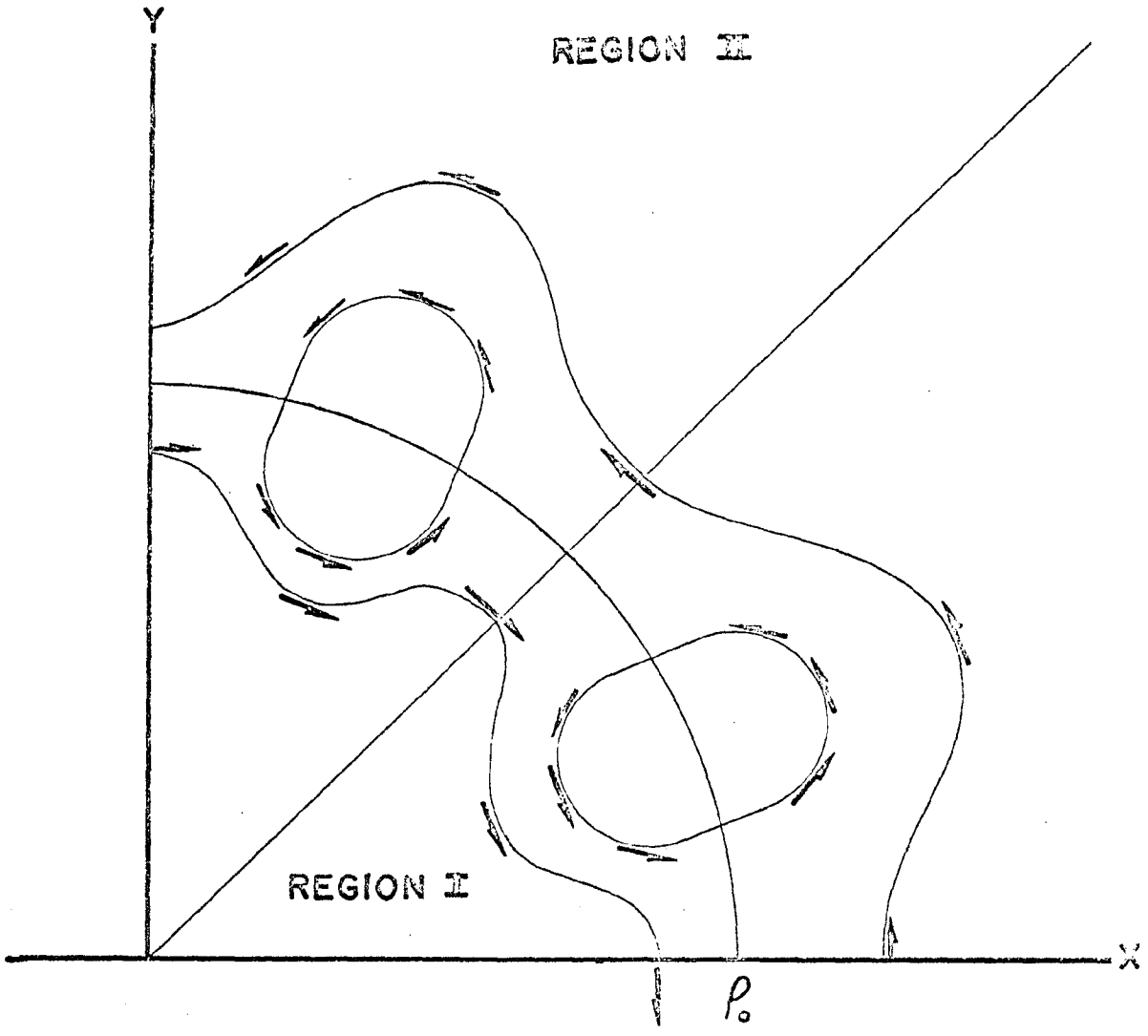

Fig. 4-2. Streamlines, unstable case for $U_1 = 0$ and $U_2 = -\text{constant}$.

(4.102) $D_3 = -0.717\ U$

(4.103) $A_2 = +0.218\ U$

(4.104) $A_1 = -.183\ U$

(4.105) $D_4 = U$

The corresponding perturbed velocities become

(4.106) $$v_{\rho I} = U(-0.183\rho^9 + 0.218\rho^7)e^{i8\theta}$$

(4.107) $$v_{\rho II} = U(-0.717\rho^{-9} + \rho^{-7})e^{i8\theta}$$

(4.108) $$v_{\theta I} = iU(-1.456\rho^9 + 0.218\rho^7)e^{i8\theta}$$

(4.109) $$v_{\theta II} = iU(0.717)\rho^{-9}e^{i8\theta}$$

The streamlines may also be calculated as follows:

for Region I, $$\frac{K_5\rho^7(U_1\cos.8\theta - U_2\sin 8\theta)}{-0.786\rho} = \frac{d\rho}{\rho d\theta}$$

(4.110) $$\rho = \left(K_6(U_1\sin.8\theta + U_2\cos.8\theta) + C_3\right)^{-1/6}$$

for Region II, $$\frac{K_7(-U_2\sin 8\theta + U_1\cos 8\theta)\rho^{-7}}{-1.692\rho} = \frac{d\rho}{\rho d\theta}$$

$$(4.111)\qquad \rho = \left(-K_8\left(U_2\cos 8\theta + U_2 \sin 8\theta\right) + C_4\right)^{1/8}$$

where the values of K_6, K_8, C_3 and C_4 are constants. The streamlines are shown in Figure 4-3. It is clear that this pattern does not resemble a cellular form as found experimentally, and if secondary motion does set in at the marginal state, it will not take the form of the plasma cells shown in Chapter 3. The difference between this case and the previous case is that this case satisfies Rayleigh's criterion as a stable case and the previous case is unstable.

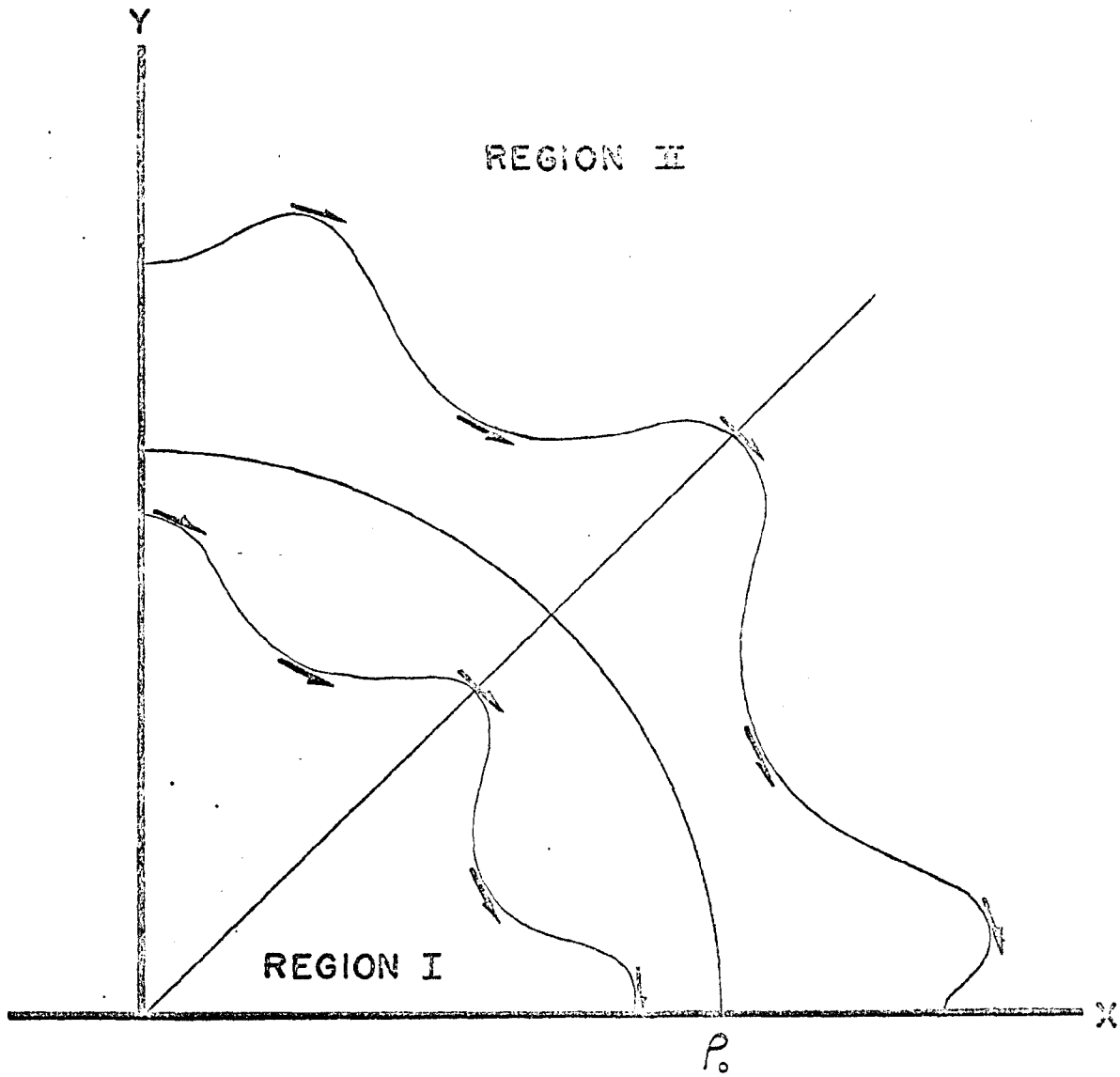

Fig. 4-3. Streamlines, stable case.

4.5 Summary

In this chapter, a theoretical analysis has been performed with the aid of experimental data. The essential results are listed as follows:

(1) Euler equations and its solution ---

By using the experimental relations between the plasma density and the electric potential, a set of differential equations, eqs. (4.42), (4.43) and (4.44) have been established in dimensionless form. The coefficients of those differential equations can be represented by viscous terms since the electromagnetic force, pressure force and inertia force are small for the perturbed state. The equations reduced to the well-known Euler's equation. The solutions have been obtained as shown in eqs. (4.62) through (4.65).

(2) Convection cells ---

By using the experimental values, the solution of Euler's equations gives a set of streamlines, the density distribution across the cross section of the plasma column, and shows a pattern of eight cells as photographed by the plasma camera.

(3) Rayleigh's criterion for stability ---

The theoretical analysis gives four possible rotations of the plasma column. One is unstable and gives convection cells. Two are very stable and provide no interesting configurations. The last one is stable and satisfies the Rayleigh's criterion. The details of the last configuration have been analyzed as shown in Figure 4-3.

(4) The concept of angular momentum interchange and its stability ---

With the evidence of the plasma camera photographs and the theoretical analysis of this chapter, the concept of angular momentum exchange between two rings leads to the verification of the mechanism for the onset instability.

CHAPTER 5

CONCLUSION

An outline of the experimental and theoretical investigation of the onset instability and the formation of cells is presented in this chapter. The special feature of the Q-machine, the developed diagnostic technique of the plasma camera, the theoretical concept of the interchange of angular momentum and a comparison of the theoretical and experimental results are described and discussed in this chapter.

5.1 Plasma Column and Diagnostics

In this dissertation, the specially designed Q-machine has the capability to produce a large potential gradient at the edge of the plasma column and to meet the requirements for the convective instability studies.

Since the conventional diagnostics of the Langmuir probe can not give the density distribution across the plasma column, the plasma camera technique has been successfully used. Due to the low energy density of the streaming plasma within the Q-machine, the original design of the plasma camera has been significantly modified.

The experimental results have shown that the plasma camera is effective in measuring the relative magnitude of the density across the column and its irregularities. By using the Langmuir probe and the plasma camera technique simultaneously, the experimental results are rather satisfactory, both qualitatively and quantitatively. The visualization of the density distribution across the plasma column is new and important, since it is very different from the concept of the existing theory. The general principle of the plasma camera is to accelerate electrons or ions from a continuously streaming plasma column onto a screen. By means of a strong electrical pulse between the screen and the scintillator, those electrons, primary or secondary, produce scintillations which in turn are photographed.

The experimental parameters are listed as follows:

Q-machine: (a) plasma density 1×10^{10} to 1.6×10^{11} particles per cu. cm.,

(b) plasma temperature 2300 degrees K,

(c) magnetic field range of plasma cells 100 to 300 gauss,

(d) column length 50 cm.

Plasma camera: (a) screen - stainless steel 50% transmissive,

(b) scintillator P-1 or P-11 phosphor on a glass disk,

(c) coating aluminum 3,000 to 5,000 anstroms,

(d) bias ±22.5 volts on the screen,

(e) pulse 7,000 volts for 1 μ sec.

5.2 Plasma Cells and Confinement

For a magnetic field of 200 gauss, photographs of a stationary cellular pattern in a Q-machine have been experimentally obtained by the use of the plasma camera. Langmuir probe measurements taken at the same time show the characteristic of zero frequency across the plasma column.

The degree of ionization and, or recombination is negligible at the magnetic fields and densities cited[46-48], therefore the increase in the plasma current must be due to an improved confinement. The increase in collector current or the improved confinement must, then, be related to the onset of the stationary cellular pattern. At higher magnetic fields, the plasma acts in a weakly turbulent manner and produces large transverse flux [49, 50] as shown by the plasma cameraphotographs in Chapter 3, basically Bohm diffusion. By going

to even higher magnetic fields some confinement is produced by strengthening the field lines but the weakly turbulent process still prevails and large transverse losses exist. In finding a region where a stationary pattern may set in, effectively laminar flow, one can truly realize improved confinement.

Plasma camera observations have also shown flute-like irregularities or plasma blobs at the periphery of the plasma column at high magnetic fields, above 700 gauss. The transverse motion of these irregularities is due to the breaking off of the flutes from the core of the plasma column and collective mass transfer across the magnetic field lines. This suggests an important mechanism in the loss of plasma transverse to the magnetic field lines, known as anomalous diffusion.

5.3 The Mechanism Producing the Cells

The convective mechanism that produced the cells is due to an adverse angular momentum caused by an inner core of plasma rotating with a constant angular momentum and an outer concentric cylinder of plasma rotating in the opposite direction, at another constant angular momentum. From the equilibrium potential profile the

magnitude of the electric field in the inner core was found to be about equal but opposite in direction to the electric field in the outer cylinder. These electric fields cause an azimuthal velocity in the inner core which is opposite to the azimuthal velocity in the outer cylinder. The resulting motion produces a shear between the inner core and the outer cylinder. This shear produces an adverse gradient of angular momentum leading to an instability. From this unstable arrangement, particles in the inner core will tend to reach a neutral state of potential energy by moving, or convecting, toward the outer cylinder. These particles will be turned back by the electric field and a loss in kinetic energy (due to collisions) prevents the particles from escaping as long as there is an electric field, and a sufficient number of collisions, the convection of plasma between the inner core and outer cylinder will continue with the formation of cells.

5.4 Theory of Stationary Convective Instability

Because of the stationary structure of the cells the principle of convective stability was proposed. By using the experimental relations between the plasma density and the electric potential, at 300 gauss, for the equilibrium conditions, a set of differential equations,

based on the two fluid equations, were established. A test for stability was performed by perturbing the density, velocity, and potential in the equilibrium equation, basically a normal mode analysis. The mechanism for this instability is due to an adverse angular momentum between concentric rings of plasma. From this analysis a set of streamlines were obtained and a comparison between the density and potential was made. The validity of the theory was established by accurately

(1) Predicting the cellular pattern,

(2) Predicting the proper location of the maximum density perturbations.

(3) Satisfying Rayleigh's stability criterion.

The theory proposed in Chapter 4 is a linear theory and only predicts the onset and form of the cells; that is, a concentration and separation of plasma, at eight distinct locations, in a cellular pattern. The normal mode analysis indicates that the cells grow exponentially. If the linear theory is valid, at larger times the cells will become infinitely large. This implies that a linear process is not valid throughout the development of the plasma cells and a nonlinear process[51, 3, 4] must control the final development of these cells.

5.5 Summary

In summary, the experimental and theoretical results are as follows:

(1) stationary convective cells were experimentally detected in a streaming plasma column and were found to improve plasma confinement,

(2) a new concept of anomalous diffusion, due to the breaking off of flute-like irregularities, has been found by the use of the plasma camera. The plasma camera has been shown to be a powerful diagnostic instrument,

(3) the principle of stationary convection was used to predict the structure of the plasma cells.

REFERENCES

1) N. D'Angelo and R. W. Motley, Phys. Fluids 6, 296 (1963).

2) N. D'Angelo and R. W. Motley, Phys. Fluids 6, 422 (1963).

3) H. Lashinsky, Phys. Rev. Letters 12, 121 (1964).

4) H. Lashinsky, Phys. Rev. Letters 13, 47 (1964).

5) N. D'Angelo, Phys. Fluids 8, 1748 (1965).

6) S. von Goeler, Phys. Fluids 9, 818 (1966).

7) S. von Goeler and N. D'Angelo, Phys. Fluids 8, 1570 (1965).

8) S. von Goeler and N. D'Angelo, Phys. Fluids 9, 309 (1966).

9) N. S. Buchelnikova, R. A. Salimov, and Yu I. Eidelman, JETP 25, 548 (1967).

10) H. W. Hendel, B. Coppi, F. Perkins and P. Politzer, Phys. Rev. Letters 18, 439 (1967).

11) T. H. Stix, Theory of Plasma Waves (McGraw-Hill, New York, 1962).

12) F. F. Chen, Phys. Fluids 7, 949 (1964).

13) F. F. Chen, Phys. Fluids 8, 912 (1965).

14) M. N. Rosenbluth and A. Simon, Phys. Fluids 8, 1300 (1965).

15) F. F. Chen, Phys. Fluids 8, 1329 (1965).

16) T. E. Stringer and G. Schmidt, Plasma Phys. 9, 53 (1967).

17) S. Chandrasekhar, Hydrodynamics and Hydromagnetic Stability (Oxford University Press, London, 1961).

REFERENCES (continued)

18) S. Chandrasekhar, Proc. Roy. Soc. (London) A, 237, 476 (1956).

19) Y. Nakagawa, Proc. Roy. Soc. (London) A, 249, 138 (1959).

20) G. W. Sutton and A. Sherman, Engineering Magnetohydrodynamics (McGraw-Hill, New York 1965).

21) W. B. Thomson, An Introduction to Plasma Physics (Pergamon Press, New York 1962).

22) G. I. Taylor, Phil. Trans. Roy. Soc. (London) A, 223. 2389, (1923).

23) S. H. Lam, Phys. Fluids 8, 73 (1965).

24) F. F. Chen, Plasma Diagnostic Techniques, R. H. Huddleston and S. L. Leonard, editors (Academic Press, New York 1965).

25) J. C. Cataldo and N. C. Jen, Phys. Fluids 11, 2057 (1968).

26) N. Rynn, N. D'Angelo, Rev. Sci. Instr. 31, 1326 (1960).

27) J. Y. Wada and R. C. Knechtli, Proc. IRE 12, 1926 (1961).

28) K. D. Sinel'nikov, B. G. Safronov, V. G. Padalka and I. I. Demidenko, Zh. Takh. Fiz 33, (1963).

29) F. H. Coensgen, W. F. Cummins, W. E. Nexsen, Jr., and A. E. Sherman, Rev. Sci. Instr. 35, 1072 (1964).

30) I. I. Demidenko and N. S. Lomino, Plasma Phys. 8, 433 (1966).

31) Optical Characteristics of Cathode Ray Tube Screens (JEDEC Electron Tube Council, New York 1966).

32) W. F. Cummins (private communications).

33) N. C. Jen and J. C. Cataldo, Bull. Am. Phys. Soc. 13, 288 (1968).

REFERENCES (continued)

34) F. C. Hoh and B. Lehnert, Phys. Fluids 3, 600 (1960).

35) F. C. Hoh, Phys. Rev. Letters 4, 559 (1960).

36) N. D'Angelo and N. Rynn, Phys. Fluids 4, 275 (1961).

37) N. D'Angelo and N. Rynn, Phys. Fluids 4, 1303 (1961).

38) N. Rynn, Phys. Fluids 5, (1962).

39) D. Bohm, E. Burhop, H. S. W. Massey and R. Williams, The Characteristics of Electrical Discharges in Magnetic Fields (A. Guthrie and R. K. Wakerling, New York, 1949).

40) L. Spitzer, Physics of Fully Ionized Gases (Wiley and Sons, New York 1965).

41) S. Chapman and T. Cowling, The Mathematical Theory of Non-Uniform Gases (Cambridge Univ. Press, London 1960).

42) F. F. Chen, Princeton Plasma Phys. Lab. Report MATT-277 (1963).

43) S. Schaaf and P. Chambre', Flow of Rarified Gases (Princeton University Press, New Jersey, 1962).

44) C. C. Lin, The Theory of Hydrodynamic Stability, (Cambridge, England, 1955).

45) E. L. Ince, Ordinary Differential Equations (Dover, New York 1956).

46) N. D'Angelo, Phys. Rev. 121, 505 (1961).

47) S. Von Goeler, Phys. Fluids 8, 463 (1964).

REFERENCES (continued)

48) N. Rynn, Phys. Fluids 9, 165 (1966).

49) B. B. Kadomtsev, Plasma Phys. 5, 31 (1962).

50) B. B. Kadomtsev, Plasma Turbulence (Academic Press, New York, 1965).

51) J. C. Cataldo and N. C. Jen, Transaction of Fluid Dynamics, Academy of Science, Poland, 1967.

VITA

Joseph C. Cataldo, born in New York on April 1, 1937, is married and father of two children.

Mr. Cataldo attended elementary school in the Bronx and graduated from Industrial Art High School in June, 1954. He went to Brooklyn Community College for two years and then came to City College in September, 1956. At City College, Mr. Cataldo majored in civil engineering and was an active member in ASCE. In January, 1960, Mr. Cataldo received a Bachelor of Civil Engineering degree. Upon graduating he went to work at the Brooklyn Naval Yard as a Naval architect, working on the structural design of the super carriers.

In January, 1963, Mr. Cataldo became a Lecturer in the Department of Civil Engineering, where he became interested in plasma physics. In 1964, after receiving a Master's degree in civil engineering at City College, he became a full-time student, working towards his Ph.D. Since 1964, he has remained at City College, working as a research assistant and/or Lecturer in the Department of Civil Engineering where he completed his dissertation in early 1969.